



Balkan Journal of Electrical & Computer Engineering

An International Peer Reviewed, Referred, Indexed and Open Access Journal

SPECIAL ISSUE: The special issue consists of recent trends on electrical & computer engineering applications. And also, some studies have been selected from International Engineering Research Symposium, (UMAS 2017) for this special issue.



This journal is supported by the Istanbul Technical University. It is abstracted and indexed in, Index Google Scholarship, the PSCR, Cross ref, DOAJ, Research Bible, Indian Open Access Journals (OAJ), Institutional Repositories (IR), J-Gate (Informatics India), Ulrich's, International Society of Universal Research in Sciences, DRJI, EyeSource, Cosmos Impact Factor, Cite Factor, SIS SIS Scientific Indexing Service, IJIF, iiiFactor. ULAKBİM-TR Dizin.



General Publication Director & Editor-in-Chief
Ş.Serhat Seker, Istanbul Technical University, Turkey

Special Issue Editor
Yunus Bicen, Duzce University, Turkey.

Scientific Committee
Abhishek Shukla (India)
Abraham Lomi (Indonesia)
Aleksandar Georgiev (Bulgaria)
Arunas Lipnickas (Lithuania)
Audrius Senulis (Lithuania)
Belle R. Upadhyaya (USA)
Brijender Kahanwal (India)
Chandar Kumar Chanda (India)
Daniela Dzhonova-Atanasova (Bulgaria)
Deris Stiawan (Indonesia)
Emel Onal (Turkey)
Emine Ayaz (Turkey)
Enver Hatimi (Kosovo)
Ferhat Sahin (USA)
Gursel Alici (Australia)
Hakan Temeltaş (Turkey)
Ibrahim Akduman (Turkey)
Jan Izykowski (Poland)
Javier Bilbao Landatxe (Spain)
Jelena Dikun (Lithuania)
Karol Kyslan (Slovakia)
Kunihiko Nabeshima (Japan)
Lambros Ekonomou (Greece)
Lazhar Rahmani (Algerie)
Marcel Istrate (Romania)
Marija Eidukeviciute (Lithuania)
Milena Lazarova (Bulgaria)
Muhammad Hadi (Australia)
Muhamed Turkanović (Slovenia)
Mourad Houabes (Algerie)
Murari Mohan Saha (Sweden)
Nick Papanikolaou (Greece)
Okyay Kaynak (Turkey)
Osman Nuri Ucan (Turkey)
Ozgur E. Mustecaplioglu (Turkey)
Padmanaban Sanjeevikumar (India)
Ramazan Caglar (Turkey)
Rumen Popov (Bulgaria)
Tarek Bouktir (Algeria)
Sead Berberovic (Croatia)
Seta Bogosyan (USA)
Savvas G. Vassiliadis (Greece)
Suwarno (Indonesia)
Tulay Adali (USA)
Yogeshwarsing Calleecharan (Mauritius)
YangQuan Chen (USA)
Youcef Soufi (Algeria)

Aim & Scope

The journal publishes original papers in the extensive field of Electrical-Electronics and Computer engineering. It accepts contributions which are fundamental for the development of electrical engineering, computer engineering and its applications, including overlaps to physics. Manuscripts on both theoretical and experimental work are welcome. Review articles and letters to the editors are also included.

Application areas include (but are not limited to): Electrical & Electronics Engineering, Computer Engineering, Software Engineering, Biomedical Engineering, Electrical Power Engineering, Control Engineering, Signal and Image Processing, Communications & Networking, Sensors, Actuators, Remote Sensing, Consumer Electronics, Fiber-Optics, Radar and Sonar Systems, Artificial Intelligence and its applications, Expert Systems, Medical Imaging, Biomedical Analysis and its applications, Computer Vision, Pattern Recognition, Robotics, Industrial Automation.



ISSN: 2147- 284X

Year: April 2018

Special Issue: The special issue consists of recent trends on electrical & computer engineering applications. And also, some studies have been selected from International Engineering Research Symposium, (UMAS 2017) for this special issue.

CONTENTS

- E. Huner, C. Akuner;** The Design and Magnetic Analysis of MultiDisc and Layer Winding Toroidal Axial Flux Permanent Magnet Open Slotted (MLTAFPMOS) Synchronous Alternator,**1-5**
- H. Bakir, A. Ozturk, and S.Tosun;** Investigation of Power Flow Effect of Serial and Parallel FACTS Devices,**6-11**
- O. Akar, U.K.Terzi and O. Ozgonenel;** A New Speed Control Technique for a Separately Excited Direct Current Motor by PID Controller,**12-17**
- M.K. Döşoğlu, M. Dursun,** Response and Analysis of Permanent Magnet Synchronous Motor According to Different Reference Signals,**18-22**
- H.Uzun, O.Akar, A.Demirci, M.C.Akuner, U.K. Terzi;** Analyzing High Efficiency Asynchronous Motors Using Scalar Control Technique,**23-26**
- K. Erhan, M. Ayaz, and Y. Icer;** Conceptual Design of a Smart Parking Lot System for Electric and Hybrid Electric Vehicles,**27-32**
- Z.B. Garip and A.F. Boz;** The FIR Filter Design based on Genetic Algorithm,**33-36**
- S. Karagol, D. Yildiz;** Transmission of Audio Signal from Reed-Solomon AWGN Channel Using Wavelet Transform Families,**37-41**
- M.S. Başarslan, F. Kayaalp;** Data Mining Through Data Visualization: A Case Study on Predicting Churners on Telecommunications Data Set,**42-45**
- B. Aslan, O. Dikmen, S. Kulaç and A. M. Elbir;** Evaluation of Reconfigurable Multiple and Compact Micro-Strip Antennas for MIMO Systems,**46-50**
- F. Katircioglu;** Noise Adaptive and Similarity Based Switching Median Filter for Salt & Pepper Noise,**51-55**
- H.S. Nogay;** Classification of Different Cancer Types by Deep Convolutional Neural Networks,**56-59**

**BALKAN
JOURNAL OF
ELECTRICAL & COMPUTER ENGINEERING**
(An International Peer Reviewed, Indexed and Open Access Journal)

Contact
Istanbul Technical University
Department of Electrical Engineering
Ayazaga Campus, Maslak, Istanbul-Turkey

Web: <https://www.bajece.com>
<http://dergipark.gov.tr/bajece>
e-mail: editor@bajece.com

The Design and Magnetic Analysis of MultiDisc and Layer Winding Toroidal Axial Flux Permanent Magnet Open Slotted (MLTAFPMOS) Synchronous Alternator


E. Huner and, M.C. Akuner


Abstract—In this study, a new multidisc and layer winding toroidal axial flux permanent magnet open slotted (MLTAFPMOS) synchronous alternators are designed and magnetic analysis was performed. Axial flux (AF) alternators are a very good candidate for wind turbine applications. However, one of the disadvantages AF alternators is to increase AF alternator diameter with AF alternator power. The junction points of AF alternator rotor shaft and disc have a very huge torques via occurring from inner rotor diameter forces to outer rotor diameter forces. Therefore mechanically problems emerge with increasing alternator powers. The ideal solution for this situation is to use a multidisc structure. In this study, a multidisc design for LTAFFPMOS synchronous alternator was developed. A 3d solid model of the developed design was obtained. Then magnetic analyzes were performed via Maxwell. It is decided that the multidisc structure is ideal to increase the alternator power as a result of analyzes. In addition, forces at the junction points is decreased via multidisc structures.

Index Terms— Axial flux alternator, Maxwell, Permanent magnet, Toroidal winding

I. INTRODUCTION

IN RECENT YEARS, a lot of study has been done to obtain electricity from wind energy, that is one of the renewable energy sources. One of them is about alternator development for wind turbines. Especially with the discovery of neodymium magnets in 1980's, with this discovery the use of permanent magnets has also begun in alternators. Especially for the last 20 years; Axial Flux Permanent Magnet (AFPM) alternators have gained importance. The axial flux machines are disk shaped and the magnetic flux path moves along the two disks. Therefore, these types of machines are called AFPM machines.

E. HUNER, is with Department of Energy Systems Engineering University of Kirklareli University, Kirklareli, Turkey, (e-mail: engin.huner@klu.edu.tr) 

M.C. AKUNER, is with Department of Mechatronic Engineering University of Marmara, Istanbul, Turkey, (e-mail: akuner@marmara.edu.tr) 

Manuscript received September 13, 2017; accepted January 08, 2018.
DOI: [10.17694/bajece.410190](https://doi.org/10.17694/bajece.410190)

Considering the work done on AFPM alternators; the air gap and the change in magnet angle of AFPM motor is examined. It is stated that a minimum magnetic flux change is performed for 26 degree in the work done. Besides, the most suitable air space value is analyzed as 4mm [1]. In the study, a coreless AFPM rhomboidal wound alternator was designed [2]. The design was run at 400 Hz. It is also emphasized that it is an ideal design for aircraft, ships and electric vehicles due to its low weight. In another study, a toroidal wound alternator was developed to apply the small wind turbine [3]. In this study; it is emphasized that it is the ideal alternator type for wind turbines due to its low cost, great moment and direct drive ability [3-4].

A hybrid design model for the coreless AFPM alternator is presented [5]. This hybrid structure includes both analytical calculations and programs using the Finite Element Method (FEM). For analytical calculations, a genetic algorithm based method was used of Powell's method. Powell's method is more suitable than the genetic algorithm that requires high processor power. Therefore, with this hybrid method, values such as minimum permanent magnet (PM), maximum power and optimum air gap are calculated in a shorter time.

In one study; an AFPM alternator that produces micro level power is produced [6]. The micro AFPM alternator consists of magnets embedded in the polymer rotor and two silicon printed circuit model stators. The design has a diameter of 7.5mm, an output power of 1.1mW and a speed of 30,000 rpm (revolution per minute). For the last 10 years, it has been emphasized that work is accelerated especially in terms of micro power generation. Many studies have used the coreless AFPM alternator structure [7-9]. This construction has advantages in terms of simple structure and low cost [1,8,10-12]. In many studies about the magnetic analysis of the AFPM alternator design have obtained ANSYS's Maxwell program. In one study, multidisc constructions have been proposed to obtain maximum power at different wind speeds than wind turbines [9,13]. In addition, they suggested field weakening methods based on varying wind speeds in the AFPM alternators [12]. They have achieved the polarization by applying the dc winding instead of the magnet. There are also

studies in the literature on vertical axis small scale alternator models with magnetic levitation for small wind turbines [14]. When we review the literature, we can sort out the studies made in the following articles.

- New type prototype development
- Alternators that generating power at micro levels
- Alternators with DC winding excitation
- Field weakening methods
- Cogging torque reduced methods
- Alternators with multidisc structure

II. MATERIAL AND METHOD

With the increase of energy demand in recent years, there has been a tendency towards renewable energy sources. One of the renewable energy sources is wind energy. One of the most important parts of turbines are alternators that designed to obtain electricity from wind energy.

For the last 20 years, especially with the discovery of the neodymium magnets, study on permanent magnet alternators has increased significantly. The most important of these studies is the axial flux permanent magnet (AFPM) alternators.

Variable wind speed has triggered studies on different methods such as field weakening, serial-parallel connection configurations, different prototype alternators. In this study, one of these methods that multidisc and layer winding toroidal axial flux permanent magnet open slotless (MLTAFPMOS) synchronous alternators.

In this study, a 3d solid model of MLTAFPMOS synchronous alternator was constituted. Then, the magnetic analysis was performed and the work was completed. In this study, MLTAFPMOS synchronous alternator is a good candidate to obtain maximum power from variable wind speeds.

2.1. 3D solid modeling of the design

The designed MLTAFPMOS synchronous alternator consists of five stators, four bi-directional rotors and two unidirectional rotors. Thus, it is possible to take five times more power than a stator-two rotor structure. In besides, depending on the wind power, MLTAFPMOS synchronous alternator step into five stages and produce maximum power at every stage. The 3D solid model of the design is given in figure 1. MLTAFPMOS synchronous alternator consisting of 5 stators is designed as open slotted and toroidal winding layer winding structure.

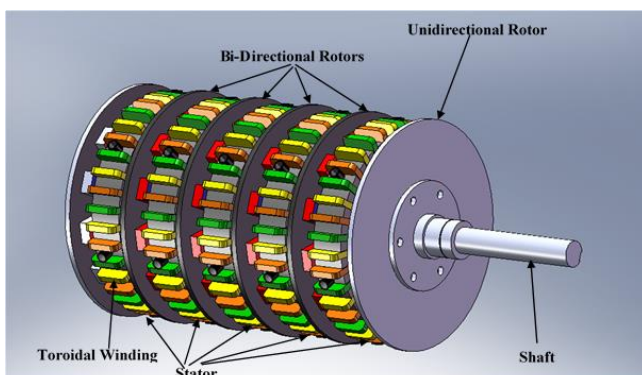


Fig.1. 3D model of MLTAFPMOS synchronous alternator

The open slotted structure used in the design reduces the production costs. However, it increases the cogging torque at high levels. The cogging torque is that are distortions in the moment due to the interaction between the magnets and the slot edges. Therefore, the cogging torque is an undesirable condition. When the literature is examined, it is seen that studies related to techniques for reducing cogging torque. The layer winding structure reduces the cogging torque while increasing the air gap. In addition to this, increasing the air gap reduces the alternator performance. In order to prevent this, a layer winding structure was applied to the increased air gap. This winding structure is given in figure 2. In Figure 2; there is two slots of the toroidal core and the toroidal winding structure is shown for a slot of the core. Outer slot winding is shown the winding in the air gap. The height of the outer slot winding is determined by the magnetic analysis with Maxwell program. In these analyzes, the average air gap magnetic flux value should be at least 0.5 Tesla. As another criterion, the air gap should be increased till close to the minimum cogging torque.

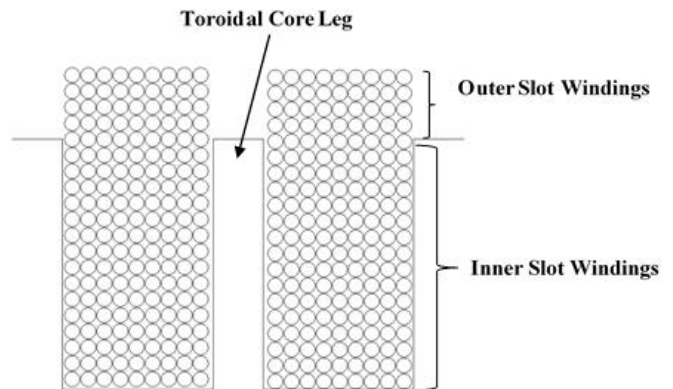


Figure 2. Slot winding structure of the MLTAFPMOS synchronous alternator

2.2. General equation of the wind turbine

Wind turbines starts with at a power of 1 kW and go up to 6 MW. The tower height and rotor diameter increment with the increase of power in the wind turbine. In particular, the increment in rotor diameter is necessary to achieve the intended power. Wind turbines are generally divided into two parts. The first is the horizontal axis turbines and the second is the vertical axis turbines.

In figure 3; wind turbines are given for horizontal and vertical axis. A basic wind turbine consists of tower, blades, anemometer, alternator, gear box (to speed up), pitch, yaw and braking systems. The wing angles are adjusted to better utilize the wind speed with the wing rotation mechanism (pitch control). Also, with tower rotation mechanism (yaw control), it is possible to catch maximum wind power by turning towards the tower wind direction in the direction of information obtained from anemometer. On the vertical axis turbines, there are no wing angles and tower rotation mechanisms.

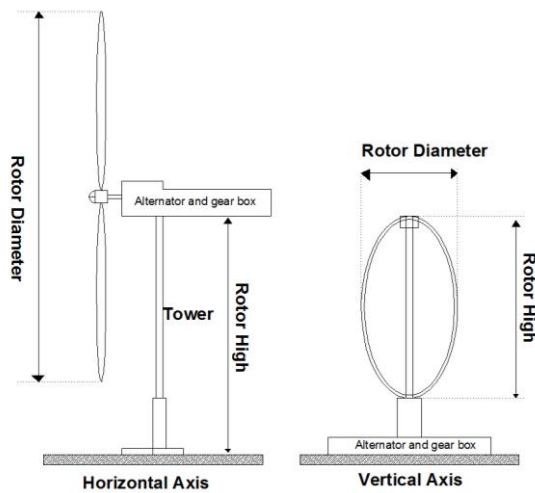


Figure 3. Horizontal and vertical axis wind turbine

The rotor diameter of the wind turbine, the density of the air, the wind speed and the rotor radius affect the power generated by the wind. The maximum power that can be achieved is given in formula (1).

$$P_m = \frac{1}{2} \rho \pi R^2 C_p u^3 \quad (1)$$

- P_m – is the maximum power to be achieved
- ρ – is the density of the air (kg/cm³)
- R – is the radius of the Rotor (m)
- C_p – is the power factor
- u – is the wind speed (m/sn)

The power factor C_p is obtained from formulas 2 and 3. β indicates rotor blade angle. λ is a coefficient related to angular velocity w , wind velocity u , and rotor blade diameter R . Therefore, from the formula 1 and 2, because of the turbine swept area increases, the larger rotor diameter, the greater mechanical power to be applied to the alternator input. However, the gear box system used in the conventional system is not available due to the direct connection to the system in the MLTAFPMOS synchronous alternator which is designed for the operation. Hence, the overall turbine efficiency is increased in this directly driven design.

$$\lambda_i = \left[\frac{1}{(\lambda + 0.08\beta)} - \frac{0.035}{(\beta^3 + 1)} \right]^{-1} \quad (2)$$

$$C_p(\beta, \lambda_i) = 0.4654 \left[\frac{116}{\lambda_i} - 0.4\beta - 5 \right] e^{-\frac{20.24}{\lambda_i}} \quad (3)$$

2.3. General equations of the design

The mechanical parameters of the designed MLTAFPMOS synchronous alternator are given in Table I.

TABLE I
GEOMETRIC DIMENSIONS OF THE MLTAFPMOS SYNCHRONOUS ALTERNATOR

Name of the Parameter	Value
Outer diameter of the stator	210 mm
Inner diameter of the stator	130 mm
Core height of the Stator	40 mm
Slot number of the Stator	42
Number of the Stator	5
Pole number of the Rotor	14
Magnet sizes of the Rotor	40x20x10 (mm)
Number of the Rotor	6

When Table I is examined, the design has six rotors and five stator. Two of the rotors are outer rotor and the other three are double sided. In the design, the input torque of the synchronous alternator of the MLTAFPMOS is calculated as in Equation 4 by dividing the input power obtained by multiplying the efficiency of formula 1 by the angular speed.

$$T = \frac{P_m \eta}{w} \quad (4)$$

The electromagnetic torque which should occur in the MLTAFPMOS synchronous alternator is obtained from formula 5.

$$T_e = \frac{1}{4} \alpha_i m_1 I_a N_1 k_{w1} B_m (D_{out}^2 - D_{in}^2) \quad (5)$$

- T_e – is the electromagnetic torque (Nm)
- α_i – is the ratio of the distance between the poles to the pole width (mm)
- m_1 – is the number of phase
- I_a – is the current of the winding
- N_1 – are the number of the phase turns
- K_{w1} – is the coefficient of the winding
- D_{out} – is the Outer diameter of the stator
- D_{in} – is the Inner diameter of the stator

2.4. Magnetic analyzes

The magnetic analysis of the MLTAFPMOS synchronous alternator was carried out with the Maxwell program of ANSYS's. The first step of the design is to create the 3D solid model to be analyzed in Maxwell. For each calculation, Maxwell divides the full model into triangular prisms and processes them based on the finite element method. So the bigger the model, the longer it takes to process. For this purpose, the points that are repeated in the program period are cut off as master and slave. Therefore, the section is taken as the slice of the model. The values obtained are multiplied by the number of cross sections taken and the actual values are reached. In the magnetic analysis of the MLTAFPMOS synchronous alternator, magnetic analysis was performed based on a stator and a rotor. Since five stator, six rotor, total 10 faces of the system is analyzed, the analysis of one face of the system is carried out, it is necessary to take 10 times the analysis results. Thus, calculations were taken 10 times faster. The full model is given in Figure 4.

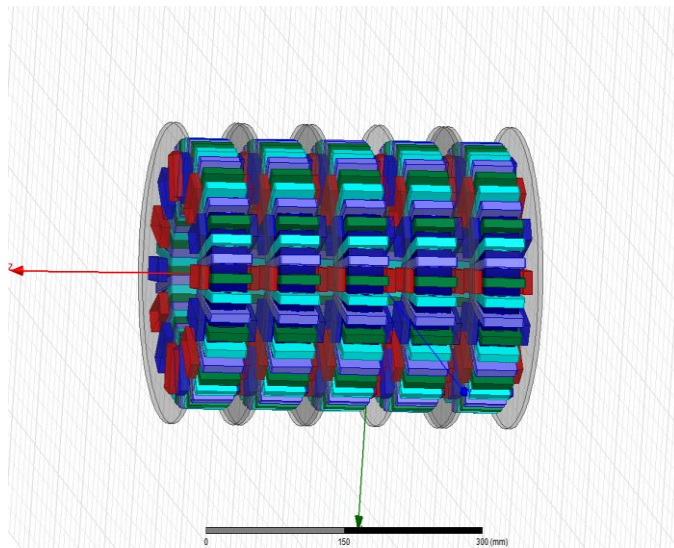


Fig.4. Full model of MLTAFPMOS synchronous alternator

In Figure 4, one out of five the full model given in Maxwell was taken and analyzes were carried out. The distribution of the magnetic flux density on the stator surface is given in Figure 5. In Figure 5, magnetic flux densities of about 1.6 tesla are observed in the core foot parts. Because of the saturating point not overcome, the received design values are suitable.

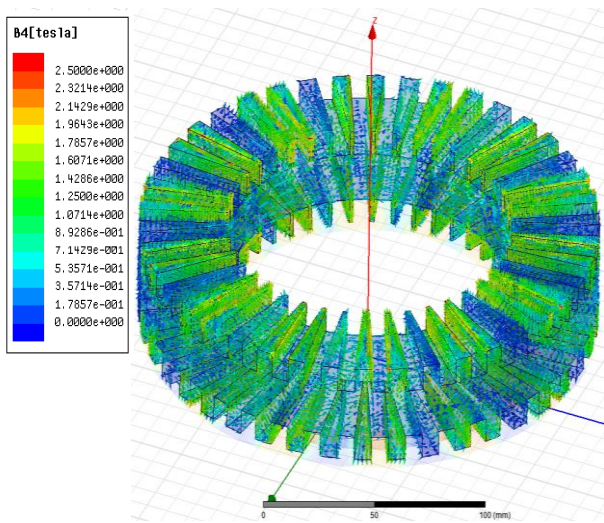


Fig.5. Magnetic flux distribution at the stator surface

Figure 6 shows the change in magnetic flux along a contour in the air gap. As shown in Figure 6, the effect of open slots is to pull down the maximum points of the curve. The magnitude of the indentations in the curves in the middle gives us an idea about the cogging torque. The greater the change, the higher the cogging torque values. In Figure 7, the magnetic flux is varied along the contour of the air gap for slot depths between 10mm and 15mm. It appears that the interaction is not too great along the 5mm difference. The reason for this is that the distance between the core and the magnet is too large because of the layer winding structure.

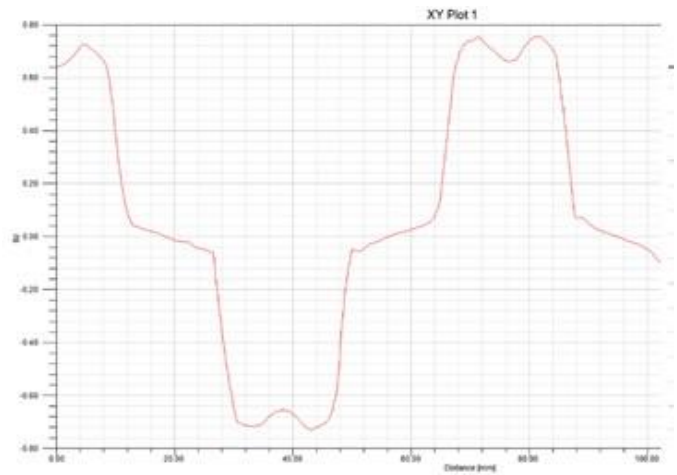


Fig.6. Magnetic flux change along a contour in the air gap

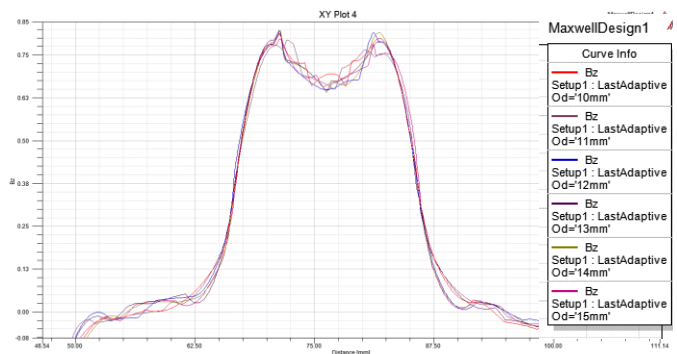


Fig.7. Magnetic flux change for slot depths values between 10mm-15mm

Table II shows the values of the slot depth from 10 mm to 15 mm at 1 mm intervals, the average value of the magnetic flux density generated in the core volume and the average magnetic flux density in the surface taken in the air gap.

TABLE II.
AVERAGE VALUE OF MAGNETIC FLUX DENSITY DUE TO SLOT DEPTH

Slot depth "Sd" (mm)	B average Core Volume (Tesla)	B average In Air Gap (Tesla)
10	0.756420485313839	0.636215991696493
11	0.80875438869431	0.691729613591648
12	0.865781444548061	0.771454864412778
13	0.923232529198211	0.861203957792007
14	0.976091446257511	0.956279998026163
15	1.02224023011257	1.07317382960829

When the magnetic flux densities for air space and core volume are examined, it is seen that they are close to each other. For this reason, the mean magnetic flux density values in the core volume can be taken instead of the air gap in the analyzes. It is also seen that the average air gap magnetic flux density value increases with the slot depth. Therefore, the appropriate value of the slot depth is determined by considering the mechanical properties, winding properties and cogging torque. In Figure 8, while the slot depth is 10mm, the generated moment value is taken. The absence of fluctuation along the figure indicates that the cogging torque is low. This

is caused by the layered winding structure. Hence, it is shown in the obtained analysis results that the alternator can operate with low cogging torque without being affected by slot depth.

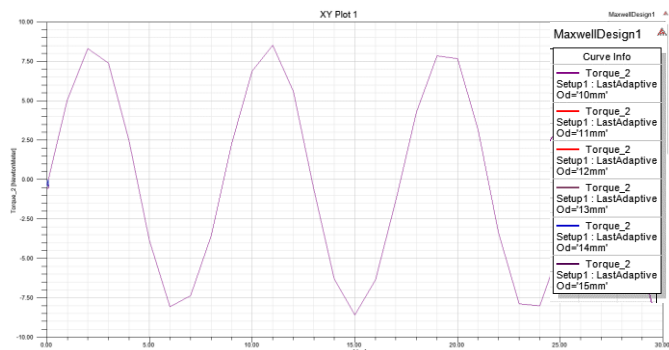


Fig.8. The moment curve of the MLTAFPMOS synchronous alternator

III. DISCUSSION AND CONCLUSION

In this study, magnetic analysis of MLTAFPMOS synchronous alternator that is a new design was analyzed. In AFPM open-slot alternators, the cogging torque is a major problem. The suggested new design is also supported by analyzes that reduce the cogging torque value to a minimum value. Increasing the diameter of the AFPM alternator for large power, however, increases production costs due to large axial forces on the shaft. There is also no continuous constant input moment in the wind turbines. Multidisc structure is presented to increase the power with the suggested system. With the multidisc structure, the power transmitted by the wind shaft each disk stator is entered to provide maximum efficiency in operation of the system. In the work done, instead of all the multidisc structure Maxwell's 3D magnetic analysis, by performing magnetic analyzes of one out of five, time savings have been achieved. A curve near the sinus value is also achieved in the obtained moment curve. It is also seen that the cogging torque is very low in this curve. The change in slot depth affects the in an open slotted AFPM alternator. With the multilayer winding structure given in the design, the cogging torque is reduced due to the increased air gap and the effect of decreasing power with the increase of the air gap is reduced to the minimum value thanks to the layered winding structure.

The proposed MLTAFPMOS synchronous alternator is easy to use and is suitable for use in wind turbines with minimum cogging torque. The multidisc structure also improves the efficiency and reduces the axial forces that force the shaft. After this work, research and development studies can be done for the use of AFPM alternators of different structures in wind turbines in multiple structures. Besides, with the multidisc structure of the present design, the potentials in different applications can be explored. In addition, the results of the analysis can be compared with the experimental data obtained by making a prototype study of the present design.

REFERENCES

- [1]. Akuner, C. & Huner, E. *The Air Gap and Angle Optimization in the Axial Flux Permanent Magnet Motor*, Electronics and Electrical Engineering, 2011, 110(4).
- [2]. Caricchi, F. Crescimbeni, F. Honorati, O. *Performance of Coreless-Winding Axial-Flux Permanent Magnet Generator with Power Output at 400 Hz, 300 r/m*, IEEE Transactions on Industry Applications, Vol.34, No.2, 1999, pp.1263–69.
- [3]. Muljadi Eduard, C.P. Butterfield, Yih huie Wan, *Axial-flux modular permanent-magnet generator with a toroidal winding for wind-turbine applications*, IEEE Transactions on Industry Applications Vol.35, No.4, 1999, pp. 831–36.
- [4]. Chalmers, B. J., W. Wu, E. Spooner, *An axial-flux permanent-magnet generator for a gearless wind energy system*, IEEE Transactions on Energy Conversion, Vol.14, No.2, 1999, pp.251–56.
- [5]. Wang Rong Jie, Maarten J. Kamper, Kobus Van Der Westhuizen, Jacek F. Gieras, *Optimal design of a coreless stator axial flux permanent-magnet generator*, IEEE Transactions on Magnetics Vol.41, No.11, 2005, pp. 55–64.
- [6]. Holmes Andrew S., Guodong Hong, Keith R. Pullen, *Axial-Flux Permanent Magnet Machines for Micropower Generation*, Journal of Microelectromechanical Systems, Vol.14, No.1, 2005, pp. 54–62.
- [7]. Chan, T. F., L. Lai, *An axial-flux permanent-magnet synchronous generator for a direct-coupled wind-turbine system*, IEEE Transactions on Energy Conversion Vol.22, No.1, 2007, pp.86–94.
- [8]. Hosseini Seyed Mohsen, Mojtaba Agha-mirsalim, Mehran Mirzaei *Permanent-Magnet Generator*, Vol.44, No.1, 2008, pp.75–80.
- [9]. Minaz Mehmet Recep, Mehmet Çelebi, *Design and analysis of a new axial flux coreless {PMSG} with three rotors and double stators*, Results in Physics (7), pp.183–88.
- [10]. Huner, Engin. Caner, Akuner. *Axial-flux synchronous machines compared with different stator structures for use in working*, Przegląd Elektrotechniczny Vol.88, No.11, 2012, pp. 174–177.
- [11]. Hüner, Engin. *Küçük Güçlü Rüzgar Türbinleri İçin 3D Sey Programı ile Ipms Alternatörün Elektromanyetik Tasarımı Ve Analizi*, Kırklareli University Journal of Engineering and Science, Vol.2, No.1, 2016, pp.60–73.
- [12]. Naeini Vahid, Mohammad Ardebili, *New axial flux PM less synchronous machine with concentrated DC field on stator*, International Journal of Electrical Power and Energy Systems, (67), 2015, pp. 651–58.
- [13]. Kalender, Osman et al., *A new axial flux permanent magnet synchronous alternator autonomously adapted to wind speeds*, Measurement: Journal of the International Measurement Confederation (69), 2015, pp. 87–94.
- [14]. Ghulam, Ahma. Uzma, Amin. *Design, construction and study of small scale vertical axis wind turbine based on a magnetically levitated axial flux permanent magnet generator*, (101), pp. 286–92.

BIOGRAPHIES



ENGİN HUNER He received Bachelor, Master and PhD degree in Electrical Education of Abant İzzet Baysal University, in Electrical Engineering of Gebze High Technology Institute and in Electrical Education of Marmara University. He has been assistant professor in the energy system engineering of Kırklareli University. He has worked mainly electrical machines and renewable energy.



M. CANER AKUNER He received Bachelor, Master and PhD degree in Electrical Education of Marmara University. He has been associate professor in the mechatronics engineering of Marmara University. He has worked mainly electrical machines and electromagnetics systems.

Investigation of Power Flow Effect of Serial and Parallel FACTS Devices


H.Bakir, A.Ozturk, and S.Tosun

Abstract— It is difficult to increase the capacity of the transmission system by establishing new lines or switching to a new voltage level to meet the rapidly rising electricity demand. Thus, there is an increased need for power flow controllers that can increase the capacity of the existing transmission line and control power flows in predetermined transmission corridors. For this reason, in recent years a new class of controllers has emerged called Flexible AC Transmission System (FACTS). It is very important to investigate the advantages of FACTS devices and to model these devices so that power systems can be operated in steady state. In this study, a comprehensive modeling of the most popular FACTS devices for power flow operation was performed. Power flow studies were first performed using the Newton Raphson method for an IEEE 5-bus power system without any FACTS devices. Then, different FACTS controllers were added to the system to perform power flow studies. As a result of the power flow studies performed, it was observed that the FACTS controllers increased the capacity of the existing transmission line and contributed to the voltage stability.

Index Terms— FACTS devices, newton-raphson, power flow, voltage stability.

I. INTRODUCTION

THE ENERGY industry is undergoing a profound transformation around the world. Decreases in natural resources and increasing demand for electricity are some of the reasons for this change. Many studies have been done to maximize the capacity of existing transmission systems with high reliability and stability. The work carried out has pointed to the need for a power electronic based controller because of the slow response times of the controllers based on electromechanical technology and high maintenance costs [1]. Until recently, active and reactive power control in Alternating Current (AC) transmission networks was done by carefully adjusting the transmission line impedances to adjusting the

H. BAKIR, is with Department of Electrical and Electronics Engineering University of Düzce University, Düzce, Turkey, (e-mail: hsynbakr@gmail.com) 

A. OZTURK, is with Department of Electrical and Electronics Engineering University of Düzce University, Düzce, Turkey, (e-mail: aliozturk@duzce.edu.tr).

S. TOSUN, is with Department of Electrical and Electronics Engineering University of Düzce University, Düzce, Turkey, (e-mail: salihtosun@duzce.edu.tr).

Manuscript received September 13, 2017; accepted January 08, 2018.
DOI: [10.17694/bajece.410204](https://doi.org/10.17694/bajece.410204)

generator excitation control and transformer step changes and terminal voltage.

FACTS technology has a critical role in transmission line planning. Because it creates new opportunities to control the power and increase the available capacity [2, 3].

Due to the increase in population and economy, there is a need to increase the flexibility, reliability and capacity of existing transmission systems. Due to changing market conditions, electrical utilities are looking for various ways to operate existing transmission lines at maximum limits. To achieve these goals, FACTS devices are used that can control the power flow and increase the transmission capacity [4]. FACTS devices commonly used in power systems are Static Var Compensator (SVC), Static Synchronous Compensator (STATCOM), Thyristor Controlled Series Compensator (TCSC), Static Synchronous Series Compensator (SSSC) and Unified Power Flow Controller (UPFC) [6].

II. POWER FLOW ANALYSIS

It is necessary to plan the operation of the power systems under the existing conditions and to carry out the load flow for the future situation. With load flow studies, voltage magnitudes and angles at each bar of the steady-state system can be obtained. Active and reactive power capacities are obtained in each line when the bus voltages and angles are calculated. Also losses in the lines can be calculated depending on the difference in the sender and receiver ends. The most preferred power flow method is the Newton-Raphson method because of its reliability in terms of convergence [7, 8].

A. Newton-Raphson Method

The Newton-Raphson method is one of the most common power flow solution methods that operate iteratively. This method is a classic method based on the Taylor series expansion and approaching well in a short time [5].

In Eq. (1) bus variables; n total number of bara i and j bara numbers [2].

$$I_i = \sum_{j=1}^n Y_{ij} V_j \quad (1)$$

In large scale power flow studies, the Newton Raphson power flow is the most successful because of its strong convergence

feature. The Newton-Raphson power flow algorithm is expressed by Eq. (2) [10, 11].

$$\begin{bmatrix} \Delta P \\ \Delta Q \end{bmatrix} = - \begin{bmatrix} \Delta P / \Delta \theta & \Delta P / (\Delta V / V) \\ \Delta Q / \Delta \theta & \Delta Q / (\Delta V / V) \end{bmatrix} \begin{bmatrix} \Delta \theta \\ (\Delta V / V) \end{bmatrix} \quad (2)$$

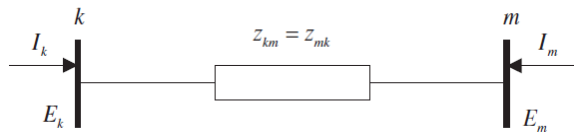


Fig. 1. Equivalent impedance

For the system in Fig. 1, the Jacobian matrix elements are constructed according to the following equations [8].

For $k \neq m$;

$$\frac{\partial P_{k,1}}{\partial Q_{m,1}} = V_k V_m [G_{km} \sin(\theta_k - \theta_m) - B_{km} \cos(\theta_k - \theta_m)] \quad (3)$$

$$\frac{\partial P_{k,1}}{\partial V_{m,1}} = V_k V_m [G_{km} \cos(\theta_k - \theta_m) + B_{km} \sin(\theta_m - \theta_k)] \quad (4)$$

$$\frac{\partial Q_{k,1}}{\partial \theta_{m,1}} = - \frac{\partial P_{k,1}}{\partial V_{m,1}} \quad (5)$$

$$\frac{\partial Q_{k,1}}{\partial V_{m,1}} = \frac{\partial P_{k,1}}{\partial \theta_{m,1}} \quad (6)$$

For $k=m$;

$$\frac{\partial P_{k,1}}{\partial \theta_{k,1}} = - Q_k^{cal} - V_k^2 B_{kk} \quad (7)$$

$$\frac{\partial Q_{k,1}}{\partial V_{k,1}} = P_k^{cal} + V_k^2 G_{kk} \quad (8)$$

$$\frac{\partial P_{k,1}}{\partial \theta_{k,1}} = - Q_k^{cal} - V_k^2 B_{kk} \quad (9)$$

$$\frac{\partial Q_{k,1}}{\partial V_{m,1}} = Q_k^{cal} - V_k^2 B_{kk} \quad (10)$$

B. Test System Data

The IEEE-5 bus power system constructed using the Power System Analysis Toolbox (PSAT) program was shown in Fig 2. The base values of the system were set at 100 MVA and 100 KV.

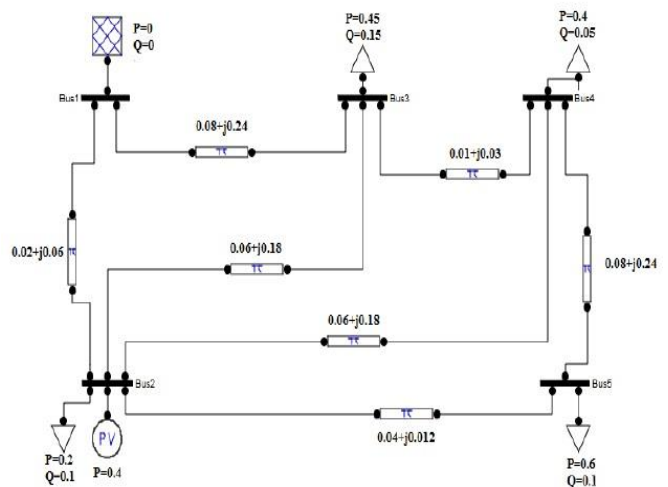


Fig. 2. IEEE-5 bus power system generated by PSAT

The generator and load data of the power system were shown in Table 1. The voltage and angle values obtained from the power flow for the IEEE 5-bus power system without FACTS were shown in Table 2.

TABLE I
GENERATOR AND LOAD DATA

Bus Type	Bus No	Voltage (p.u)	Active Power (p.u)	Reactive Power (p.u)
Slack	1	1.06	-	-
P-V	2	1.00	0.4	-
P-Q	3	-	0.45	0.15
P-Q	4	-	0.4	0.05
P-Q	5	-	0.6	0.1

TABLE II
VOLTAGE AND ANGLE VALUES WITHOUT FACTS

Parameters	Bus 1	Bus 2	Bus 3	Bus 4	Bus 5
VM (p.u.)	1.06	1	0.987	0.984	0.972
VA (degree)	0.00	-2.06	-4.640	-4.96	-5.770

III. POWER FLOW MODEL OF FACTS DEVICES

A. Static Var Compensator (SVC) Power Flow Model

Two alternative power flow models are commonly used to assess the effect of the SVC controller on power system applications. These are the variable shunt susceptance model and the trigger angle model.

Variable shunt susceptance SVC model was shown in Fig. 3. The equivalent circuit shown in Fig. 3 is used to derive nonlinear power equations. In the equivalent circuit shown in Fig. 3, the SVC current equation was shown in Eq. (11). The reactive power equation of the SVC was shown in Eq. (12) [12].

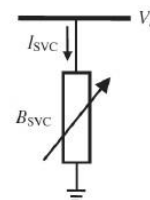


Fig. 3. Variable shunt susceptance SVC model

$$I_{SVC} = j B_{SVC} V_k \quad (11)$$

$$Q_{SVC} = -V_k^2 B_{SVC} \quad (12)$$

At the end of each iteration, the variable shunt susceptance is updated according to Eq. (13) [8].

$$B_{SVC}^i = B_{SVC}^{(i-1)} + \left\{ \frac{\Delta B_{SVC}}{B_{SVC}} \right\} B_{SVC}^{(i-1)} \quad (13)$$

Another SVC model is the trigger angle model. An alternative SVC model, which circumvents the additional iterative process, consists in handling the thyristor controlled reactor trigger angle α as a state variable in the power flow formulation. The SVC susceptance is obtained by Eq. (14) [8].

$$Q_k = \frac{-V_k^2}{X_C X_L} \left\{ X_L - \frac{X_C}{\pi} [2(\pi - \alpha_{SVC}) + \sin(2\alpha_{SVC})] \right\} \quad (14)$$

Using the above equation, the linearized SVC equation is expressed by Eq. (15) [12].

$$\begin{bmatrix} \Delta P_k \\ \Delta Q_k \end{bmatrix} (i) = \begin{bmatrix} 0 & 0 \\ 0 & \frac{2V_k^2}{\pi X_L} [\cos(2\alpha_{SVC}) - 1] \end{bmatrix} (i) \begin{bmatrix} \Delta Q_k \\ \Delta \alpha_{SVC} \end{bmatrix} (i) \quad (15)$$

The trigger angle is updated according to equation (16) at the end of each iteration [12].

$$\alpha_{SVC}^{(i)} = \alpha_{SVC}^{(i-1)} + \Delta \alpha_{SVC}^{(i)} \quad (16)$$

B. Thyristor Controlled Series Compensator (TCSC) Power Flow Model

Two alternative power flow models have been introduced to assess the effect of the TCSC controller in power system applications. The simple TCSC model uses the concept of variable series reactance. In this model, the series reactance is automatically adjusted to provide active power flow within the specified limits. The advanced model uses a nonlinear reactance trigger angle graph. In this model, the TCSC trigger angle is selected as the state variable in the Newton Raphson power flow solution [13].

The TCSC power flow model presented in this section is based on the simple concept of variable series reactance. The value is automatically set to limit the power flow to a certain value. The amount of reactance is determined effectively using Newton's method. Thyristor controlled series compensator equivalent circuit was shown in Fig. 4 [8].

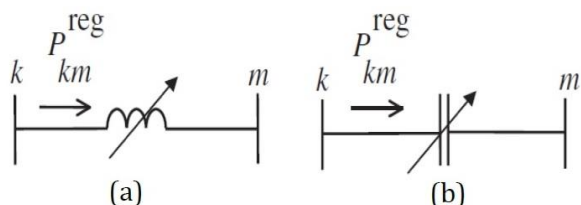


Fig. 4. Thyristor controlled series compensator equivalent circuit (a) inductive and (b) capacitive regions

The transfer matrix of the variable series compensator was shown in Eq. (17) [14].

$$\begin{bmatrix} I_k \\ I_m \end{bmatrix} = \begin{bmatrix} jB_{kk} & jB_{km} \\ jB_{mk} & jB_{mm} \end{bmatrix} \begin{bmatrix} V_k \\ V_m \end{bmatrix} \quad (17)$$

The equations for inductive operation were shown in Eq. (18) and (19). For capacitive operation, the signals are inverted [14].

$$B_{kk} = B_{mm} = -\frac{1}{X_{TCSC}} \quad (18)$$

$$B_{km} = B_{mk} = \frac{1}{X_{TCSC}} \quad (19)$$

The active and reactive power equations were shown in equations (20) and (21) [8].

$$P_k = V_k V_m B_{km} \sin(\theta_k - \theta_m) \quad (20)$$

$$Q_k = -V_k^2 B_{kk} - V_k V_m B_{km} \cos(\theta_k - \theta_m) \quad (21)$$

The state variable X_{TCSC} is updated at the end of each iterative step as in Eq. (22) [8].

$$X_{TCSC}^{(i)} = X_{TCSC}^{(i-1)} + \{ \Delta X_{TCSC} / X_{TCSC} \} (i) X_{TCSC}^{(i-1)} \quad (22)$$

The trigger angle model presented in this section uses the concept of equivalent series reactance to represent TCSC. After the reactance value is determined using the Newton method, the angle can be calculated. However, this calculation requires an iterative solution since the TCSC reactance value and the trigger angle α_{TCSC} are nonlinearly related [15].

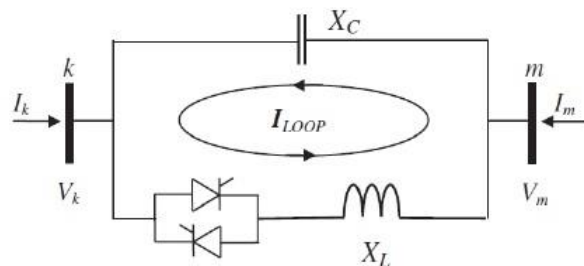


Fig. 5. TCSC Equivalent Circuit

The equivalent reactance of TCSC shown in Fig. 5 is calculated according to Eq. (23) [8].

$$X_{TCSC} = -X_C + C_1 \{ 2(\pi - \alpha) + \sin[2(\pi - \alpha)] - C_2 \cos^2(\pi - \alpha) \{ \omega \tan[\omega(\pi - \alpha)] - \tan(\pi - \alpha) \} \} \quad (23)$$

$$C_1 = \frac{X_C + X_{LC}}{\pi} \quad (24)$$

$$C_2 = \frac{4X_{LC}^2}{X_L \pi} \quad (25)$$

$$X_{LC} = \frac{X_C X_L}{X_C - X_L} \quad (26)$$

The active and reactive power equations of TCSC are as follows [14].

$$P_k = V_k V_m B_{km} \sin(\theta_k - \theta_m) \quad (28)$$

$$Q_k = -V_k^2 B_{kk} - V_k V_m B_{km} \cos(\theta_k - \theta_m) \quad (29)$$

$$B_{kk} = -B_{km} = B_{TCSC} \quad (30)$$

C. Static Synchronous Compensator (STATCOM) Power Flow Model

The static synchronous compensator (STATCOM) is represented by a synchronous voltage source with minimum and maximum voltage magnitude limits. The synchronous voltage source represents the fundamental fourier series component of the switched voltage waveform at the AC converter terminal of STATCOM [9]. The STATCOM equivalent circuit shown in Figure 6 is used to obtain the mathematical model of the controller to be included in power flow algorithms [16].

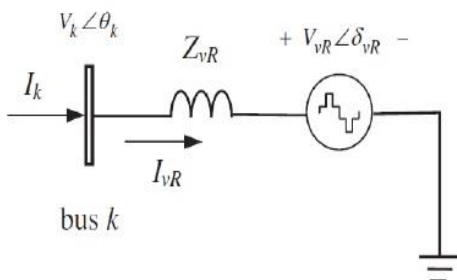


Fig. 6. STATCOM Equivalent Circuit

Based on the shunt connection shown in Figure 6, power flow equations for STATCOM can be written following.

$$E_{vR} = V_{vR} (\cos \delta_{vR} + j \sin \delta_{vR}) \quad (31)$$

$$S_{vR} = V_{vR} I_{vR}^* = V_{vR} Y_{vR}^* (V_{vR}^* - V_k^*) \quad (32)$$

The active and reactive power equations for the converter and k bus are obtained as follows.

$$P_{vR} = V_{vR}^2 G_{vR} + V_{vR} V_k [G_{vR} \cos(\delta_{vR} - \theta_k) + B_{vR} \sin(\delta_{vR} - \theta_k)] \quad (33)$$

$$Q_{vR} = -V_{vR}^2 B_{vR} + V_{vR} V_k [G_{vR} - B_{vR} \cos(\delta_{vR} - \theta_k)] \quad (34)$$

$$P_k = V_k^2 G_{vR} + V_k V_{vR} [G_{vR} \cos(\theta_k - \delta_{vR}) + B_{vR} \sin(\theta_k - \delta_{vR})] \quad (35)$$

$$Q_k = -V_k^2 B_{vR} + V_k V_{vR} [G_{vR} \sin(\theta_k - \delta_{vR}) - B_{vR} \cos(\theta_k - \delta_{vR})] \quad (36)$$

IV. SIMULATION RESULTS

A. Power Flow With SVC

SVC was added to the IEEE-5 bus power system to

examine the voltage control capability of the SVC controller. The power system with SVC controller was shown in Fig. 7. Before running the simulation, the amplitude value of the slack bus was set to 1.06 p.u and the amplitude of the PV bus was set to 1 p.u. SVC was placed in the Bus-3 to hold the bus voltage at 1 p.u. The inductive reactance value of the SVC was 0.288 p.u, and the capacitive reactance value was 1.07 p.u. The SVC trigger angle was initially set to 140 degrees. This value allows the SVC to operate in the capacitive region. The voltage magnitude and phase angle values obtained as a result of the power flow was shown in Table 3.

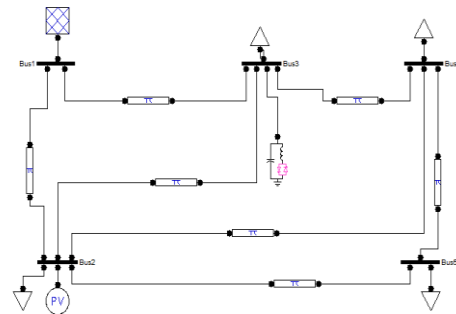


Fig. 7. IEEE-5 bus power system with SVC

TABLE III
VOLTAGE AND ANGLE VALUES OBTAINED FROM LOAD FLOW OF SYSTEM INCLUDING SVC

Parameters	Bus 1	Bus 2	Bus 3	Bus 4	Bus 5
VM (p.u.)	1.06	1	1	0.994	0.9752
VA (degree)	0.00	-2.053	-4.837	-5.107	-5.797

B. Power Flow With TCSC

As shown in Fig. 8, the IEEE-5 bus power system was modified to include the TCSC to compensate the transmission line between Bus 3 and Bus 4. The TCSC was added to the transmission line to control the active power flowing from Bus 3 to Bus 4. The initial value of the TCSC was set to be equal to % 50 of the inductive reactance value of the transmission line. The TCSC initial capacitive reactance value was 0.015 p.u and the triggering angle was 145 degrees.

As a result of the power flow, it was observed that the TCSC sets the active power value of the transmission line 3-4 to 21 MW. The voltage magnitude and phase angle values obtained from the power flow result for the system in Fig. 8 were shown in Table 4.

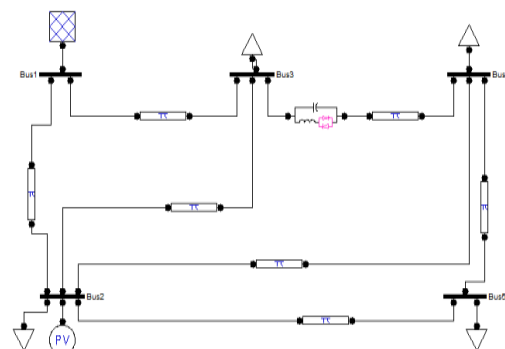


Fig. 8. IEEE-5 bus power system with TCSC

TABLE IV
VOLTAGE AND ANGLE VALUES OBTAINED FROM LOAD FLOW OF
SYSTEM INCLUDING TCSC

Parameters	Bus 1	Bus 2	Bus 3	Bus 4	Bus 5
VM (p.u.)	1.06	1	0.987	0.988	0.984
VA (degree)	0	-2.04	-4.72	-4.46	-4.81

C. Power Flow With STATCOM

STATCOM was added to Bus 3 of the IEEE-5 bus power system in order to maintain the node voltage at 1 p.u. The initial source voltage of STATCOM was 1 p.u, the phase angle was 0 degree and the transformer reactivity was 10 p.u.

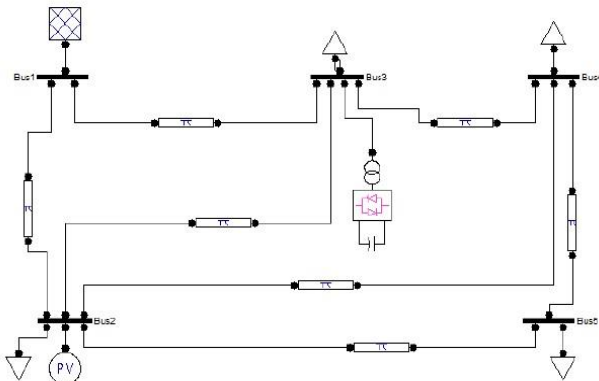


Fig. 9. IEEE-5 bus power system with STATCOM

It was observed from the power flow results that STATCOM produced 20.5 MVAR of power to hold the voltage at 1 p.u in Bus 3. The results in Table 5 showed that the use of STATCOM could improve the voltage profile.

TABLE V
VOLTAGE AND ANGLE VALUES OBTAINED FROM LOAD FLOW OF
SYSTEM INCLUDING STATCOM

Parameters	Bus 1	Bus 2	Bus 3	Bus 4	Bus 5
VM (p.u.)	1.06	1	1	0.994	0.974
VA (degree)	0	-2.05	-4.82	-5.11	-5.81

V. CONCLUSION

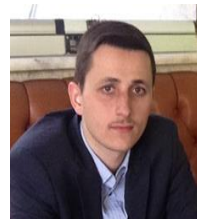
In this study, the power flow of the IEEE-5 bus power system using the Newton-Raphson method was performed for situations with and without FACTS devices. Serial and parallel FACTS devices were added to the power system and serial and parallel compensation was performed. STATCOM and SVC from the parallel FACTS controllers were added to the system. In addition, TCSC is added to the system from serial FACTS controllers.

From the simulation results it is observed that parallel FACTS devices have an important role in voltage control and serial FACTS devices have an important role in increasing transmission line capacity. In series compensation, the line impedance is changed, which means that the net impedance is reduced and thus the transmittable active power is increased. In shunt compensation, it has been observed that even reactive current is injected to adjust the voltage at the connection point.

REFERENCES

- [1] N.G. Hingorani, L. Gyugyi, and M. El-Hawary, *Understanding FACTS: Concepts And Technology of Flexible AC Transmission Systems*, IEEE press, 2000.
- [2] N.G. Hingorani, "Flexible AC Transmission." IEEE Spectrum, Vol.30, No. 4, 1993, pp.40-45.
- [3] R.M. Mathur, R.K. Varma, *Thyristor-based FACTS Controllers For Electrical Transmission Systems*, John Wiley & Sons, 2002.
- [4] X.P. Zhang, C. Rehtanz and B. Pal. "Congestion Management and Loss Optimization with FACTS. flexible ac transmission systems: modelling and control", 2006, pp.239-258
- [5] V. Yamaçlı, K. Abacı, "Güç sistemlerinde aktif güç kaybının optimizasyonu", Elektrik – Elektronik – Bilgisayar ve Biyomedikal Mühendisliği Sempozyumu, Kasım 2014.
- [6] B. Gao, G.K. Morison and P. Kundur, "Towards the development of a systematic approach for voltage stability assessment of large-scale power systems", IEEE transactions on power systems, Vol.11, No.3, 1996, pp.1314-1324.
- [7] C.R. Fuerte-Esquivel and E. Acha, "A Newton-type algorithm for the control of power flow in electrical power networks", IEEE Transactions on Power Systems, Vol.12, No.4, 1997, pp.1474-1480
- [8] E. Acha, C.R. Fuerte-Esquivel, H. Ambriz-Perez and C. Angeles-Camacho, *FACTS: Modelling and Simulation in Power Networks*, John Wiley & Sons, 2004.
- [9] Y.H. Song, A. Johns, *Flexible AC Transmission Systems (FACTS)*, IET, 1999.
- [10] F. Milano, "Continuous Newton's method for power flow analysis", IEEE Transactions on Power Systems, Vol.24, No.1, 2009, pp.50-57.
- [11] R. Bonert, "A laboratory for power systems control with static converters", IEEE transactions on power systems, Vol.13, No.1, 1998, pp.15-20.
- [12] H. Ambriz-Perez, E. Acha C. R. Fuerte-Esquivel, "Advanced SVC models for Newton-Raphson load flow and Newton optimal power flow studies", IEEE transactions on power systems, Vol.15, No.1, 2000, pp.129-136.
- [13] Fuerte-Esquivel, C. R. and Acha, E. "Newton-Raphson algorithm for the reliable solution of large power networks with embedded FACTS devices. IEEE Proceedings-Generation, Transmission and Distribution", Vol.143, No.5, 1996, pp.447-454.
- [14] A.K. Sahoo, S.S. Dash and T. Thyagaraja, "Power flow study including FACTS devices", Journal of applied sciences, Vol.10, 2010, pp. 1563-1571.
- [15] C.R. "Fuerte-Esquivel, E. Acha and H. Ambriz-Perez, A thyristor controlled series compensator model for the power flow solution of practical power networks", IEEE transactions on power systems, Vol.15, No.1, 2000, pp.58-64.
- [16] L. Gyugyi, "Dynamic compensation of AC transmission lines by solid-state synchronous voltage sources", IEEE Transactions on Power Delivery, Vol.9, No.2, 1994, pp. 904-911.

BIOGRAPHIES



Hüseyin BAKIR was born in Sakarya, Turkey in 1991. He received the Bachelor of Science and Master on Science degrees on Electrical and Electronics Engineering in 2015 and 2017 respectively, both from the Düzce University. Presently he is a Ph.D. student at Düzce University, Department of Electrical and Electronics Engineering. His research interests include power systems and renewable energy systems.



Ali ÖZTÜRK received his B.S. in Electrical Engineering Yıldız Technical University, Turkey, in 1996, his M.Sc. in Electrical Engineering from Sakarya University, Sakarya, Turkey, in 2001 and his Ph.D. in 2007 from the same university. His research interests include voltage stability and optimization in electric power systems.



Salih TOSUN received his B.S. in Electrical Education Marmara University, Turkey, in 1986, his M.Sc. in Electrical Engineering from Marmara University, Istanbul, Turkey, in 1991. His research interests include voltage stability and optimization in electric power systems.

A New Speed Control Technique for a Separately Excited Direct Current Motor by PID Controller

O.Akar, U.K.Terzi and O.Ozgonenel

Abstract—In this study, by deriving electro-mechanic mathematical model of separately excited direct current motor (SEDCM) via equivalent circuit, a new control block diagram has been formed. By using this block diagram, state space model of SEDCM has been created and block diagram of motor has been formed in Matlab Simulink environment. Steady state and transient values of armature current, emf, produced torque, speed and position angle have been obtained using this new model. By adding PID controller to block diagram, SEDCM has been remodeled. Finally, results of steady state and transient analysis of SEDCM have examined through speed control of the proposed model.

It is reported that the suggested modeling technique is able to analyze the speed control of the SEDCM.

Index Terms—PID controller, separately excited direct current motor (SEDCM), speed control, equivalent circuit.

I. INTRODUCTION

THIS DOCUMENT is in parallel to rapid development of technology, from toy production to industry even from robots to space devices, many products contain motors powered by electrical energy. One of them is Direct Current motor. In comparison to alternating current motor, speed control of direct current motor is easier [1,2]. Therefore, as it used to be, today they still take their place in industrial applications. Day by day, by the development of technology, their use in new products increases. High power DC motors are generally used in paper factories, weaving machines, ship propellers, printing machines and elevators and, low power DC motors are frequently used with motor controllers for the parts which especially require speed and position control in robotics, 3D printers, copying machines, moving parts of computers, radar tracking systems [3,4].

O. AKAR, is with Department of Mechatronic Program, Gedik Vocational High School Istanbul Gedik University, 34700, Istanbul, Turkey, (e-mail: onur.akar@gedik.edu.tr)

U.K.TERZI, is with Department of Electrical-Electronics Engineering, Marmara University, Istanbul, Turkey, (e-mail: terzi@marmara.edu.tr)

O. OZGONENEL, is with Department of Electrical-Electronics Engineering, Ondokuz Mayıs University, Samsun, Turkey, (e-mail: okanoz@omu.edu.tr)

Manuscript received September 13, 2017; accepted January 08, 2018.

DOI: [10.17694/bajece.410209](https://doi.org/10.17694/bajece.410209)

There are many types of DC motors which can be classified according to their winding and connection types and purpose of usage. The constant increase in the number of direct current motors and their dependence on the technology has made the development of the control of these motors important. In parallel to developing technology, the variety of DC motors and continuous increase of their usage area have made the development of the control of these motors important.

II. DIRECT CURRENT MOTORS AND PID CONTROLLER

The Electrical motors can be classified as alternating current motors and direct current motors. Direct current motors among themselves also can be classified in two groups according to their excitation type and connection type. According to excitation type, there are separately excited and self-excited direct current motors and, according to connection type there are shunt, serial and compound direct current motors. Except these, there are step and servo motors driven with DC [5].

A. Separately Excited DC Motors

Armature and excitation windings of SEDCM are independent from each other. They need to be excited by two different DC source. These are called separately excited DC motors [5]. As known, DC motors consist of two electrical parts which are armature and excitation circuit and one mechanical part which transmits torque. As known, DC motors consist of two electrical parts which are armature and excitation circuit and one mechanical part which transmits torque. While DC machine works as generator, torque is applied to DC machine, but while DC machine works as motor, torque is applied to load which is coupled to shaft. A dc machine which works as motor is represented with general equivalent electromechanic system given in Fig. 1 [3].

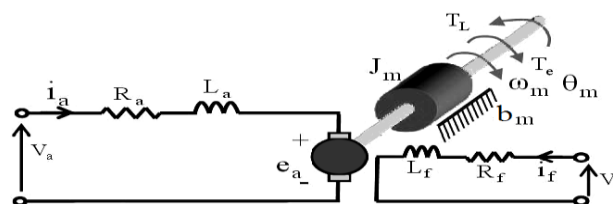


Fig.1. Equivalent electromechanic scheme of separately excited DC motors [3,6-8].

Where;

- R_a : Armature resistance;
- L_a : Armature inductance;
- i_a : Armature current;
- V_a : Input voltage;
- e_a : Back electromotive force (EMF);
- R_f : Field resistance;
- L_f : Field inductance;
- i_f : Field current;
- V_f : Field voltage;
- T_e : Motor torque;
- θ_m : Position angle;
- ω_m : An angular velocity of rotor;
- J_m : Rotational inertia of motor bearing;
- b_m : Friction constant;
- K : EMF-Torque constant.

These types of motor are not preferred in industry because they are separately excited. Even if they are used, excitation windings are connected in parallel with armature and it is used as shunt DC motor. Apart from this, they are used for experimental purposes in the organizations provided with technical training.

B. Proportional- integral and derivative (PID) controller

PID controller is built up by using three controllers as seen in Fig. 2. In system, by using proportional, integral and derivative controls, control signal is generated. The system works with K_P , K_I and K_D constants. A low pass filter is used to reduce noise of derivative control [8-10]

$$K_D S \approx \frac{K_D S}{1 + S\tau} \tag{1}$$

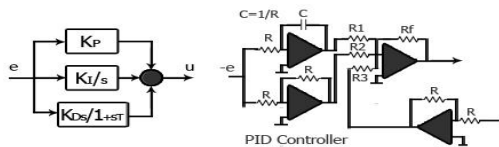


Fig.2. Block and circuit diagram of PID controller [6-11]

III. STATE SPACE MODEL

IDEs of armature circuit of SEDMC are given in Eq. 2 and Eq. 3. IDEs of excitation circuit of SEDMC are given in Eq. 4 and Eq. 5, and IDEs of mechanical system of SEDMC are given from Eq. 6 through Eq. 9.

$$V_a(t) = L_a \cdot \frac{di_a(t)}{dt} + R_a \cdot i_a(t) + e_a(t) \tag{2}$$

$$L_a \cdot \frac{di_a(t)}{dt} = V_a(t) - R_a \cdot i_a(t) - e_a(t) \tag{3}$$

$$V_f(t) = L_f \cdot \frac{di_f(t)}{dt} + R_f \cdot i_f(t) \tag{4}$$

$$L_f \cdot \frac{di_f(t)}{dt} = V_f(t) - R_f \cdot i_f(t) \tag{5}$$

$$\frac{d\theta_m(t)^2}{dt^2} = \frac{d\omega_m(t)}{dt} \tag{6}$$

$$\frac{d\theta_m(t)}{dt} = \omega_m(t) \tag{7}$$

$$T_e(t) = J_m \cdot \frac{d\omega_m(t)}{dt} + b_m \cdot \omega_m(t) + T_L(t) \tag{8}$$

$$J_m \cdot \frac{d\omega(t)}{dt} = T_e(t) - b_m \cdot \omega_m(t) - T_L(t) \tag{9}$$

The electromechanical interaction of the SEDCM is given in equations Eq.10- Eq.23 [6-8,10-18].

$$B = k_f \cdot i_f \tag{10}$$

$$k_m = 2 \cdot N \cdot l \cdot r \tag{11}$$

$$K = k_m \cdot k_f \tag{12}$$

$$T_e = N \cdot l \cdot r \cdot i_a \cdot B \tag{13}$$

$$T_e = k_m \cdot i_a \cdot k_f \cdot i_f \tag{14}$$

$$T_e = k_m \cdot k_f \cdot i_a \cdot i_f \tag{15}$$

$$T_e = K \cdot i_a \cdot i_f \tag{16}$$

$$e_a = 2 \cdot N \cdot l \cdot r \cdot \omega_m \cdot B \tag{17}$$

$$e_a = k_m \cdot \omega_m \cdot k_f \cdot i_f \tag{18}$$

$$e_a = k_m \cdot k_f \cdot \omega_m \cdot i_f \tag{19}$$

$$e_a = K \cdot \omega_m \cdot i_f \tag{20}$$

$$L_a \cdot \frac{di_a(t)}{dt} = V_a(t) - R_a \cdot i_a(t) - K \cdot \omega_m(t) \cdot i_f(t) \tag{21}$$

$$L_f \cdot \frac{di_f(t)}{dt} = V_f(t) - R_f \cdot i_f(t) \tag{22}$$

$$J_m \cdot \frac{d\omega_m(t)}{dt} = K \cdot i_a(t) \cdot i_f(t) - b_m \cdot \omega_m(t) - T_L(t) \tag{23}$$

Block diagram which is shown in Fig.3 is formed by using IDEs given in Eq. 21,22,23. [6-8,10-18].

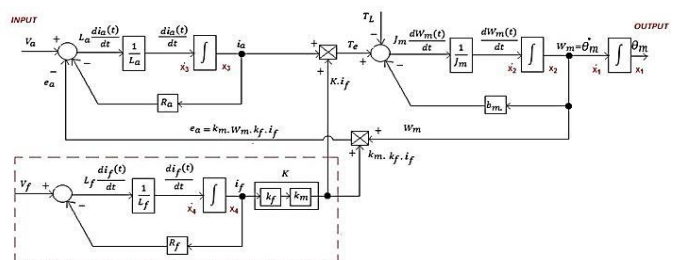


Fig.3. Block diagram of SEDCM [3,10]

On the basis of simulation block diagram shown in Fig. 3, state space equation formulated in Eq.24-30 of SEDCM is obtained by assigning $X_1, \dot{X}_1, X_2, \dot{X}_2$ variables.

$$\dot{X}_1 = X_2 \tag{24}$$

$$\dot{X}_2 = \frac{1}{J_m} \cdot [-b_m \cdot X_2 + k_f \cdot N \cdot l \cdot r \cdot X_3 \cdot X_4 + k_f \cdot N \cdot l \cdot r \cdot X_4 \cdot X_3 - T_L] \tag{25}$$

$$\dot{X}_3 = \frac{1}{L_a} \cdot [-R_a \cdot X_3 - k_f \cdot N \cdot l \cdot r \cdot X_2 \cdot X_4 - k_f \cdot N \cdot l \cdot r \cdot X_4 \cdot X_2 + V_a] \tag{26}$$

$$\dot{X}_4 = \frac{1}{L_f} \cdot [-R_f \cdot X_4 + V_f] \tag{27}$$

$$\begin{bmatrix} \dot{X}_1 \\ \dot{X}_2 \\ \dot{X}_3 \\ \dot{X}_4 \end{bmatrix} = \begin{bmatrix} 0 & 1 & 0 & 0 \\ 0 & -\frac{b_m}{J_m} & \frac{k_f \cdot N \cdot l \cdot r}{J_m} \cdot X_4 & \frac{k_f \cdot N \cdot l \cdot r}{J_m} \cdot X_3 \\ 0 & -\frac{k_f \cdot N \cdot l \cdot r}{L_a} \cdot X_4 & -\frac{R_a}{L_a} & -\frac{k_f \cdot N \cdot l \cdot r}{L_a} \cdot X_2 \\ 0 & 0 & 0 & -\frac{R_f}{L_f} \end{bmatrix} \cdot \begin{bmatrix} X_1 \\ X_2 \\ X_3 \\ X_4 \end{bmatrix} + \begin{bmatrix} 0 & 0 & 0 \\ -\frac{1}{J_m} & 0 & 0 \\ 0 & \frac{1}{L_a} & 0 \\ 0 & 0 & \frac{1}{L_f} \end{bmatrix} \cdot \begin{bmatrix} T_L \\ V_a \\ V_f \end{bmatrix} \tag{28}$$

$$[y] = [1 \ 0 \ 0 \ 0] \cdot \begin{bmatrix} X_1 \\ X_2 \\ X_3 \\ X_4 \end{bmatrix} \tag{29}$$

By using Eq. 24 through Eq. 29, Eq.30 is obtained [10,19].

$$y = X_1 \tag{30}$$

IV. MATLAB SIMULINK ENVIRONMENT AND SIMULATION OF CONTROL SYSTEM

A. Simulation model in Matlab Simulink Environment for SEDCM

Motor parameters of SEDCM are given in Table 1. By using these values, Matlab/Simulink model of system which is shown in Fig.4 is formed. Display modules are inserted to the certain points to monitor the results of steady state and transient analysis.

TABLE II MOTOR PARAMETERS OF SEDCM

DC Motor Parameters		
Parameter	Value	Unit
R_a	0.26	Ohm
R_f	260	Ohm
L_a	0.025	Henry
L_f	0.28	Henry
V_a	420	Volt
k_f	0.08135	V·s/rad
B_m	0.028	Nm·s/rad
J_m	0.5	kg·m ²
T_L	8	Nm

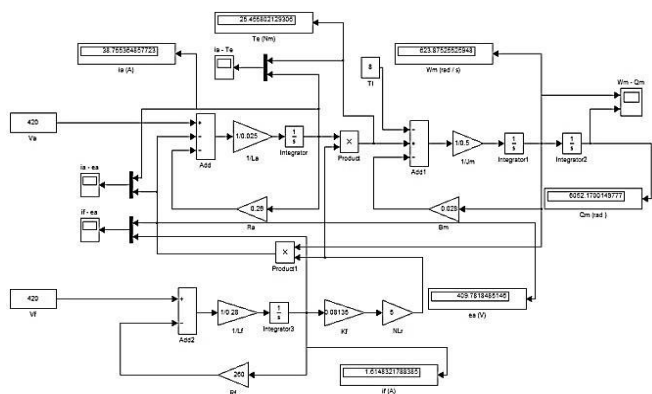


Fig.4. Matlab/Simulink simulation model of SEDCM

The graphs of some values such as armature current, emf, armature current, produced torque, excitation current and position angle vs time are given below before PID controller is added to system in Matlab/Simulink environment for SEDCM.

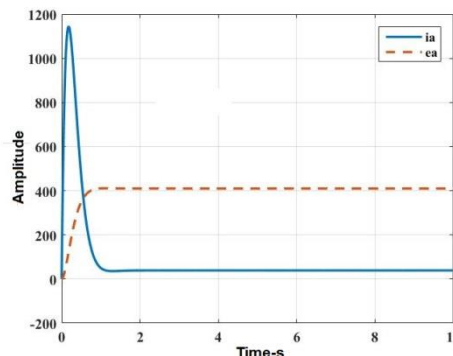


Fig.5. Graphs of armature current and emf vs time of SEDCM

When Fig. 5 is examined, it is figured out that armature current increases logarithmically approximately up to 1150 A in a few hundred milliseconds and after 1 second, it gets stable and takes value of 38.755 A. Emf reaches 409.781 V in a few hundred milliseconds and gets stable.

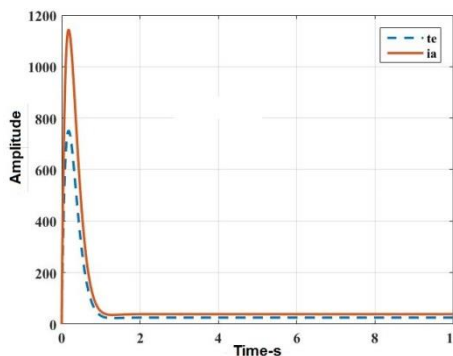


Fig.6. Graphs of armature current and produced torque vs time of SEDCM

When Fig. 6 is examined it is figured out that armature current increases up to 1150 A in a few hundred milliseconds and after 1 second, it gets stable and takes value of 38.755 A. Produced torque simultaneously with armature current increases up to 700Nm in a few hundred milliseconds and after 1 second, it gets stable and takes value of 24.455 Nm.

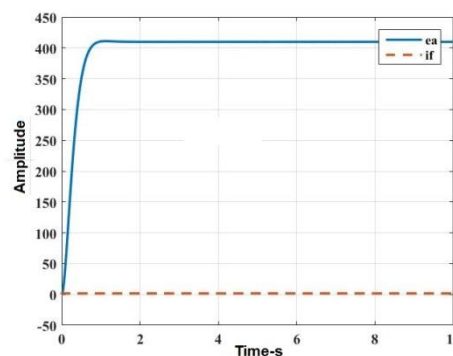


Fig.7. Graphs of excitation current and emf vs time of SEDCM

When Fig. 7 is examined, it is figured out that with excitation current of 1.614 A emf reaches 409.781 V in a few hundred milliseconds and then gets stable.

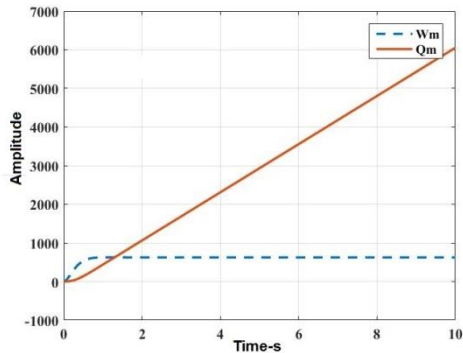


Fig.8. Graphs of speed and position angle vs time of SEDCM

When Fig. 8 is examined, it is figured out that speed of motor reaches approximately 600 rad/s in a few hundred milliseconds and after 1 second, it gets stable and takes value of 623.87 rad/s. Position angle increases logarithmically in a few hundred milliseconds and after that it keeps increasing linearly and get value of 6052.17 rad at 10th second.

The speed value of motor is measured as 623.87 rad/s which is equal to 5957.33 rpm and this value is used as a reference value for control models.

B. Simulation model in Matlab Simulink Environment with PID controller for SEDCM

The model of control system with PID controller in the Matlab/Simulink environment can be seen in Fig. 9. Since the speed of motor is normally 623.87 rad/s, reference value is fixed to this value. After that, by varying resistance and capacity values in related layers of control circuit control parameters K_P , K_I , K_D and K_{P1} , K_{I1} and K_{D1} are adjusted and it is ensured that the output speed is 653,87 rad/s.

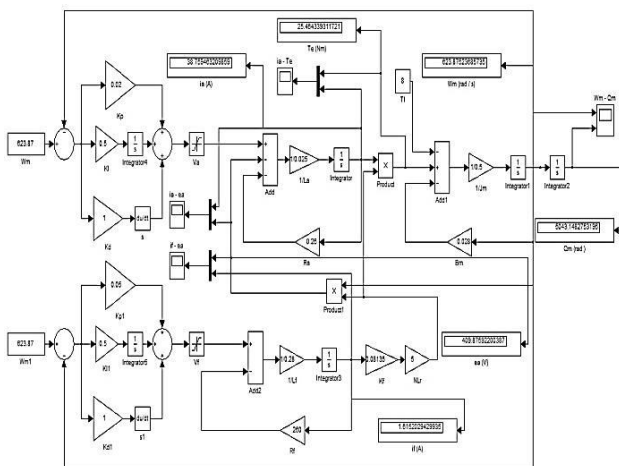


Fig.9. Matlab/Simulink simulation model with PID controller of SEDCM.

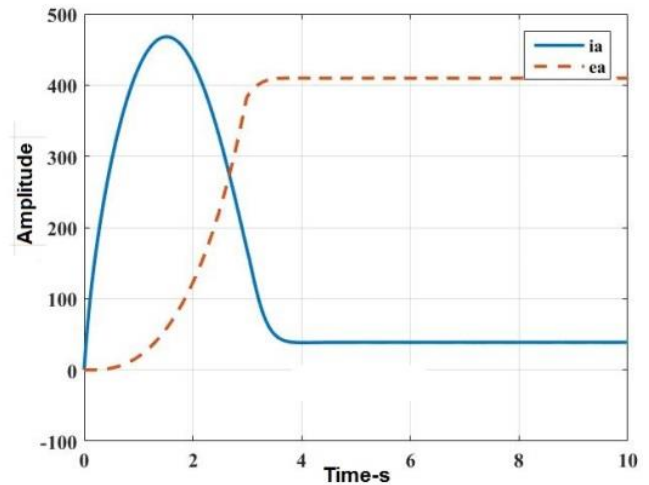


Fig.10. Graphs of armature current and emf vs time of SEDCM with PID controller

When Fig. 10 is examined, it is figured out that armature current increases logarithmically approximately up to 500 A in a few seconds and decreases logarithmically approximately up to 38.755 A. Later on, it gets stable. Emf reaches 409.781 V in a few seconds and gets stable.

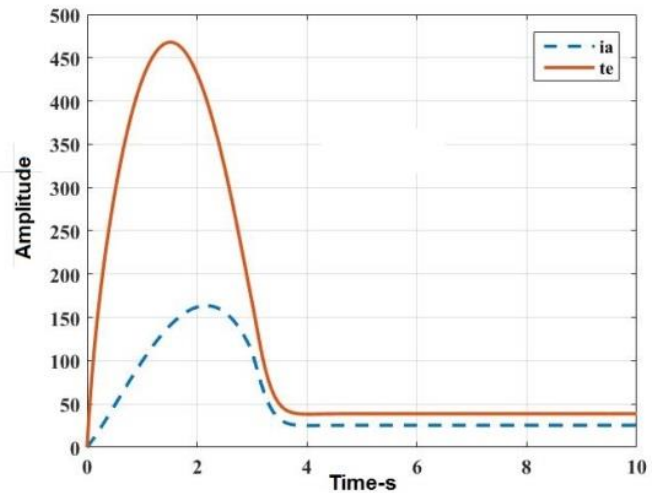


Fig.11. Graphs of armature current and produced torque vs time of SEDCM with PID controller

When Fig. 11 is examined, it is figured out that armature current increases logarithmically approximately up to 500 A in a few seconds and decreases logarithmically approximately up to 38.759 A. Later on, it gets stable. Produced torque logarithmically increases up to 150Nm in a 2.2 seconds and decreases logarithmically up to 25.464 Nm in 3.5s. Later on, it gets stable with value of 25.464 Nm.

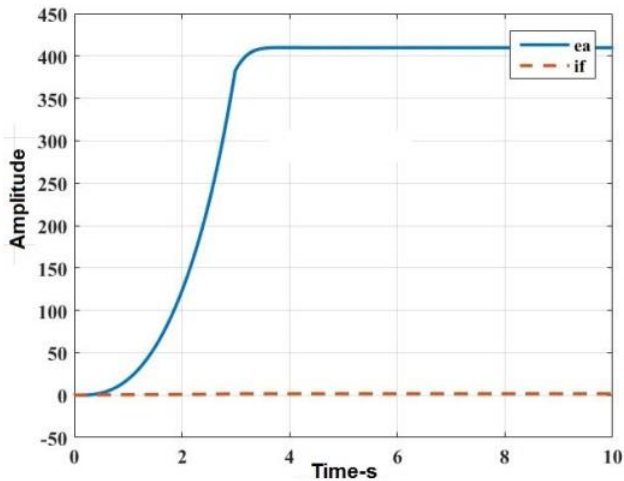


Fig.12. Graphs of excitation current and emf vs time of SEDCM with PID controller

When Fig. 12 is examined, it is figured out that with excitation current of 1.615 A, emf increases logarithmically and reaches 409.781 V in 3 seconds. Later on, then gets stable.

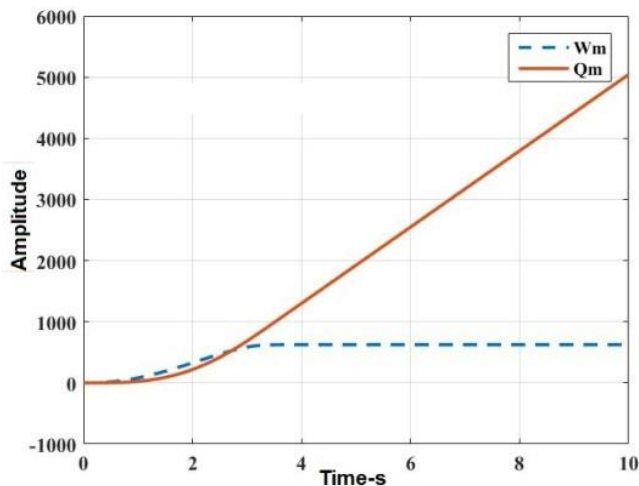


Fig.13. Graphs of speed and position angle vs time of SEDCM with PID controller

When Fig. 13 is examined, it is figured out that speed of motor reaches approximately 623.87 rad/s in 3 seconds, it gets stable and takes value of 623.87 rad/s. Position angle increases logarithmically in 3 seconds and after that it keeps increasing linearly and get value of 5043.14 rad at 10th second.

The speed value of motor is measured as 623.87 rad/s which is equal to 5957.33 rpm and this value is used as a reference value for control models.

V. CONCLUSION

Measured steady state values of SEDCM are almost same with and/or without proposed new speed control technique except for position angle. But, the results for transient values are not the same and show difference as seen in related graphs. The harmonization, peak and stability values and durations provided by proposed new speed control technique differ. It is

figured out that SEDCM with proposed speed control technique has lower startup current in shorter duration and reaches stable sooner.

REFERENCES

- [1] ALLAOUA, B.; GASBAOUI, B.; MEBARKI, B.: "Setting Up PID DC Motor Speed Control Alteration Parameters Using Particle Swarm Optimization Strategy", Leonardo Electronic Journal of Practices and Technologies ISSN 1583-1078, Issue 14, January-June 2009, p. 19-32
- [2] BANSAL, U., K.; NARVEY, R.: "Speed Control of DC Motor Using Fuzzy PID Controller, Advance in Electronic and Electric Engineering, ISSN 2231-1297, Volume 3, Number 9 (2013), pp. 1209-1220
- [3] ALTAŞ, İ.,H.: "Endüvi ve Uyarma Birleşik Kontrollü DA Motorlarının Modellenmesinde Sebep-Sonuç Yaklaşımı", Otomasyon Dergisi, Bileşim yayınları, Mart 2008, Sayfalar: 102-110.
- [4] GEORGE, M.: "Speed Control of Separately Excited DC Motor", American Journal of Applied Sciences 5 (3): 227-233, 2008 ISSN 1546-9239
- [5] ÖZDEMİR, A.: "Elektrik Motorları ve Sürücüleri", Birsen yayınevi, ISBN: 978-975-511-489-7, 2007, İstanbul.
- [6] SINGHAL, R.; PADHEE, S.; KAUR, G.: "Design of Fractional Order PID Controller for Speed Control of DC Motor", International Journal of Scientific and Research Publications, Volume 2, Issue 6, June 2012 1 ISSN 2250-3153
- [7] HUANG, G.; LEE, S.: "PC-based PID Speed Control in DC Motor", 978-1-4244-1724-7/08/\$25.00 ©2008 IEEE, ICALIP2008
- [8] ALI, F., H.; HUSSEIN, M., M.; ISMAEL,S.; M.; B.: "LabVIEW FPGA Implementation Of a PID Controller For D.C. Motor Speed Control", 2010 1 st International Conference on Energy, Power and Control (EPC-IQ), Collage of Engineering, University of Basrah, Basrah, Iraq, November 30-December 2. 2010
- [9] <http://www.yildiz.edu.tr/~omurlu/CF/OKI/12.pdf> , 07.05.2017
- [10] ALTAŞ, İ.,H.: "Otomatik Kontrol Sistemleri Ders Notları", KTÜ, Mühendislik Fakültesi, Elektrik-elektronik Mühendisliği, 2009, Trabzon.
- [11] KANOJIYA, R., G.; MESHARAM, P., M.: "Optimal Tuning of PI Controller for Speed Control of DC motor drive using Particle Swarm Optimization", 978-1-4673-2043-6/12/\$31.00 ©2012 IEEE
- [12] TANG, J.: "Pid Controller Using The Tms320c31 Dsk With On-Line Parameter Adjustment For Real-Time Dc Motor Speed And Position Control", 0-7803 -7090-2/01/ \$10.00 © 2001IEEE, ISIE 2001, Pusan, KOREA
- [13] YU, G., R.; HWANG, R.,C.: "Optimal PID Speed Control of Brushless DC Motors Using LQR Approach", 2004 IEEE International Conference on Systems, Man and Cybernetics, 0-7803-8566-7/04/\$20.00 © 2004 IEEE.
- [14] SHIN, H., B.; PARK, J., G.: "Anti-Windup PID Controller With Integral State Predictor for Variable-Speed Motor Drives", IEEE Transactions On Industrial Electronics, Vol. 59, No. 3, March 2012
- [15] DUMAN, S.; MADEN, D.; GÜVENÇ, U.: "Determination of the PID Controller Parameters for Speed and Position Control of DC Motor using Gravitational Search Algorithm", ", 7th International Conference on Electrical and Electronics Engineering (ELECO 2011), 1-4 December, Bursa, TURKEY, pp. 226-230, 2011.
- [16] THOMAS, N.; POONGODI, P.: "Position Control of DC Motor Using Genetic Algorithm Based PID Controller", Proceedings of the World Congress on Engineering 2009 Vol II WCE 2009, July 1 - 3, 2009, London, U.K.
- [17] MESHARAM, P., M.; KANOJIYA, R., G.: "Tuning of PID Controller using Ziegler-Nichols Method for Speed Control of DC Motor", IEEE-International Conference On Advances In Engineering, Science And Management (ICAESM -2012) March 30, 31,2012 117
- [18] NASRI, M.; NEZAMABADI, H.; MAGHFOORI, M.: "A PSO-Based Optimum Design of PID Controller for a Linear Brushless DC Motor", Proceedings Of World Academy Of Science, Engineering And Technology Volume 20 April 2007 Issn 1307-6884
- [19] SALEH, A.; AL-MASHAKBEH, O.: "Proportional Integral and Derivative Control of Brushless DC Motor", European Journal of Scientific Research ISSN 1450-216X Vol.35 No.2 (2009), pp.198-203
- [20] Matlab/SimulinkTM, The Mathworks, Inc, <http://www.mathworks.com/> (10 Mayıs 2017 tarihinde aktif olan link

BIOGRAPHIES



Onur AKAR was born in Giresun in 1981. He received his B.S. degree from Electrical Education Department of Technical Education Faculty of University of Marmara, Istanbul, in 2005 and his M.Sc. degree from Electrical Education Department of Institute of Pure and Applied Sciences, University of Marmara, İstanbul, in 2011. He also received B.S degree from Electrical and Electronics Engineering Department of Engineering Faculty of Karadeniz Technical University, Trabzon, in 2017. He has been

currently attending doctorate programme in Electrical and Electronics Engineering department of Institute of Pure and Applied Sciences of Marmara University, Istanbul.

He has been working as a Lecturer at Mechatronics Program of Vocational High School of Istanbul Gedik University since 2010. He served as the Head of Electrical Department of Vocational High School of Gedik University in Istanbul between 2012 and 2015. He is the author of 2 article and one book chapter. His research interests include Control Systems, Renewable Energy Systems and Power Systems.



Umit K. TERZI was born in Zonguldak in 1968. He received his B.S. degree from Electrical Education Department of Technical Education Faculty of University of Marmara, Istanbul, in 1989 and his M.Sc. and Ph.D. degree from Electrical Education Department of Institute of Pure and Applied Sciences, University of Marmara, Istanbul, in 1994 and 2000 respectively.

From 1989 to 1996, he worked as a research assistant, from 1996 to 2000 as a lecturer, from 2000 to 2013 as an Assistant Prof. Dr. for university of Marmara. Since 2013 he has been working as an Associate Prof. Dr. for Electrical and Electronics department of Technology Faculty of Marmara University and Electrical Education Department of Technical Education Faculty where he is head of department.

His research interests include Electrical Machinery, Power Systems, Energy Transmission and Distribution, Renewable Energy Systems.



Okan OZGONENEL was born in Samsun in 1967. He received his B.S and MSc. degrees from Marmara University in 1989 and 1991, respectively. He received his PhD degree from Sakarya University in 2001.

From 1989 to 1991, he worked for Goztepe SSK Hospital as an engineer. Then he received a special grant and promoted as Lecturer in Amasya Technical and Vocational Higher School by means of World Bank Second Industrial Training Project. He has worked there for 10 years and then joined Ondokuz Mayis University, Electrical & Electronic Engineering Department in 2002. He was promoted as full Professor in 2014 and since then he has been working for Ondokuz Mayis University where he is head of department.

His main researches include power system modeling and protection and renewables, too. applications.

Response and Analysis of Permanent Magnet Synchronous Motor According to Different Reference Signals

M.K. Döşoğlu, and M. Dursun

Abstract— Permanent magnet synchronous motors (PMSM) are frequently used in many applications, and so great importance in response to variable speed conditions. These engines, which are also used in electric vehicles, can be given to the best response in different road conditions. For this reason, a simulation is performed using vector control technique in MATLAB / Simulink environment. By giving different reference signals, the response of the motor is analyzed with current, speed and torque curves, and the study to be done in the future is provided with light.


Index Terms— PMSM, MATLAB/Simulink, Vector control.

I. INTRODUCTION

THE field oriented control (vector control) method developed in 1965 started to be implemented only in the 1980s. The propose of this application allows to discrete control rotating in field-based electric machines, and free-excitation DC motors. Nowadays vector control method is widely used in industrial drive systems. Thus, it is possible to use asynchronous motor, synchronous motors in alternating current motors, and in servo systems classically designed with only direct current free excitation motors [1].

Besides, in the DC motor, torque control can also be achieved by controlling motor currents in AC motors. However, only the currents controlled as amplitude in DC motors can be controlled both in amplitude and phase and angle in AA motors. That is, the current can be controlled not only as amplitude but also as a space vector. In this way control of the current space vector has occurred to the vector control terminology [2].

M.K. DÖŞOĞLU is with Department of Electric-Electrincs Engineering Technologies Faculty of Duzce University, Düzce, Turkey, (e-mail: kenandosoglu@duzce.edu.tr)

M. DURSUN is with Department of Electric-Electrincs Engineering Technologies Faculty of Duzce University, Düzce, Turkey, (e-mail: mustafadursun@duzce.edu.tr) 

Manuscript received September 13, 2017; accepted January 08, 2018.
DOI: [10.17694/bajece.410213](https://doi.org/10.17694/bajece.410213)

A new simulation model for the brushless motor drive system has been proposed in the MATLAB environment, and it is stated that the proposed model is very easy to use because it is cost-effective in the design phase and is prepared in MATLAB environment [3]. Simulation of engine control with PMSM's Direct Torque Control (DTC) has been discussed in detail. The simulation results, the system performance and the effect of PI controller are examined [4]. The vector control performance of the PMSM fed from the matrix converter is discussed in detail with the Matlab / Simulink model [5].

Detailed field oriented control of the PMSM driver system has been performed in Simulink. All components of the system are designed to depending on mathematical reality. The application was carried out in Matlab/Simulink. Simulation results were obtained from two reference speeds, above and below of the nominal speed, and the validity of the experiment was tried to be proved [6]. Modeling, simulating and implementing of vector control for variable-speed drive systems of multi-phase PMSMs is described. A simplified model in Matlab / Simulink was developed depending on this control method. Then the application was done using DSP [7]. In the study, PMSM vector control system application is developed by using the SVPWM algorithm, the PMSM vector control was implemented with the TMS320F2812 DSP, photoelectric encoder, hall current sensor and IPM module [8].

In this study, field oriented control method of PMSM was performed using space vector pulse width modulation (SVPWM) technique in various operating conditions. Under various operation conditions, field oriented control method enhanced in PMSM is successful on parameters such as speed, currents, and torque.

II. PMSM DYNAMIC MODELING

The mathematical modeling of the PMSMs fed by the sinusoidal current is carried out in the rotor reference frame. The model obtained by transferring of the stator magnitudes, rotor reference plane, similar to free excitation DC motor model. The motor control structure is created using this model. Thus, the PMSM can be controlled such as a free-excitation motor. Another advantage of the rotor plane is faster in solution because the equation level is reduced. The equivalent circuit of the PMSM in the rotor reference plane is given in Figure 1.

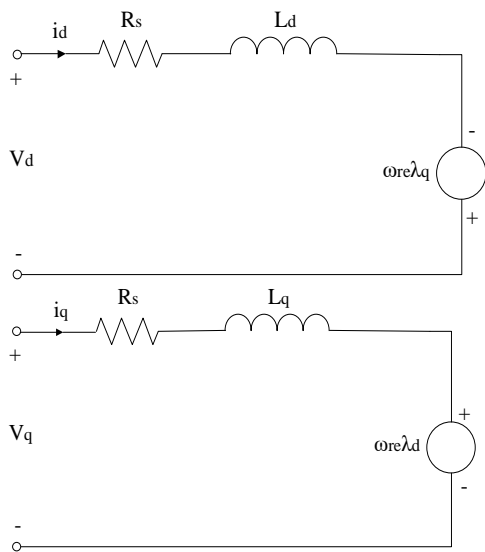


Fig.1. dq-axis dynamic equivalent circuits of PMSM

$$\begin{bmatrix} v_d \\ v_q \end{bmatrix} = \begin{bmatrix} R_s & -\omega_{re} L_q \\ \omega_{re} L_d & R_s \end{bmatrix} \cdot \begin{bmatrix} i_d \\ i_q \end{bmatrix} + \begin{bmatrix} L_d & 0 \\ 0 & L_q \end{bmatrix} \cdot p \begin{bmatrix} i_d \\ i_q \end{bmatrix} + \omega_{re} \lambda_d \begin{bmatrix} 0 \\ 1 \end{bmatrix} \quad (1)$$

$$V_d = R_s i_d + L_d \frac{di_d}{dt} - \omega_{re} \lambda_q \quad (2)$$

$$V_q = R_s i_q + L_q \frac{di_q}{dt} + \omega_{re} L_d i_d + \omega_{re} \lambda_m \quad (3)$$

Where, R_s is stator resistance, V_d and V_q are dq-axis voltages, i_d and i_q are dq-axis currents, ω_{re} is electrical rotor angular speed, λ_d and λ_q are dq-axis fluxes.

$$\lambda_d = L_d i_d + \lambda_m \quad (4)$$

$$\lambda_q = L_q i_q \quad (5)$$

Where, λ_m represents the mutual magnetic flux occurring due to the permanent magnet. The induced electrical moment is given in equation 6 [9].

$$T_e = \frac{3}{2} P \lambda_m i_q + \underbrace{\frac{3}{2} P \cdot (L_d - L_q) i_d i_q}_{\text{Reluctance Moment}} \quad (6)$$

Where, P indicates the number of poles. In the case of the moment expression, the first term is the moment produced by the magnet, and the second term is the reluctance moment achieved by difference reluctance. In the surface SMSM, the reluctance moment will be zero since the d-q axis inductances are equal to each other. So,

$$T_e = \frac{3}{2} P (\lambda_m i_q) \quad (7)$$

From Equation 7, it is clear that the control of the torque in the motor resulting from the interaction of the magnetizing flux and the vertical axis current is only dependent on the q-axis current. The torque obtained by energy conversion is used to meet the mechanical load. Electromagnetic moment in terms of motor dynamic equations s given in equation 8.

$$T_e = J \frac{d\omega_r}{dt} + B\omega_r + T_L \quad (8)$$

Where T_e is the torque generated by the motor and shows the ω_r , the mechanical speed, J , the moment of inertia, B , the friction coefficient, T_L , the load torque in the equation according to the selected reference plane. If we subtract ω_r from this equation, the equation becomes as follows [9].

$$\frac{d\omega_r}{dt} = \frac{T_e - B\omega_r - T_L}{J} \quad (9)$$

III. FIELD ORIENTED CONTROL

The general block diagram of the field oriented control in the PMSM drive system is shown in Fig 2.

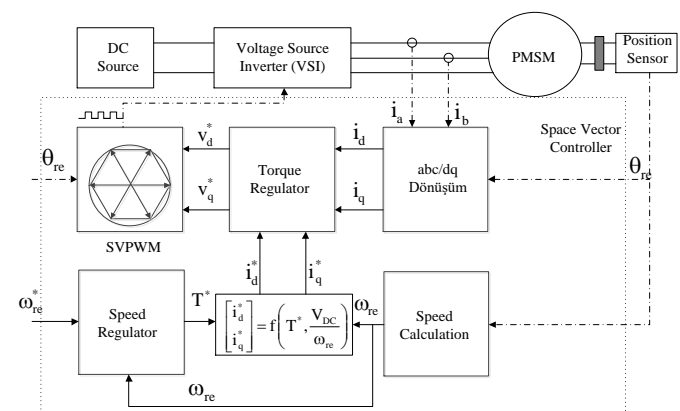


Fig.2. Field oriented control design

While, the reference torque obtained from the output of the speed controller, The i_q reference current is obtained by using Equation. The error value obtained by comparing the reference and measured i_q currents is applied to the input of the Proportional Integral (PI) controller, which is a torque controller. The V_q value is obtained from the output of the controller. Similarly, the error value obtained by comparing the reference and measured i_d currents is applied to the input of the PI controller which is also the torque controller. The V_d value is obtained from the output of the controller. These voltages are sent to the switching block. The switching signals obtained from the SVPWM switch block are sent to the voltage source inverter and three-phase sinusoidal voltages.

IV. SIMULATION RESULTS

Simulation studies of PMSM's field oriented control were performed in Matlab / Simulink environment. This simulation

were first carried out using equations relation with the mathematical model of the previously given PMSM. The

contents of PMSM's Matlab / Simulink simulation block are shown in Fig 3.

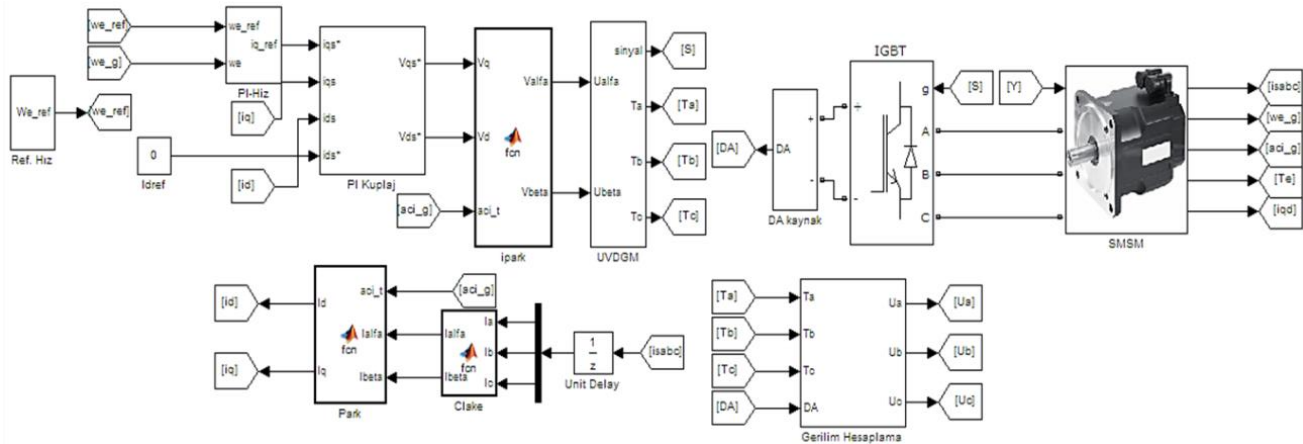
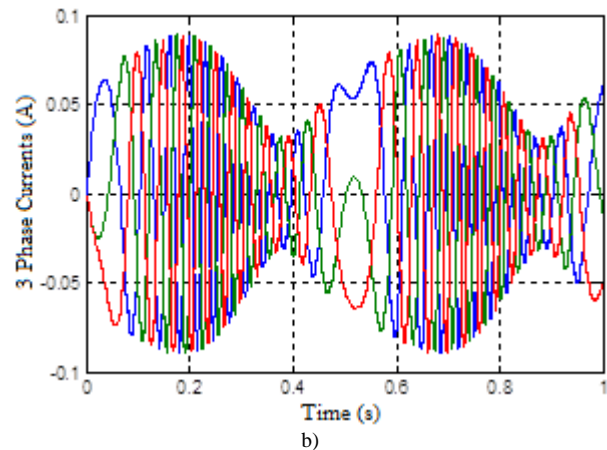
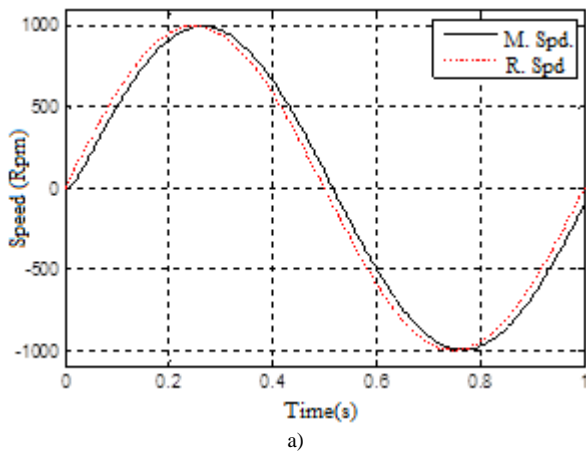


Fig. 3 Field oriented control Simulink overall blocks



The figures of the field oriented control of the PMSM made at variable input speed reference values are given below. In the following, the speed change of the sinusoidal wave from 1000 rpm to -1000 rpm is investigated, then the speed change of the square wave from 1000 rpm to -1000 rpm, and the speed change of the triangle wave from 1000 rpm to -1000 rpm were investigated.

When the simulation results in Fig. 4 are examined, it is seen that the field oriented control is steadily following the reference speed. In addition, when the results of PMSM speed, stator three phase currents are examined, it can be seen that the stator currents increase in first in parallel with the moment of inertia of the motor.

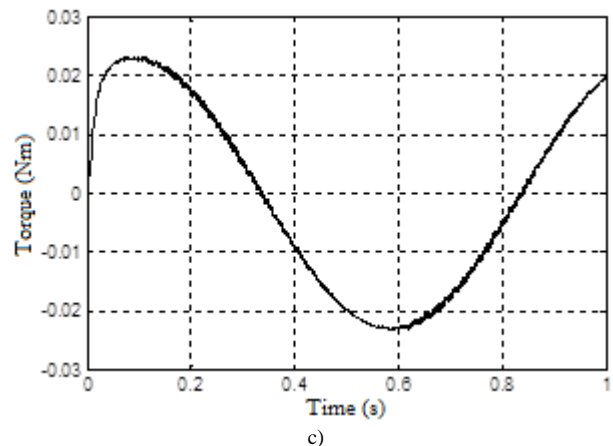


Fig. 4 1000 rpm. -1000 rpm. results for sinus reference speed a) speeds b) three phase currents c) moment

In Figure 5, when the simulated results of the square wave reference velocities is examined, the system response is fast and as steady it is in the same sine wave.

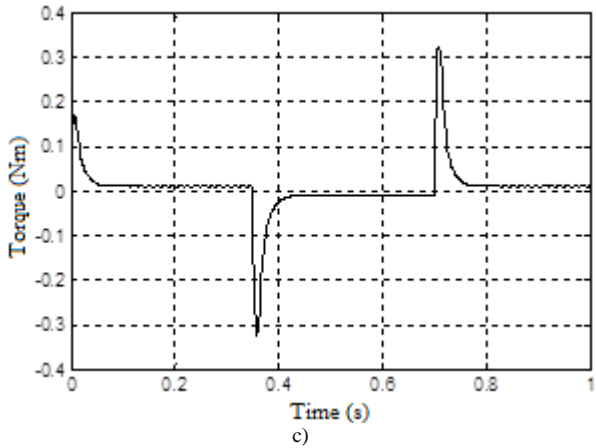
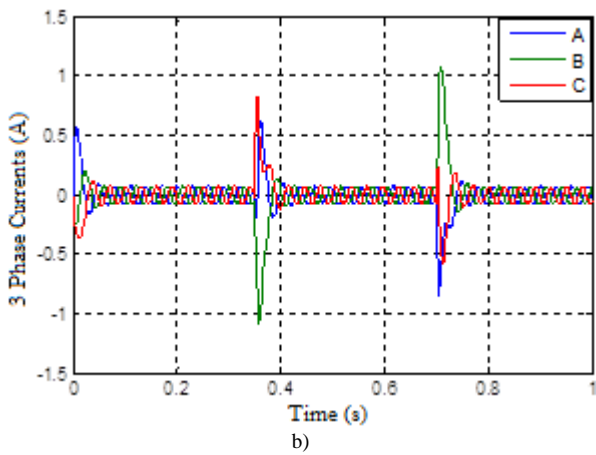
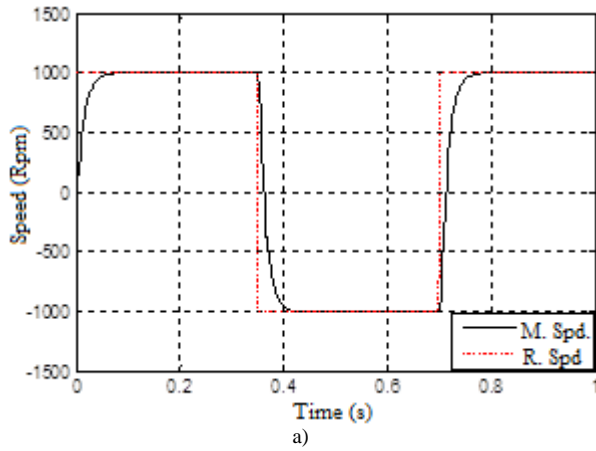


Fig. 5 1000 rpm. -1000 rpm. results for square wave reference speed a) speeds b) three phase currents c) moment

In figure 6, when the simulated results of the triangular wave reference velocities is examined, the system response is fast and as steady it is in the same sine wave and square wave.

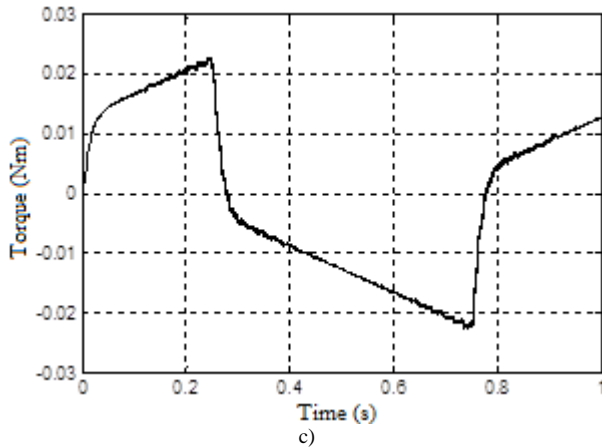
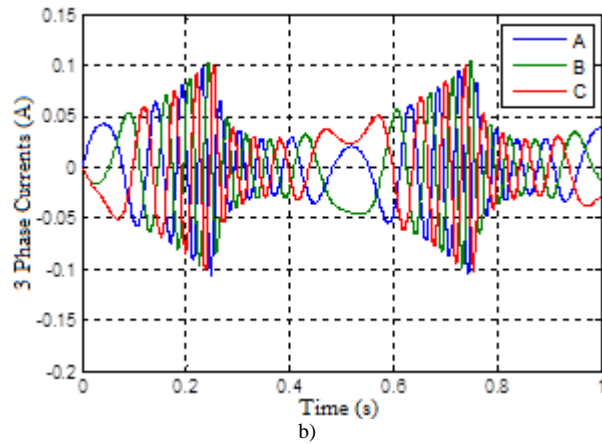
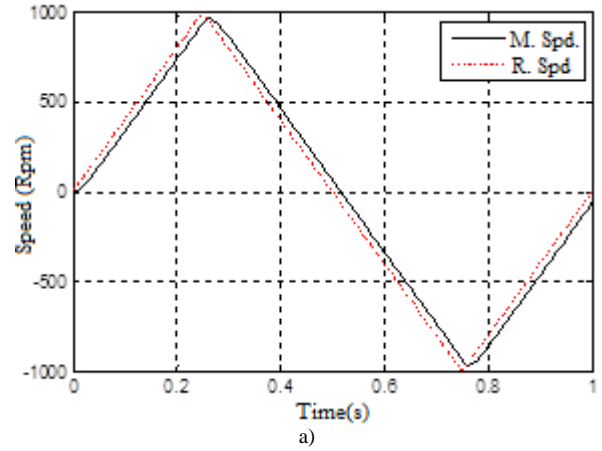


Fig. 6 1000 rpm. -1000 rpm. results for triangle wave reference speed a) speeds b) three phase currents c) moment

V. RESULTS AND DISCUSSION

The FOC performance of the PMSM for these three variable speeds it is clear that the motor speed follows the reference speed. In general, simulation carried out for field-oriented control of PMSM has shed a light on us before going to a real-time system. In this respect, it proved the validity of the study in order to determine the situations that can occur without conducting experimental work and to contribute to the research both in terms of cost and time.

REFERENCES

- [1] Gümüş B., Sürekli mıknatıslı senkron motorun bulanık mantık gözlemleyicisi kullanarak vektör kontrolü, Phd Thesis, Fırat University Institute of Science and Technology, 2004, Elazığ.
- [2] ASKER M.E., Sürekli mıknatıslı senkron motorlara vektör ve doğrudan moment kontrol yöntemlerinin uygulanması, Graduate Thesis, Fırat University, Institute of Science and Technology, 2009, Elazığ.
- [3] Matsui N., Sensorless operation of brushless DC motor drives, Proc. of the 19th. Annual Conference of IEEE Industrial Electronics Society, Vol.2, pp.739-744 Hawaii, 1993, November 15-19.
- [4] Lu Z. Sheng, H. Hess, H.L. and Buck, K.M, The modeling and simulation of a permanent magnet synchronous motor with direct torque control based on Matlab/Simulink, IEEE International Conference on Electric Machines and Drives, 2005, 1156-1162.
- [5] Sünter S., Altun H, Control of a permanent magnet synchronous motor fed by a direct AC-AC converter, Electrical Engineering, Springer Verlag, 2004, New York.
- [6] Arroyo E. L. C., Modeling and simulation of permanent magnet synchronous motor drive system, Degree Of Master Of Science In Electrical Engineering. University Of Puerto Rico Mayagüez Campus, 2006.
- [7] Zhu D., Vector control of multiphase permanent magnet synchronous motors, Faculte Des Sciences Et De Genie Universite Laval Quebec (M. Sc.), 2006.
- [8] Sun T., Liu C., Lu N., Gao D., Xu S., Design of PMSM Vector Control System Based on TMS320F2812 DSP, IEEE 7th International Power

Electronics and Motion Control Conference-ECCE Asia, 2012, June 2-5, Harbin, China.

- [9] Pillay P. and Krishnan R., "Modeling of permanent magnet motor drives", IEEE Transactions on Industrial Electronics, 35(4), 1998, 537-541.

BIOGRAPHIES



M. Kenan DÖŞOĞLU was born in 1983. He received the M.Sc. degree of Electrical Education at Technical Education Faculty of Abant İzzet Baysal University, 2010. He received Ph. D. in 2014 with thesis "Dynamic modelling and analyzing of wind plants". From 2007 he is assistant in the department of Electrical Education in University of Duzce. From 2015 he is assistant professor by in Department of Electrical and Electronics Engineering, Faculty of Technologies in the University of Duzce in Turkey. His research interests include: wind farm dynamic modeling,

FACTS application in power systems, economic load dispatch in power systems.



Mustafa DURSUN was born in 1981. He received the M.Sc. degree of Electrical Education at Technical Education Faculty of Afyonkocatepe University, 2009. He received Ph. D. in 2015 with thesis "Sensorless Speed Control of Permanent Magnet Synchronous Motor with Hybrid Adaptation Mechanism". From 2008 he is assistant in the department of Electrical Education in University of Duzce. From 2016 he is assistant professor by in Department of Electrical and Electronics Engineering, Faculty of Technologies in the University of Duzce in Turkey. His

research interests include: electrical machine control, sensorless algorithms, inverter topologies, C programming and microprocessors.

Analyzing High Efficiency Asynchronous Motors Using Scalar Control Technique

H.Uzun, O.Akar, A.Demirci, M.C.Akuner, and U.K. Terzi

Abstract— In industry, more than half of the total electrical energy produced in developed countries is converted into mechanical energy by electric motors. The usage rate of asynchronous motors is estimated to be 90% of all electric motors. For these motors, an improvement in efficiency may result in huge savings. These electric motors which have minimized losses can be improved with speed control drives to be more efficient in terms of energy consumption and performance. In speed control drives of asynchronous motors widely used in industry; scalar, vector control and direct torque control are used.

In this study, in a Matlab/Simulink environment, high efficiency and standard asynchronous motors with the same characteristics were driven with scalar control technique and the simulations were compared in detail. From the point of view of both speed control performance and energy saving, it observed that high efficiency motors have more advantages.

Index Terms—Asynchronous motor, High Efficiency Motors, Speed Control, Scalar Control.


I. INTRODUCTION


WORLD industrial production mostly relies on electric motors and electric motors are performing the work of billions of people. Therefore, it is of great importance that the electric motor is highly efficient. Efficiency improvements can provide big savings. By minimizing the losses in the motor, the obtained high-efficiency motors, can not only prevent heat loss, but also minimizes any other losses. Other big advantages of high efficiency motors are that when used with variable speed drive they have advanced control characteristic [1-4].

H. UZUN, is with Department of Electrical and Electronic Technologies, Yenidoğan Vocational and Technical Anatolian High School, 34791, Istanbul, Turkey, (e-mail: hasanuzun2@hotmail.com)

O. AKAR, is with Department of Mechatronic Program, Gedik Vocational High School Istanbul Gedik University, 34700, Istanbul, Turkey, (e-mail: onur.akar@gedik.edu.tr)

A. DEMIRCI, is with Department of Electrical Engineering, Yıldız Technical University, 34220, Istanbul, Turkey, (e-mail: ademirci@yildiz.edu.tr)

M. C. AKUNER, is with Department of Mechatronic Engineering, Marmara University, 34722, Istanbul, Turkey, (e-mail: akuner@marmara.edu.tr) 

U. K. TERZI, is with Department of Electrical and Electronics Engineering, Technology Faculty, Marmara University, 34722, Istanbul, Turkey, (e-mail: terzi@marmara.edu.tr) 

Manuscript received September 13, 2017; accepted January 08, 2018.
DOI: [10.17694/bajece.410219](https://doi.org/10.17694/bajece.410219)

II. HIGH EFFICIENCY ASYNCHRONOUS MOTORS

It is known that the industry is the biggest electricity consuming sector in a country. In the industry of advanced countries three-quarters of the energy consumed is used in electric motors. Efficiency improvements in these motors can provide big savings.

In the production phase electric motors are generally manufactured in three classes. These classes are named according to European standards as High Efficiency Motor Class (EFF1), Standard Efficiency Motor Class (EFF2) and Low Efficiency Motor Class (EFF3). Nowadays EFF3 class motors, totally or partially disappeared from production and EFF1 and EFF2 have been used mostly in industry. In our study, subjects will be motors of these two classes.

Two different Technologies are used in the manufacture of high efficiency motors. Extending the length of the packet motor sheet is raising efficiency, and the other design is made by using higher quality sheet metal and copper. In addition, motors with rotors produced with copper injection technique do also step forward as new generation high- efficiency motors. Also in this type of motor the fan structure is designed specifically to provide better cooling. Thus the heat losses to the energy are minimized.

An electric motor cannot convert the entire energy it draws from the network which it's connected into mechanical energy. The useful power from the electric motor shaft; losses from the power drawn from the mains power out of the state. Energy losses in the motor during operation of the engine are converted into heat energy. The high efficiency motors gained from minimization of these losses, not only prevents heat loss, but also minimizes any other losses [1-11].

III. SCALAR CONTROLS

Due to the ease of implementation, scalar control nowadays is the best known and most widely used method of speed control for variable speed motor drives. The essential feature of this method; at speeds from zero to the rated value is that the voltage applied to the stator frequency (V / F) ratio, and thus the flux and induced torque is kept constant. At speeds above the rated speed, the increase in frequency and the voltage is kept constant; therefore, the attenuation of the flux through the rate control can be performed. Asynchronous Motor (ASM) speed drive systems using scalar methods of control have a good variable dynamic steady-state performance, but the dynamic response is not good answered. Oscillations in the air flow

range worsens dynamic response and causes electromagnetic torque oscillation. In high-performance drive systems, oscillations in torque and speed are not required. In this type of application, high accuracy, fast position and speed control is required. If the flux and torque are controlled separately, these problems can be overcome. A method of controlling the flux and torque individually is called the vector control (field oriented control) [6, 12-18].

IV. STUDIES

In this section, studies performed in the MATLAB/ Simulink environment are described. In the simulation study performed with MATLAB/Simulink blocks asynchronous motors with scalar control methods have been proposed. For the realization of these simulations of both efficiency classes of the Gamak motor brand and tag information of the motor equivalent circuit parameters were utilized. In Table 1 and Table 2, the tag information and equivalent circuit parameters of the motor are given.

TABLE I
HIGH EFFICIENCY MOTOR INFORMATION (EFF1 YIELD CLASS)

Motor Nameplate Value							
	Voltage	Frequenc y	Current	Power	cosφ	Rotation	J (kgm ²)
triangle	220/240V	50Hz	4.04/4.01 A	1.1 kW	0.82	2900d/d	0.00066
star	380/415V	50Hz	2.34/2.32 A	1.1 kW	0.82	2900d/d	0.00066
Equivalent Circuit Parameters							
R ₂	R ₂	L ₂	L ₂	L _m			
10.5 Ω	0.2294 Ω	33.7 mH	33.7 mH	0.627 H			

TABLE II
STANDARD MOTOR INFORMATION (EFF2 YIELD CLASS)

Motor Nameplate Value							
	Voltage	Frequenc y	Current	Power	cosφ	Rotation	J (kgm ²)
triangle	220V	50Hz	4.4 A	1.1 kW	0.83	2800d/d	0.00066
star	380V	50Hz	4.4 A	1.1 kW	0.83	2800d/d	0.00066
Equivalent Circuit Parameters							
R ₂	R ₂	L ₂	L ₂	L _m			
13.4 Ω	0.4834 Ω	40.3 mH	40.3 mH	0.51 H			

For scalar control experiment, the block diagram given in Figure 1 is used. After entering the motor tag information and equivalent circuit parameters from Table 1 and Table 2 and

entering appropriate settings, the stator current and rotor speed graphics were obtained from the screen.

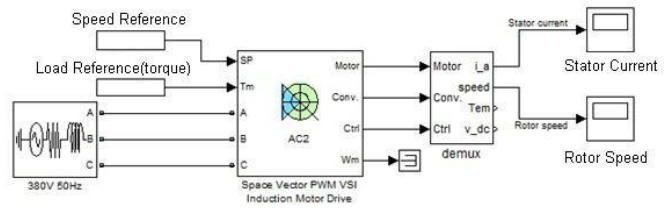


Fig.1. Scalar Control Block Diagram

In order to measure the response of asynchronous motor during loading, the motor speed reference of 3000 rpm including 0-1 sec in the range of load (ie. 0 Nm) and 1-2 sec in the range of nominal motor torque with 3.7 Nm load reference has been entered. In Figure 2, It can be seen that the current drawn of EFF1 efficient motor at the very beginning is higher than the current drawn by the EFF2 motor. In Figure 3, EFF1 efficient motor 1 sec at 3.7 Nm loads the implementation of the reduction by reference speed of the rotor speed is less than EFF2 efficient motor.

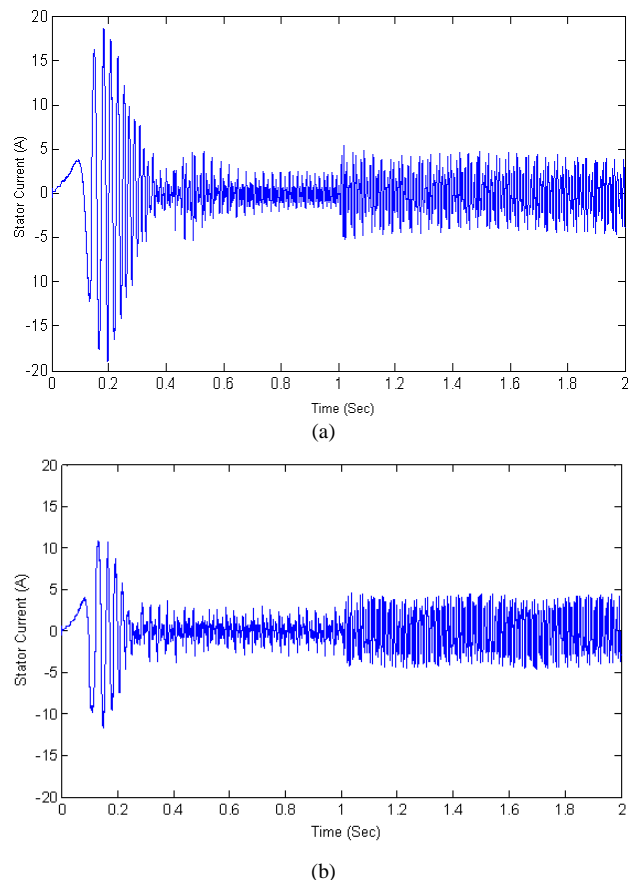
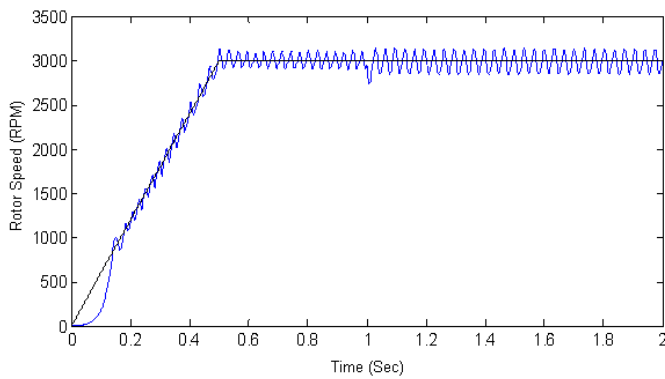
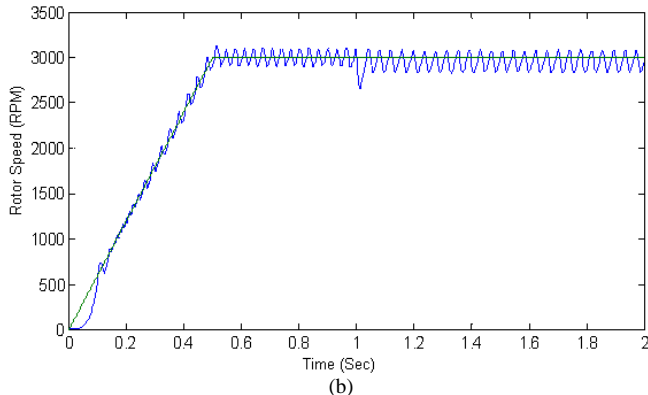


Fig.2. Scalar Control in The Idle and 3.7 Nm Load Current in The Stator
a) EFF1 Motor b) EFF2 Motor



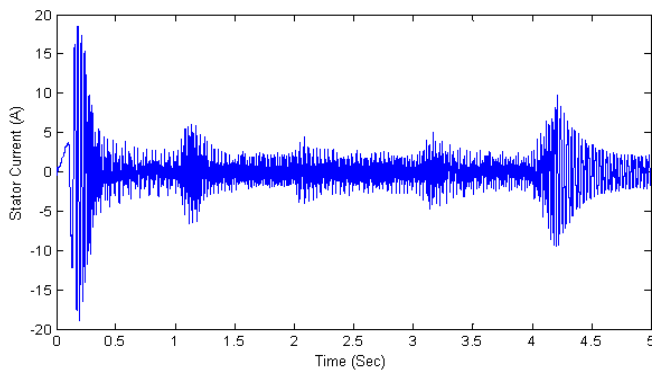
(a)



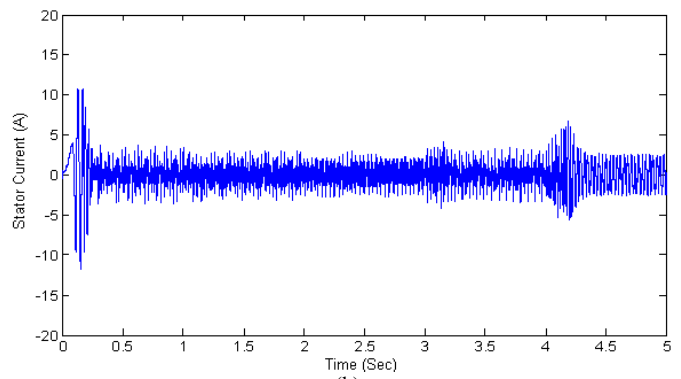
(b)

Fig.3. In The Idle and 3.7 Nm Load Variation of Rotor Speed for Scale Control a) EFF1 Motor b) EFF2 Motor

To monitor the response of the asynchronous motor against variable speed references, under no load conditions, speed references; 2000 rpm for duration of 0-1 sec, 3000 rpm for duration of 1-2 sec, 3500 rpm for duration of 2-3 sec, 2500 rpm for duration of 3-4 sec and 1000 rpm for duration of 4-5 sec were applied to motors. Figure 4 shows that at the start up stage, EFF1 motors with no load draw more current than the efficient EFF2 motor. In Figure 5, the responses of EFF1 and EFF2 efficient motors to variable speed references are seen. It can be seen that fluctuations of high efficiency motor while reaching to reference speed are less than those in the standard motor.

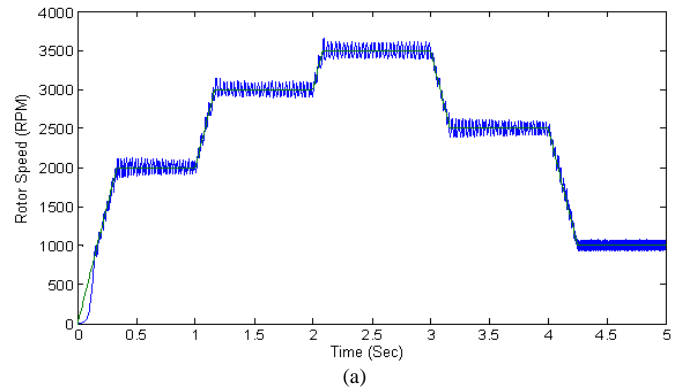


(a)

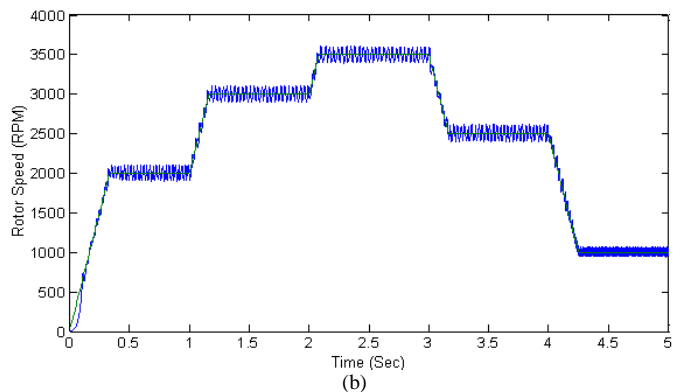


(b)

Fig.4. Stator Current Changes in The Mixed Speed Reference for Scale Control a) EFF1 Motor b) For EFF2 Motor



(a)



(b)

Fig.5. Variations of rotor speed in The Mixed Speed Reference for Scale Control a) For Eff1 Motor b) For Eff2 Motor

V. CONCLUSION

Performed in this paper, a study was done on the standard motors and highly efficient asynchronous motors which have same characteristics (power, voltage, speed) and their stator currents and speeds were compared. In the simulation study done, it is observed that the starting current in the EFF1 efficient motor is higher than the starting current of the EFF2 efficient motor. This shows that the highly efficient motor start-up torque is higher. It is also observed that the current of the efficient motor, after getting the steady state, is lower. This means that less energy is spend in continuous operation. On the other hand, it is seen that EFF1 efficient motor response to changes in motor speed is faster than the EFF2 efficient motor and fluctuations were less. This also shows that speed control characteristic in highly efficient motors is better. Generally, this study shows that high efficiency asynchronous motors are

superior to standard motors in terms of energy saving and speed controlling characteristic. However, because the starting current in the EFF1 efficient motor is higher than the starting current of the EFF2 efficient motor, this situation causes using more sensitive protection devices.

REFERENCES

- [1] H. Uzun, "Yüksek Verimli ve Standart Asenkron Motorların Farklı Hız Kontrol Yöntemleri Kullanılarak Karşılaştırılması", Master Thesis, Marmara University, İstanbul, Turkey, 2013.
- [2] H. Uzun, M. C. Aküner, İ. Temiz, & E. Hüner, (2012). "Comparison of high efficiency and standard induction motors with different speed control methods", Energy Education Science and Technology Part A Energy Science and Research. Sayı SI-1. Cilt 30 sf 533-538
- [3] C. Tekin, "Yüksek Verimli Asenkron Motorların Analizi" Master Thesis, Marmara University, İstanbul, Turkey, 2008 [in Turkish].
- [4] F. Akova, "Elektrik Motor Sistemlerinde Enerji Verimliliğine Bakış. Verimli Endüstriyel Komponentler İç ve Dış Tic Ltd Sti" [Online]. Available: www.uevf.com.tr/uevf1/sunumlar/ot08-05.doc. [Accessed: August 16, 2011]. [in Turkish].
- [5] E. Goren, "Elektrik Motoru ve Hız Kontrol Sistemleri ile Enerji Verimliliği. Siemens San ve Tic AS" [Online]. Available: www.uevf.com.tr/uevf1/sunumlar/ot08-01.doc. [Accesses: August 16, 2011] [in Turkish].
- [6] MK .Sarioglu, M . Gokasan, S. Bogosyari, "Asenkron Makinalar ve Kontrolü", Birsen Print House, İstanbul, 2003 [in Turkish].
- [7] B. Widell, D. Danfoss, L. Park, "High Efficiency Motors And Nuisance Starting Trips", Illinois, USA, 2007.
- [8] J. Pyrhonen, J. Haataja, K. Luostarinen, "High Efficient Induction Motors", Lappeenranta University of Technology.
- [9] [Online]. Available: www.energysc.org/energy_tips.html high_efficiency_MOTORS.PDF, [ACCESSES: AUGUST 10, 2011].
- [10] ABB. ACS 800 Programlama Kilavuzu [in Turkish].
- [11] S. Dursun, "Energy utilization and energy efficiency", Ener Educ Sci Tech 2005;15:59-70.
- [12] N. Ozturk, "Yumusak Anahtarlama Asenkron Motorun Dolaylı Vektör Denetiminin Gerçekleştirilmesi", PhD Thesis, Gazi University, Ankara, Turkey, 2006.
- [13] A. Saygin, "Asenkron Motor Hız Kontrolünün Matris Konverter ile Hızının Denetlenmesi", PhD. Thesis, Gazi University, Ankara, Turkey, 2004 [in Turkish].
- [14] O.A. Karaman, "Doğrudan Moment Kontrollü Motor Surucu Sisteminin İncelenmesi", Master Thesis, Firat University Elazığ, Turkey, 2010 [in Turkish].
- [15] MK. Sarioglu, M. Gokasan, S. Bogosyari, "Asenkron Makinalar ve Kontrolü", Birsen Print House, İstanbul, 2003 [in Turkish].
- [16] A. Boglietti, A. Cavagnino, M. Lazzari, M. Pastorelli, "International Standards for the Induction Motor Efficiency Evaluation: A Critical Analysis of the Stray-Load Loss Determination", 2003.
- [17] J. Lepka, P. Stekl, "3-Phase AC Induction Motor Vector Control Using a 56F80x, 56F8100 or 56F8300 Device. Design of Motor Control Application", 2005.
- [18] A. Hazzab, M. Rahli, B. Kamli, B. Mazari, "Direct Field-Oriented Control Design using Backstepping Technique for Induction Motor Speed Control", University of Sciences and Technology of Oran, Algeria, 2009.

BIOGRAPHIES



Hasan UZUN was born in İstanbul in 1986. He received his B.S. degree from Electrical Education Department of Technical Education Faculty of University of Gazi, Ankara, in 2008 and his M.Sc. degree from Electrical Education Department of Institute of Pure and Applied Sciences, University of Marmara, İstanbul, in 2013. From 2011 to 2012, he was a Lecturer in İstanbul Gedik University. Since 2012, he has been a Technical Teacher with the electrical and electronic department, İstanbul,

Vocational and Technical High School. He is the author of 1 article. His research interests include power electronic, speed control of electrical motors, energy efficiency.



Onur AKAR was born in Giresun in 1981. He received his B.S. degree from Electrical Education Department of Technical Education Faculty of University of Marmara, İstanbul, in 2005 and his M.Sc. degree from Electrical Education Department of Institute of Pure and Applied Sciences, University of Marmara, İstanbul, in 2011. He also received B.S degree from Electrical and Electronics Engineering Department of Engineering Faculty of Karadeniz Technical University, Trabzon, in 2017. He has been currently attending doctorate programme in Electrical and Electronics Engineering department of Institute of Pure and Applied Sciences of Marmara University, İstanbul.

He has been working as a Lecturer at Mechatronics Program of Vocational High School of İstanbul Gedik University since 2010. He served as the Head of Electrical Department of Vocational High School of Gedik University in İstanbul between 2012 and 2015. He is the author of 2 article and one book chapter. His research interests include Control Systems, Renewable Energy Systems and Power Systems.



Alpaslan DEMIRCI was born in İstanbul in 1985. He received his B.S. degree from Electrical Education Department of Technical Education Faculty of University of Marmara, İstanbul, in 2007 and his M.Sc. degree from Electrical Education Department of Institute of Pure and Applied Sciences, University of Marmara, İstanbul, in 2011. He also received B.S degree from Electrical and Electronics Engineering Department of Engineering Faculty of Sakarya University, Sakarya, in 2017.

From 2012 to 2015, He was a Lecturer with the Electricity and Energy Department, İstanbul Yıldız Technical University, Vocational and High School. Since 2016, He has been a Lecturer with the Electrical Engineering Department, İstanbul Yıldız Technical University. His research interests include Power electronics, Energy Transmission and Distribution, Renewable Energy Systems.



M. Caner AKUNER was born in Samsun in 1968. He received his B.S. degree from Electrical Education Department of Technical Education Faculty of University of Marmara, İstanbul, in 1990 and his M.Sc. and Ph.D. degree from Electrical Education Department of Institute of Pure and Applied Sciences, University of Marmara, İstanbul, in 1993 and 1999 respectively.

From 1990 to 1996, he worked as a research assistant, from 1993 to 1999 as a lecturer, from 1999 to 2012 as an Assistant Prof. Dr. for university of Marmara. Since 2012 he has been working as an Associate Prof. Dr. for Mechatronics Department of Technology Faculty of Marmara University.

His research interests include Electrical Machinery, Power Systems, Energy Transmission and Distribution, Renewable Energy Systems.



Umit K. TERZI was born in Zonguldak in 1968. He received his B.S. degree from Electrical Education Department of Technical Education Faculty of University of Marmara, İstanbul, in 1989 and his M.Sc. and Ph.D. degree from Electrical Education Department of Institute of Pure and Applied Sciences, University of Marmara, İstanbul, in 1994 and 2000 respectively.

From 1989 to 1996, he worked as a research assistant, from 1996 to 2000 as a lecturer, from 2000 to 2013 as an Assistant Prof. Dr. for university of Marmara. Since 2013 he has been working as an Associate Prof. Dr. for Electrical and Electronics department of Technology Faculty of Marmara University and Electrical Education Department of Technical Education Faculty where he is head of department.

His research interests include Electrical Machinery, Power Systems, Energy Transmission and Distribution, Renewable Energy Systems.

Conceptual Design of a Smart Parking Lot System for Electric and Hybrid Electric Vehicles

K. Erhan, M. Ayaz, and Y. Icer

Abstract—Today, demand to electric and hybrid electric vehicles (EVs, HEVs) increases day by day due to both environmental factors and limited fossil fuel resources. With EVs and HEVs becoming widespread, some basic problems arise. One of the most important of these problems is that the users who want to charge their vehicles cause to over load on the power grid. Another problem is that charging stations are not widespread and charging station installation cost is high. This study deals with the design of a smart parking lot system that can provide collective charging services for electric and hybrid electric vehicles. In the proposed smart parking system, online booking assistance is provided and the location of charging stations is marked on the navigation so that users of EVs and HEVs can easily access the charging stations. Also, users via the designed mobile application can follow up and control booking inquiry, battery charge status, battery sharing permission and payment services. Another important feature provided by the proposed parking system is that the problem of excessive and irregular load to the power grid occurred during charging of vehicles located in the parking lot solve with the developed energy management algorithm. In the developed energy management algorithm, in case of the over loading of the power grid, the energy requirement for charging is provided from other vehicles for which prior permission for battery sharing has been obtained instead of the power grid. Thus, overloading of the power grid is prevented and, also drivers who give permission for battery sharing can derive a profit.

Index Terms—Electric vehicle, plug-in hybrid electric vehicle, charge station, smart parking lot system, energy management.

I. INTRODUCTION

IT is envisaged that fossil fuel resources will be consumed away within 30-40 years. A study supporting this predicts that the oil will deplete in 2057 [1]. For this reason, research on electric and hybrid electric vehicles (EVs and HEVs) continues with an increasing rate. Usage of EVs and HEVs instead of only fossil fuel-based vehicles will significantly reduce both environmental pollution and dependence on oil.

K. ERHAN, is with Department of Energy Systems Engineering University of Kocaeli, Kocaeli, Turkey, (e-mail: koray.erhan@kocaeli.edu.tr)

M. AYAZ, is with Department of Electric and Energy University of Kocaeli, Kocaeli, Turkey, (e-mail: murat.ayaz@kocaeli.edu.tr) 

Y. ICER, is with Department of Energy Systems Engineering University of Kocaeli, Kocaeli, Turkey, (e-mail: yusuf.icer92@gmail.com)

Manuscript received September 13, 2017; accepted January 08, 2018.
DOI: [10.17694/bajece.410230](https://doi.org/10.17694/bajece.410230)

According to the values published by a manufacturer, EVs have a high efficiency of 88%, while the efficiency is 30% for vehicles having internal combustion engine. Furthermore, the maximum torque can be achieved in large speed range in EVs compared with conventional vehicles [2]. In this context, the widespread usage of electric vehicles will increase driving comfort. Despite all these positive developments, EVs have not reached widespread use at the desired level in our country. The main reason for this situation is that sufficient number of charging stations have not been established yet. This causes that users of EVs worry about being stranded on the road [3]. The fuel tank of conventional vehicles can be filled with fuel in very short time as approximately 3-4 minutes and depending on fuel tank capacity, about 600 – 1200 km distance can be driven with a fully loaded tank. On the other hand, users of EVs and HEVs to drive 150 km distance need to an average of 6-8 hours on a standard charge, or a minimum of half an hour on a quick charge. Several R&D studies are being carried out on battery technologies to solve this problem. A vehicle manufacturer company introduced an electric vehicle battery capable with a 480 km driving range that could reach 100% capacity in 5 minutes [4].

Users who want to charge their vehicles at the time when the power grid is overloaded will cause the power grid to load even more. This causes some problems on the power grid such as distribution fault, power interruption and poor power quality [5]. Issues such as reservation, location information and battery sharing are being studied to solve these problems. With the reservation option, the users are able to charge vehicles by going to the pre-booked charging station and avoid the stress of finding the right charging station. Also, with location support option, users who want to charge their vehicles can find the nearest charging station that the program directs them instead of searching for a charging station. In addition of these features, extra overloading situation occurred on the power grid due to the charging process of the vehicles can be solved with battery sharing in the afternoon and evening hours when the power grid is overloaded. At times when the power grid is overloaded, energy is transferred to vehicles having empty battery from vehicles having fully charged battery. Thus, the power grid is not overloaded and power demand is balanced [6].

In this study, a smart parking automation system consisting

of several features such as reservation, location information and battery sharing permission allows the vehicles to fill their batteries without overloading the power grid while parked. The proposed smart park automation system is recommended for places such as hospitals and airports where power interruption can cause major problems. By applied the proposed system to the vehicle parks of these enterprises, in case of energy interruption, energy supply can be provided using batteries of EVs and HEVs. In such a case, the vehicles in the vehicle park constitute an important backup energy source.

II. ELECTRIC AND HYBRID ELECTRIC VEHICLES

Electric vehicles take their energy from the batteries and have no other energy sources. Fully electric vehicles do not have fuel tank, internal combustion engine and generator units. Electric vehicles consist of an electric motor that provide mechanical power to traction system of the vehicle, a driver that drives the motor, and a battery group that supplies energy to the entire system. The battery group needs to be charged when the energy is consumed. Figure 1 shows the structure of the electric vehicle.

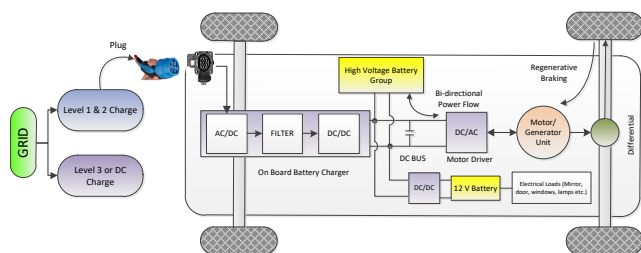


Fig.1. General structure and system components of the electric vehicle

Hybrid electric vehicles have more than one energy source. HEVs are subdivided into four classes according to the driving range [7]. These are summarized as following.

- Micro hybrid vehicles are the simplest hybrid electric vehicles. In case of starting movement of the vehicle, the electric motor provides mechanical power to traction system in urban traffic. Also, these HEVs have start-stop feature.
- Mild hybrid vehicles provide energy gain by stopping internal combustion engine when necessary. These types of vehicles can store energies that occur during braking (regenerative braking). When necessary, the electric motor provides mechanical power for traction in order to support internal combustion engine and vehicle performance can be improved. The ratio of electric motor to the total vehicle power is between 10% and 30%.
- The difference between Full Hybrid vehicles and the mild hybrid vehicles is that they can only be driven using the electric motor. Except for this, they have same features of mild HEVs. The power ratio of the electric motor to the total power of vehicle is 30% or more.
- The plug-in HEVs have all the features of the other HEVs. Apart from these features, the plug-in HEVs can be charged from the power grid.

The general structure of the hybrid electric vehicle is shown in Figure 2.

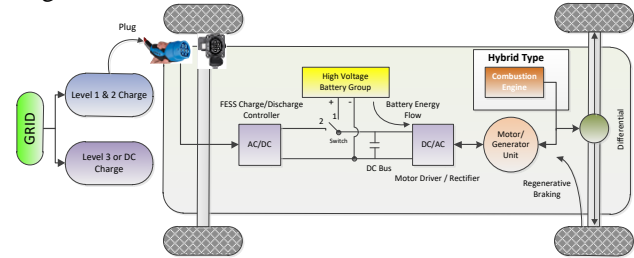


Fig.2. General structure and system components of a hybrid electric vehicle

It is stated that electric and hybrid electric vehicles will replace conventional vehicles in the near future. In this respect, various standards related to EVs and HEVs are put forward by many international institutions. Many of these standards relate to the equipment and procedures of chargers [8]. Japan adopts the CHADEMO standard and can deliver energy to vehicles up to 62.5 kW with direct current [9]. The IEC 62196 standard accepted in Europe can transfer energy up to 43.5 kW with 3-phase alternating voltage [10]. The USA allows the AC charging up to 19.2 kW with the SAE J1772 standard [11]. Society of Automotive Engineers (SAE) has developed SAE J-1772 and SAE J-1773 standards for conductive and inductive connection respectively. In SAE standards, 3 different power levels are defined for chargers. Level 1 (120V-15A) is at 1.5 kW of power and is the recommended power level for emergencies. These chargers are used when level 2 chargers are unavailable. These types of chargers are lightweight, cheap and portable. They can charge the vehicle battery in 10-15 hours. Level 2 (230V-40A) charging system is at 6.6 kW power and is the recommended power level for nominal charging. This level is suitable for home and commercial chargers. Depending on the battery type, they can charge the battery in 3-8 hours. Level 3 is in the 25-160 kW range and contains large and heavy power electronics equipment. For this reason, electronic equipment is located in the station and provides DC charging. These devices capable of rapid charging within minutes can be thought of as petrol stations for EVs and HEVs [12, 13]. Expert personnel are required for the usage of Level 3 charger [14].

III. DESIGN OF SMART PARKING SYSTEM

The goals of the designed intelligent parking system are follows: the integration of EVs and HEVs into the power grid, elimination the extra waiting time for the battery charging, easily finding and reservation of the charging station, and preventing overloading of the power grid with battery sharing. Furthermore, batteries of vehicles can be used as a backup energy source in places such as hospitals and airports where energy interruptions cause major problems in emergencies. Today, with a standard charge (level 1-2), the required battery charge time for a 150 km driving range is 6-8 hours on average. A quick charge (level 3) requires a half hour of charging time to provide the same driving range. This long charging time is an important problem for users of EVs and HEVs in terms of the efficient use of the vehicle. Vehicles wait in park for an average of 22 to 23 hours per day [15, 16].

In the developed system, vehicles are charged while waiting in the parking lot, so there is not any extra waiting time for charging. This is made by communicating the vehicles with the smart parking management system.

One of the most important advantages of the system is the possibility of battery sharing. On this point, users do not increase the power grid load by charging their vehicles except for the hours when the power grid is overloaded (hours when the energy is expensive). In case of necessary or preference, users whose vehicle battery is fully charged can deliver energy to the power grid or the other users. Thus, they can derive a profit.

A daily energy distribution graph recorded on 11/01/2018 In Turkey is shown in Figure 3. It is seen that the consumption of electricity in the graph is maximum between 9.00-11.00 hours and between 14.00-15.00 hours. At these times, it is not desirable that additional energy is drawn from the power grid in order to prevent overloading of the power grid. This high energy consumption during daytime hours will increase in the event of charging of electric vehicles, these unbalanced load profiles will increase costs and reduce the quality of the power.

Transient regime, short-time voltage fluctuations, long-term voltage fluctuations, interruptions, voltage fluctuations (flicker), frequency fluctuations and harmonics are events that degrade the quality of the power. These can be attributed to nonlinear loads, conveyor applications, train drivers, large motors, arc induction furnaces, sudden load changes, lightning, switching events, failures. The power quality disruption caused by the non-linear load will increase further as the EVs and HEVs are charged. This problem can be minimized, if EVs and HEVs are charged during night hours when electricity consumption is low. Also, the temperature of the distribution transformers increases with the unbalanced load profiles caused by the switching power supplies. As the value of power drawn from the transformer decreases, its temperature decreases to normal levels. The service life is shortened due to the mechanical wear caused by this temperature change in the transformer.

Users who want to charge their vehicles at times when electric power is sorely demanded may prefer to use energy obtained from the battery sharing option provided by other users in the smart parking system. With this option, extra load to the power grid can be avoided and users who give permission to the battery sharing can get a profit. In this case, the energy is not drawn from the power grid and is transferred between the vehicles. Thus, the energy consumption versus to the hours shown in Figure 3 can be balanced as shown in Figure 4.

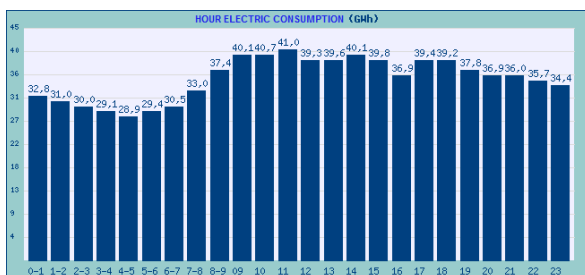


Fig.3. General hourly electricity consumption graph recorded on 11/01/2018 in Turkey (GWh) [17].

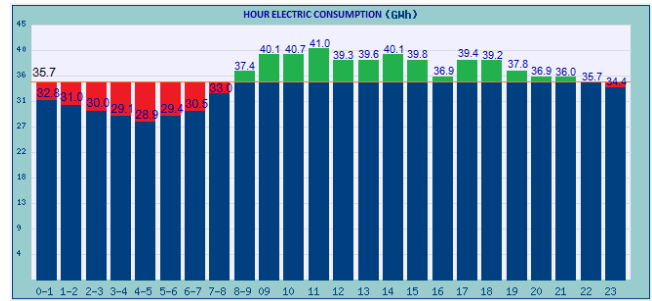


Fig.4. Balanced energy consumption graph using vehicle batteries for the day of 11.01.2018 [17].

Electric vehicle batteries can be charged by the power grid at times of low consumption. In the hours when energy demand on the power grid is above the average value, this excess demand can be supplied by electric vehicle batteries. Thus, the 24-hour energy demand can be held on average value.

A. Mobile application design for the proposed system

It is an important problem that charging of the vehicles causes overloading in the power grid. With smart parking system designed for EVs and HEVs, overloading of the power grid is prevented by the automation system capable with energy management during the charging of vehicles. The designed smart vehicle parking lot system has 16 vehicles capacity and 8 charge stations. With the developed interface software, the users are guided and it is expected that the charging procedure desired by each user will be set into the program. The mobile application has been designed with several features such as reservation, location of the closest parking lot, battery charge status monitoring, and battery sharing for deriving a profit and etc. Mobile application screens of the proposed smart parking lot system are shown in Figure 5.



Fig.5. Some of the mobile application screens

Users often prefer vehicle park lots near their offices or residences to park their vehicles. This preference will not change even if fossil-fueled vehicles are replaced by electric and hybrid electric vehicles. However, EVs and HEVs need to

be charged different from conventional vehicles. This situation should not prevent the efficient usage of the vehicles. If the users can charge their vehicles during parked, there will be no extra waiting time for charging. Thus, the usage efficiency of vehicle is not reduced.

Users who want to charge their vehicles using this system need to create an account first through the mobile application. After the account creation process, the users can perform the booking process for parking and charging the vehicle by detecting the parking lot closest to them. When making a reservation through the mobile application, the user is asked whether request charging, permission for battery sharing as well as the vehicle model, the date and time information. Thus, the users make reservation by giving the necessary information beforehand, without having to come to the parking lot. In addition, the users who have parked the vehicles for charging will be able to monitor the charge status of the vehicles and the battery state of charge online via the application. The consumption values of the vehicles and the payment amounts can be updated instantly and displayed on the system. If necessary, the user will be able to cut charging process online.

An energy management is carried out taking into consideration the reservation and battery sharing information, which is made on a daily and hourly basis. The required energy for the users who make the charging reservation at time when overloading of power grid will be supplied from

the vehicles of the users who give permission for battery sharing. Furthermore, in case of extreme power demand, battery sharing offer is asked to all drivers of vehicles fully charged which will be waiting for long periods in the parking lot. The users who are allowed to share the battery are provided with discounts at a considerable rate. Thus, the battery sharing is encouraged.

B. Automation System of Smart Parking Lot

The block diagram of the control structure for energy management and monitoring of the proposed smart parking system is shown in Figure 6. In the system, the data of the charging stations and the energy demand values are collected and controlled by PLC. Communication network have been also established to increase the accessibility of the system among operator panel, PC and mobile application.

The priority of the developed algorithm is that perform the requested charging process on the scheduled time for all vehicles in the parking lot. However, there are many other factors to consider when providing this. While the number of vehicles dependent on electricity increases, the power grid loading factor increases with same rate. Some methods need to be developed to compensate or balance this increase such as installing new power generation plant, increasing energy efficiency, design efficient energy management systems.

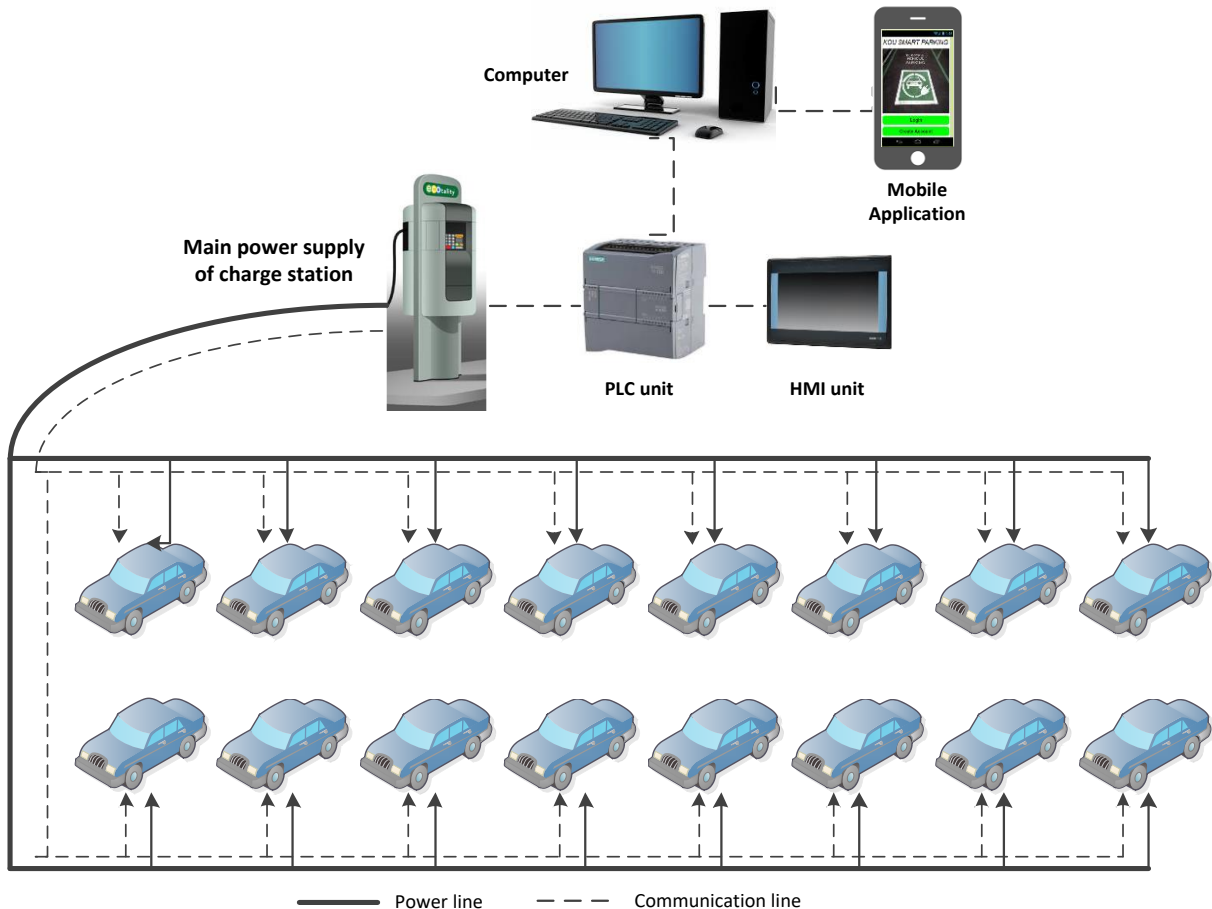


Fig.6. The proposed automation system block diagram

The proposed system algorithm performs control of the energy management and charging schedule by considering the data obtained from the operator panel or via the mobile application. Apart from the data obtained from the application, it also evaluates the instantaneous demand situation of the power grid. In this way, it is decided how and which source that the energy required to charge vehicles will be supplied. In addition, state of charge of the vehicle battery is taken into account. The algorithm uses the battery capacities of the vehicles previously entered into the system when calculating the charging time. The proposed control algorithm of the smart parking lot system is shown in Figure 7.

First, it is checked whether a user who want to charge the vehicle has made a reservation through the mobile application. If no reservation is made, it is checked whether there is a suitable parking lot available. If no reservation is made and there is no suitable parking lot space, charging cannot be carried out. However, if there is a parking lot space, charging service can be provided.

Users are encouraged to make reservations in advance. Thus, daily energy demands can be predicted and necessary actions can be taken. If the user has made a prior reservation, parking usage and charging process can be started at the planned time.

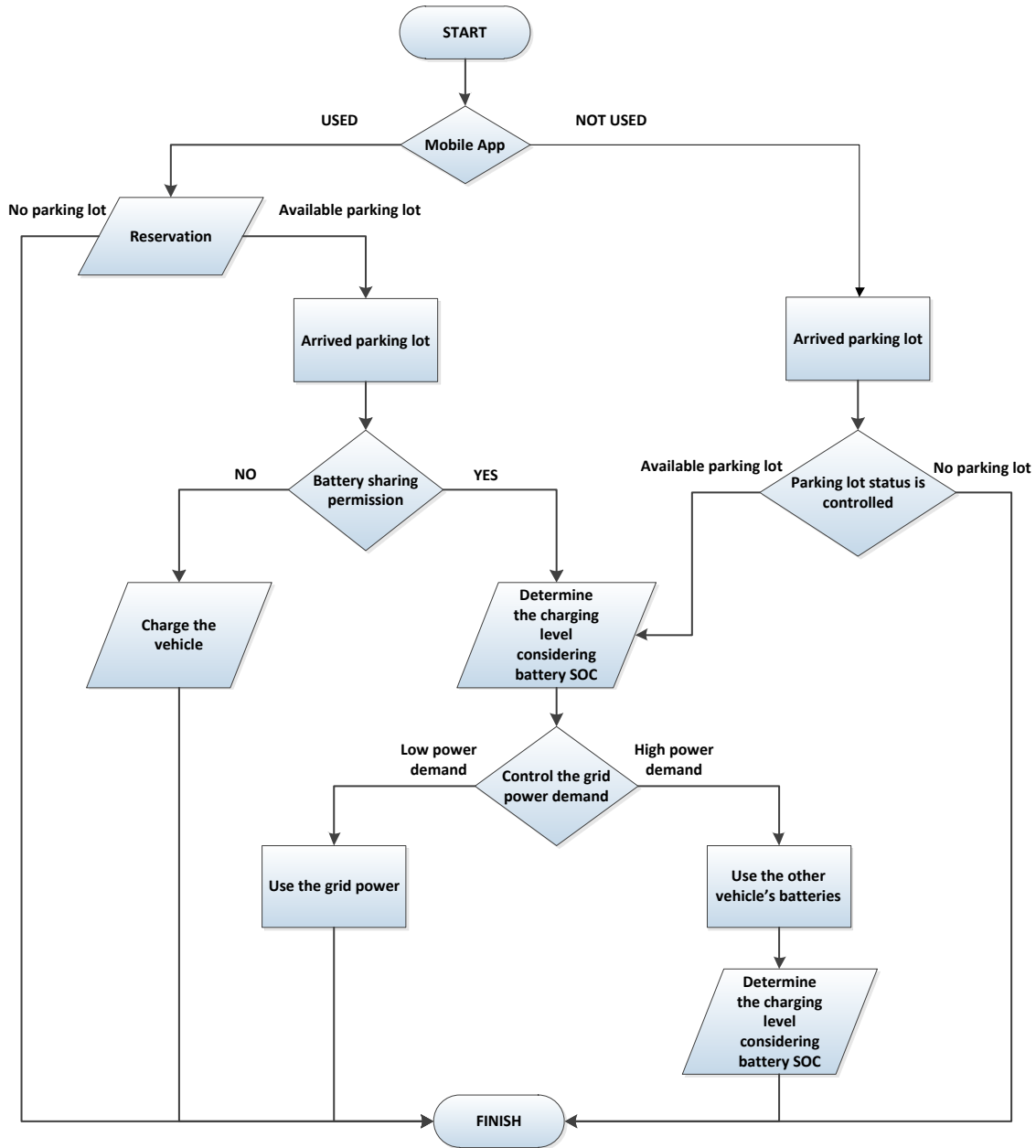


Fig.7. The proposed control algorithm of the smart parking lot system

Battery sharing approval may be given through the mobile application during or after the reservation process. If battery sharing permission is given, it ensures positive results for both

the users and the power grid. Besides the users derive a profit and overloading of the power grid is prevented by means of the battery sharing option.

IV. CONCLUSION

The widespread usage of electric and hybrid electric vehicles will reduce environmental pollution rate and the use of fossil fuels. In addition, there will be positive results such as reduced energy costs, improved driving and comfort features. However, besides the positive aspects mentioned above, long charging time, insufficient number of charge stations, additional load on the power grid and disruption of the power quality are disadvantages emerged by using EVs and PHEVs. The proposed smart parking lot system offers solutions to some of these problems. The smart parking lot system ensures optimum power flow between vehicle battery and power grid. In the proposed system, charging service to users who want to charge their vehicles during the hours when electricity consumption reached peak value is aimed to perform without overload to the power grid. In cases of that the energy demand from power grid is high, the required energy are supplied by the battery of vehicles which is given permission to share. The more users give permission to share of the battery, the more effective balance of the power demand can be achieved. Therefore, users should be encouraged to share battery. Encouragement of users to share battery can be increased by discount of fee or providing a profit.

Referring to the hourly energy consumption in Turkey, the energy consumption changes depend on energy demands of daytime and night. By means of the proposed system, the vehicles are encouraged to be charged at night. In the daytime hours, the vehicles that are required to be charged in the parking lot are charged by using the energy in the batteries of other unused vehicles instead of the power grid. Thus, energy demand to vehicle charging from the power grid is minimized. At this point, electricity generation and distribution companies will not have to increase the energy production capacity. In addition, system components such as transformer and transmission lines are prevented to strain during peak times.

ACKNOWLEDGMENT

Koray ERHAN is supported by ASELSAN Graduate Scholarship for Turkish Academicians.

REFERENCES

- [1] T.Appenzeller, *End of cheap oil*, National Geographic Online Magazine, 2004, Available: <http://ngm.nationalgeographic.com/ngm/0406/feature5/>, 01.03.2018.
- [2] Y. Gürbüz, A. A. Kulaksız, "Elektrikli araçlar ile klasik içten yanmalı motorlu araçların çeşitli yönlerden karşılaştırılması", *Gümüşhane Üniversitesi Fen Bilimleri Enstitüsü Dergisi*, Vol.6, No.2, 2016, pp.117-125.
- [3] N. Adrenacci, R. Ragona, G. Valenti, "A demand-side approach to the optimal deployment of electric vehicle charging stations in metropolitan areas", *Applied Energy*, Vol.182, No.1, 2016, pp.39-46.
- [4] <https://spectrum.ieee.org/energywise/green-tech/fuel-cells/storedot-wants-to-charge-your-ev-in-5-minutes>, Available: 3.06.2015.
- [5] S. Deilami, A. S. Masoum, P. S. Moses, M. A. S. Masoum, "Real-Time Coordination of Plug-In Electric Vehicle Charging in Smart Grids to Minimize Power Losses and Improve Voltage Profile", *IEEE Transaction on smart grid*, Vol.2, No.3, 2011, pp.456-467.
- [6] T. Kupka, M. Patt, "Hybrid Photovoltaic Inverter for Smart Grids", *Balkan journal of electrical & computer engineering*, Vol.2, No.1, 2014, pp.20-22.
- [7] A. Keskin, *Hibrit Taşıt Teknolojileri ve Uygulamaları*, Mühendis ve Makine, 2009, pp. 12-20.

- [8] C. C. Chan, "The state of the art of electric, hybrid and fuel cell vehicles", *Proceedings of the IEEE*, Vol.95, No.4, pp.704-718.
- [9] TEPCO (2010-03-15). "General Outline of CHAdeMO Association".
- [10] Volker Lazzaro (2010-02-14). "The interface between the electric vehicle and infrastructure"p13.
- [11] SAE Electric Vehicle Conductive Charge Coupler, SEAJ1772, Rev.Month01.
- [12] N. H. Kutkut, D. M. Divan, D. W. Novotny, "Design considerations and topology selection for a 120-kW IGBT converter for EV fast charging", *IEEE Transactions on Power Electronics*, 1998, Vol.13, No.1, pp.169-178.
- [13] I. A. Khan, "Battery chargers for electric and hybrid vehicles", *Power Electronics in Transportation*, 1994, proceedings, pp.103-112.
- [14] S. Dhameja, *Electric Vehicle Battery Systems*, Newnes Press, 2002, p.4-30.
- [15] S. Yardım, "Bölgesel otopark yönetimi", 1. Kentiçi ulaşımında otopark politikaları ve uygulamaları konferansı, 2009, pp.90-107.
- [16] T. Litman, *Parking management best practices*, American planning association, Victoria Transport Policy Institute, 2006.
- [17] <http://www.enerjiatlasi.com/elektrik-tuketimi/>, available: 01.03.2018.

BIOGRAPHIES



Koray ERHAN (Research Assistant) was born in 1987 in Turkey. He received his B.Sc. in Electrical Engineering from Yıldız Technical University, Turkey in 2010. Then he completed his MSc in Electrical Engineering at Istanbul Technical University in 2013. He became a Research and Teaching assistant in 2010 at Istanbul Technical University. Then he has transferred to Kocaeli University as a Research and Teaching assistant in 2013. He is already continues his PhD education in

Energy Systems Engineering at Kocaeli University. He has published many papers in different subjects including photovoltaic power generation systems, renewable energy sources, energy storage technologies, smart grid integration, automation systems and electrical, hybrid electrical vehicles. He has been a referee in SCI and other indexed journals. He is currently holding position of research assistant at Kocaeli University.



Murat AYAZ received his B.S., M.S., and Ph.D. degrees from the Department of Electrical Education, Kocaeli University, Kocaeli, Turkey, in 2005, 2008, and 2015, respectively. Between 2005 and 2009, he worked as a project engineer in Beck & Pollitzer, Kocaeli, Turkey. From 2009 to 2015, he served as a research assistant in the Electrical Education Department of Kocaeli University, Kocaeli. Currently, he is an assistant professor at Electric and Energy Department of Kocaeli

University. His current research includes design of electrical machines, hybrid electric vehicles, and industrial automation systems.



Yusuf ICER was born in 1992 in Turkey. He received his B.Sc. in Energy Systems Engineering from Kocaeli University, Turkey in 2016. He is already continues his Master education in Energy Systems Engineering at Kocaeli University.

The FIR Filter Design based on Genetic Algorithm

Z. B. GARIP, and A. F. BOZ


Abstract— Especially, in the signal and image processing fields of electronics, filters are most often used parts. Also, rapid advances in digital systems have expanded the use of digital filters. Therefore, it is very important to understand and learn the filters and calculation of their coefficients. Thus, in this work, interactive graphical user interface software which can be used for educational purposes and also accessible via the Internet is designed in the MATLAB environment. In the software, genetic algorithm, which is one of the popular methods in recent years, is used for designing the Finite Impulse Response (FIR) filters. In this program, when the parameters of filter, which will be designed, are entered by the user, the coefficients are obtained from genetic algorithms, and many features of the filter are presented numerically and graphically. Thus, the FIR filter design can easily be carried out for practical or educational purposes using the software. Further, the superiority of the genetic algorithm over the classical design in this field has been shown by comparing the obtained filter coefficients for both methods.

Index Terms— Digital filters, genetic algorithms, FIR filter

I. INTRODUCTION

FILTERING is a fundamental process in the field of electrical and electronics including signal and image processing. Analog and digital filters are used in this field for selecting the desired frequencies, suppressing the undesired noises etc. Rapid advances in the digital electronics have increased the use of digital filters as well as advantages of them. Amongst the advantages of the use of digital filters, low costing, adjusting or changing the filter parameters or structures using only software etc. can be counted. Thus, Finite Impulse Response (FIR) and Infinite Impulse Response (IIR) filters have established themselves in very general application areas.

Today, there are many methods available for obtaining the FIR or IIR filter coefficients [1-4]. It is required to design higher degree filters for obtaining almost ideal frequency responses. On the other hand, increasing the degree of the filters brings many difficulties in the design processes.

Z. B. GARIP is with the Institute of Natural Sciences, Sakarya University, Turkey (e-mail: zbatik@sakarya.edu.tr) 

A. F. BOZ is with the Faculty of Technology, Electrical-Electronics Eng. Dept., Sakarya University, Sakarya, Turkey (e-mail: afboz@sakarya.edu.tr)

Manuscript received September 13, 2017; accepted January 08, 2018.
DOI: [10.17694/bajece.410234](https://doi.org/10.17694/bajece.410234)

Genetic Algorithms (GA) are one of the heuristic calculation methods and they have reached the solutions by producing the values from different search points. Also they have used for the situations where the classical calculation methods are insufficient or different solutions ways are required [5-8]. Similarly, using genetic algorithms to obtain filter coefficients is located in [9-12]. In the proposed work, both the classical methods and genetic algorithms have been used for calculation of the FIR filter coefficients.

In this context, the simulator program, which can also be used for educational purposes, has been designed to operate offline. Some parts of the program have been designed using the MATLAB GUI [13] that works offline. In the developed software, FIR filter coefficients can be calculated using both the classical methods and the genetic algorithms in accordance with the criteria set by the user. Many features of the resulting filters such as the list of coefficients, the amplitude response, phase response, unit impulse response, unit step response, root locus, group and phase delays and so on can be displayed both numerically and graphically. This program is also very easily be used for educational purposes. In the program, animation aided filter design theory is presented and students can easily see the effects of the parameters to the filters by simply changing the coefficients. So, the FIR filter design can easily be carried out by using genetic algorithms for whether theoretical or practical purposes, whether offline or online on the web environment.

While the FIR filter designs are summarized in the second part of the paper, the third section provides information on genetic algorithms. The Fourth section gives information about the developed simulator together with the comparative simulation examples. Finally, the results are summarized in the fifth section.

II. FIR FILTER DESIGN

Finite impulse response and linear phase characteristic is given as in the Fig.1. Its output can be obtained by using;

$$y_n = \sum_{i=0}^k a_i \cdot x_{n-i} \quad (1)$$

Filter coefficients can be symmetric or asymmetric according to the center value. Four different types of designs may be carried out (Table 1) [1-4]. FIR filter design methods are usually simple, linear and reliable. Calculation equations of

un-normalized filter coefficients for the ideal FIR filters are given in Table 2[1-4].

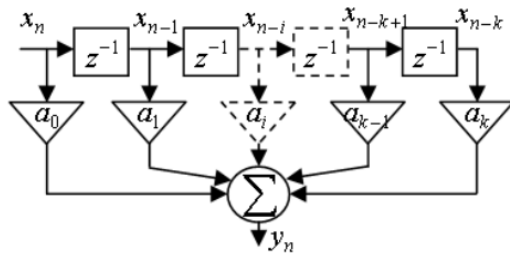


Fig. 1. FIR filter architecture

TABLE 1. FIR FILTER PROPERTIES

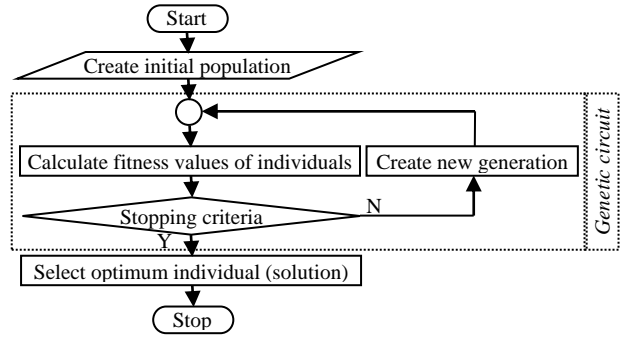
Type	Properties			
	Length of filter	Filter coefficients	Frequency response	
			$\Omega = 0$	$\Omega = \pi$
I.	Odd integer	Symmetric	Even symmetry	Even symmetry
II.	Even integer	Symmetric	Even symmetry	Odd symmetry
III.	Odd integer	Asymmetric	Odd symmetry	Odd symmetry
IV.	Even integer	Asymmetric	Odd symmetry	Even symmetry

TABLE 2. IDEAL FIR FILTER COEFFICIENTS

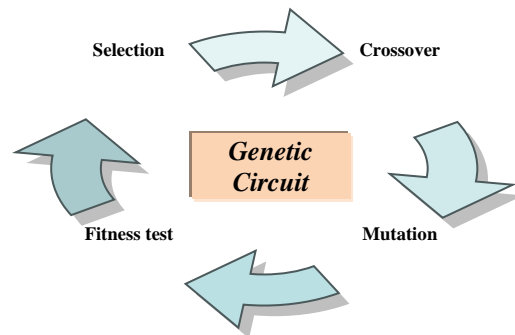
Filter	Center coefficient	Other coefficients
Low-pass	$h[0] = \frac{\omega_c}{\pi}$	$h[n] = \frac{\sin(n\omega_c)}{n\pi}$
High-pass	$h[0] = 1 - \frac{\omega_c}{\pi}$	$h[n] = -\frac{\sin(n\omega_c)}{n\pi}$
Band-pass	$h[0] = \frac{\omega_{c2} - \omega_{c1}}{\pi}$	$h[n] = \frac{\sin(n\omega_{c2}) - \sin(n\omega_{c1})}{n\pi}$
Band-stop	$h[0] = 1 - \frac{\omega_{c2} - \omega_{c1}}{\pi}$	$h[n] = \frac{\sin(n\omega_{c1}) - \sin(n\omega_{c2})}{n\pi}$

III. GENETIC ALGORITHM

Genetic algorithms, which is a heuristic method based on the nature of evolutionary / biological process, is developed and used for the first time in 1975. The genetic algorithms, which are a part of evolutionary computation, are an iterative and probabilistic solution method that emerges by modeling the relevant process. They use random search techniques for the solution and they are based on the parameter encoding. The genetic algorithms are used in the solution of optimization problems from different fields, such as in the information systems, in the machine learning and so on [5], [14]. Stages of the solution with genetic algorithms can be summarized as in the Figure 2.



(a) Flow chart



(b) Genetic circuit

Fig. 2. Genetic algorithms

IV. DESIGNED SIMULATOR AND SIMULATIONS

In this study, an offline and online working FIR filter design simulator has been developed. The main screen capture of the simulator software that works offline is given in Fig. 4. In this module, the filter (LPF, HPF, BPF and BSF) and the coefficient type (symmetrical, asymmetrical) are selected and their parameters (filter order, sampling frequency, the lower / upper cut-off frequency) are entered. By arranging the genetic algorithm settings using main menu options of the simulator (population size, the fitness scaling function {linear, proportional, top, rank}, selection function {remainder, uniform, roulette, tournament, stochastic uniform}, mutation function {uniform, Gaussian, adaptive}, crossover function {heuristic, intermediate, single point, two point, arithmetic, scattered} and crossover fraction), desired FIR filter design using both the classical methods and genetic algorithms can be obtained in the simulator.

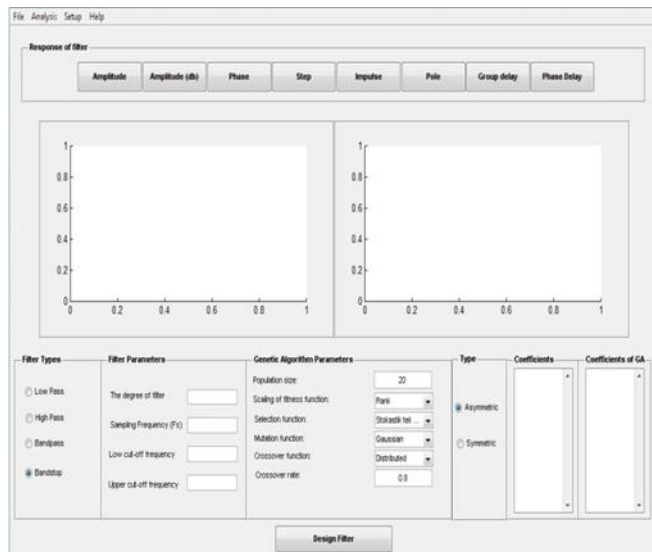
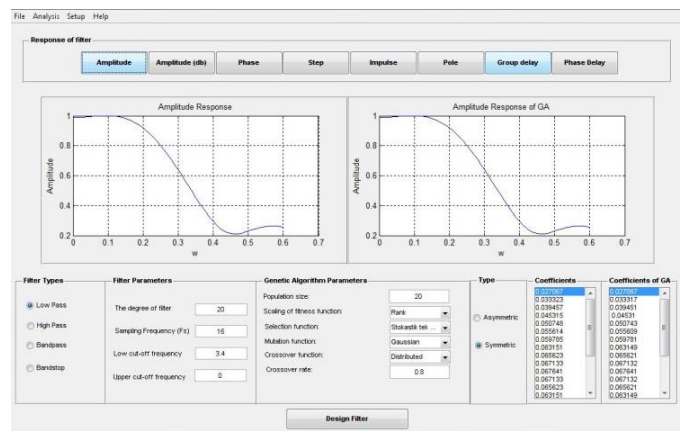


Fig. 4. Main screen capture of the offline working simulator

As an example, simulation design and results screen captures of a low pass filter are given in Fig 8. In the example, degree of the filter was chosen 20, low cut-off frequency was 3.4 kHz and it was assumed that the filter has symmetrical coefficients.



(a)

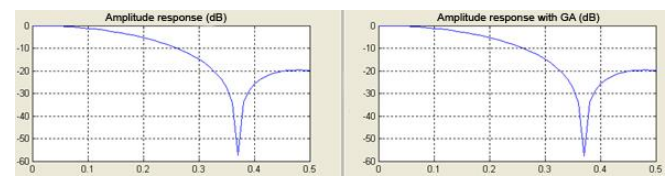
First of all, fitness functions are prepared for obtaining the selected filter coefficients using the genetic algorithms. Optimization procedure can be implemented after the genetic algorithm settings/options are organized. For example, the MATLAB codes are given in Fig 5 according to LPF equations, which are given in Table 2, and the optimization result is given in Fig 6.

```

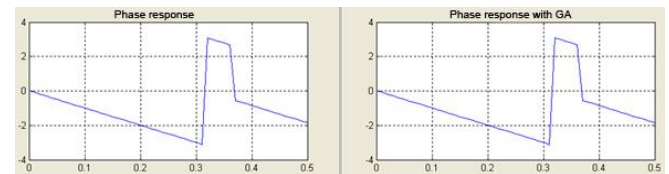
% Fitness function for center coefficient of LPF
function y=h0_lpf(k)
global wc1
y=((k*wc1)/(k*pi));
end

% Fitness function for other coefficients of LPF
function y=hn_lpf(k)
global wc1
y=(sin(k*wc1)/(k*pi));
end
    
```

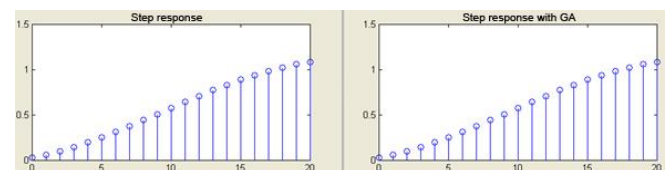
Fig. 5. Sample fitness function codes



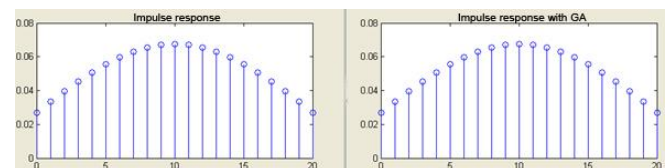
(b) Amplitude response of the low-pass filter (db)



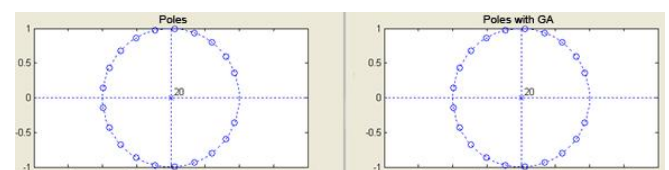
(c) Phase response of the low-pass filter



(d) Step response of the low-pass filter



(e) Impulse response of the low-pass filter



(f) Poles of the low-pass filter

Fig. 7. Screenshots of the LPF design simulation example

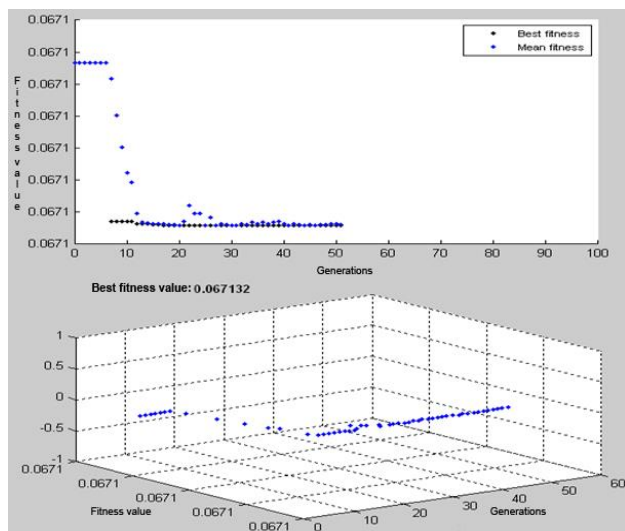


Fig. 6. Result of optimization example

V. CONCLUSIONS

In this work, a simulator program has been developed for designing the FIR filters. Developed software allows user to design the FIR filter using the classical and genetic algorithm methods. It offers many features of the filter both graphically and numerically. Filters with the desired characteristics can be designed and compared quickly, effectively, and easily by using this software and thus it can also be used for educational purposes. As a future work, it is considered to include IIR filter design module.



Ali Fuat BOZ received B.Sc. degree in Electronics Education Department from Gazi University, Ankara, Turkey and Ph.D. degree in Control Engineering from the University of Sussex, Brighton, U.K. He has been with the Sakarya University, Turkey, Faculty of Technology, and Electrical-Electronics Engineering Dept. as a Professor. He performs research in the areas of control systems, engineering education, circuits and systems.

REFERENCES

- [1] S. Winder, Analog and Digital Filter Design, Second Edition, -Newnes, USA, 2002.
- [2] W.-K.Chen (Ed.), The Circuits and Filters Handbook, Second Edition CRC Press, 2003.
- [3] V.K. Ingle, J.G. Proakis, Digital Signal Processing Using MATLAB ,V.4, PWS Publishing Company, Boston, 1997
- [4] L. Thede, Practical Analog and Digital Filter Design, Artech House Publication, 2004
- [5] D.E. Goldberg, Genetic Algorithms in Search Optimization and Machine Learning, Addison Wesley, 1989
- [6] S. Duman, A. Öztürk, Robust Design of PID Controller for Power System Stabilization by Using Real Coded Genetic Algorithm, International Review of Electrical Engineering (IREE), vol. 5 n. 5, pp. 2159– 2170, 2010.
- [7] M. Eslami, H. Shareef, A. Mohamed, M. Khajehzadeh, Damping of Power System Oscillations Using Genetic Algorithm and Particle Swarm Optimization, International Review of Electrical Engineering (IREE), vol. 5 n. 6, pp. 2745 – 2753, 2010.
- [8] M. Rashidi, F. Rashidi, Power System Stabilizer Tuning Using Multi-Objective Genetic Algorithm, International Review of Electrical Engineering (IREE), vol. 6 n. 4, pp. 356 – 363, 2011.
- [9] A. Dey, A. Saha, S. Saha, S.A. Ghosh, A Method of Genetic Algorithm (GA) for FIR Filter Construction: Design and Development with Newer Approaches in Neural Network Platform, International Journal of Advanced Computer Science and Applications, vol. 1, no. 6, 2010
- [10] S. Goyal, J. Raina, Design of Low Power FIR Filter Coefficients Using Genetic Algorithm, vol. 1, no. 2, pp. 1-5, 2010.
- [11] A. Ahmad, Design of Digital Filters Using Genetic Algorithms, Ph.D. dissertation, University of Victoria, Electrical and Computer Engineering, 2010.
- [12] D. Suckley, Genetic algorithm in the design of FIR filters, IEE Proceedings-G, vol. 138, no. 2, 1991.
- [13] The Matworks, MATLAB 2008
- [14] J.H. Holland, Adaption in Natural and Artificial Systems, Cambridge, MA, MIT Press, 1975.

BIOGRAPHIES



Zeynep B. GARIP received B.Sc. and M.Sc. degree in Electronics and Computer Education Department from Sakarya University, Sakarya, Turkey. She has been with the Sakarya University, Institute of Natural Sciences as a Research Assistant. She performs research in the areas of software development, mechatronics, robotic.

Transmission of Audio Signal from Reed-Solomon AWGN Channel Using Wavelet Transform Families


S. Karagol, and D. Yildiz

Abstract— Mobile communication has become an important part of our daily lives for voice communication, data sharing and access over the Internet. Mobile communication is an open network, so maintaining the privacy and reliability of data has always been anxiety. The reliability of the data against channel noise can be achieved by various error correction codes. The primary purpose of the channel coding process is to reduce the effect of disturbing influences to the minimum level. In this way, the receiver will be able to receive the data sent by the transmitter with the minimum error. In this research paper, it is required to acquire two audio signals with 8 bits of resolution and 8 kHz sampling frequency for 5 seconds in MATLAB. In the first part of this study, Reed-Solomon (RS) Coding Method was used to transmit two audio data recorded in .wav format with minimum error. Binary Phase Shift Keying (BPSK) modulation was used as the modulation method. The Bit Error Rate (BER) performance curve was plotted and the difference between the original and the received signal was observed. According to the BER performance curve, as the signal to noise ratio increases, less false data is received at the receiver. In the second part of the study, four wavelet transform families at different levels were applied to the audio signal, and the performances of these classes were compared.

Index Terms— Audio Signal, Channel Coding, Reed-Solomon Coding, Wavelet Transform Families.

I. INTRODUCTION

TO TRANSMIT data along the channel, the digital information is converted into electrical impulses or waveforms. This process is called channel coding. Channel coding aims to bring a digital signal into conformity with the physical characteristics of the transmission channel and to ensure synchronization in the receiver [1]. The other purpose of the channel coding process is to reduce the effect of some disturbing elements that the data has encountered in the transmission phase as much as possible. The process ensures that the data is delivered to the receiver with minimum error.

S. KARAGOL is with Department of Electrical and Electronics Engineering, Ondokuz Mayıs University, Samsun, Turkey, (e-mail: serap.karagol@omu.edu.tr) 

D. YILDIZ, is with Department of Electrical and Electronics Engineering, Ondokuz Mayıs University, Samsun, Turkey, (e-mail: dogan.yildiz@omu.edu.tr)

Manuscript received September 13, 2017; accepted January 08, 2018.
DOI: [10.17694/bajece.410238](https://doi.org/10.17694/bajece.410238)

The Reed-Solomon (RS) coding is one of the error correction methods that can be used to obtain the message properly. This form of transmission is commonly known as the Forward Error Correction (FEC) [2]. An error correction code comprises of algorithms and techniques that include two basic operations which are encoding and decoding [3]. Recently, several studies have been carried out using different channel coding methods in order to realize data transmission with minimum loss. Miah and Rahman [4] used a wireless communication simulator that included Gray coding, modulation, different channel models (frequency selective fading channels, smooth fading channels, Additive White Gaussian Noise (AWGN)), channel estimation, adaptive equalization and demodulation. Subsequently, they tested the effects of different channel models on transmitted data using Quadrature Phase Shift Keying (QPSK) schemes at the receiver. In [5], a system for data transmitting over a mobile audio channel based on the M-Phase Shift Keying (M-PSK) modulation with optimized parameters was proposed. Rashed et al. [6] investigated the effects of Cyclic Residual Codes and convolutional codes on the transmission performance of audio signals from AWGN and Rayleigh, Rician faded channels. In [7], measuring voice quality in VOIP communication was aimed. More specifically, besides the channel coding and compression methods, the effect of wireless channel conditions on the quality of the voice signal received was investigated.

In the study of [8], audio signal that is 5 sec and in .wav format where each sample was expressed with 8 bits that has 8 kHz sampling frequency was recorded in the MATLAB environment. This obtained audio signal was coded with the Cyclic Coding Method by applying to the AWGN noisy channel. Binary Phase Shift Keying (BPSK) is used for the modulation of the audio signal. Finally, the difference between the original signal and the received signal was observed by drawing the Bit Error Rate (BER) performance curve. In [9], Bhatti used Reed-Solomon coding and Code Division Multiple Access (CDMA) methods unlike in [8].

Wavelet transforms have also been used in some topics on channel coding. In the study [10], a wavelet-based voice-coded communication system was applied to compress the size of the audio signal and the performance evaluation of this algorithm was performed. In [11], some applications of Discrete Wavelet Transform (DWT) have been described for the problem of extracting information from non-speech sounds.

In the first part of this study, two audio signals were recorded for 5 sec, in .wav format where each samples were expressed with 8 bits that has 8 kHz sampling frequency in MATLAB environment. These obtained audio signals were coded with the Reed-Solomon Coding Method by applying to the AWGN noisy channel. Binary Phase Shift Keying (BPSK) was used for the modulation of the audio signals. After modulating with BPSK, CDMA encoded signals were spread. The signals were then dispread and demodulated after passing through the AWGN channel. Finally, the differences between the original signals and the received signals were observed by drawing the Bit Error Rate (BER) performance curve. In the second part of the study, four wavelet transform families at different levels were applied to the audio signals and the performances of these classes were compared.

II. AUDIO TRANSMISSION STEPS

In this study, the five second length audio signals are passed through the steps of sampling, quantization and A/D conversion and AWGN noisy RS coded channel.

A. Channel Coding

The main aim of the channel coding process, which has an important place in communication systems, is to reduce transmission errors. Therefore, the coding made for this aim can also be called error control coding. To minimize the error in communication systems, control bits which contain no information and only provide error checking are added to the data directory. Since the added control bits do not contain information, redundancy occurs in the transmitted data. If the receiver decodes each bit independent from the others, it decides on the majority of the information bits. This is also a method for reducing the error to the minimum.

In this study, Reed-Solomon coding method is used for channel coding process.

B. Reed-Solomon Codes

Irving Reed and Gus Solomon published a paper in the Journal of the Society for Industrial and Applied Mathematics in 1960 [12]. These codes are used in many applications today due to their powerful performances. As example of these applications, compact disc players and deep space applications can be shown.

Reed-Solomon (R-S) Codes are cyclic and non-binary codes. They have symbols consisting of m -bit arrays where m is an integer greater than 2. R-S (n, k) codes on m -bit symbols exist for all k and n for which

$$0 < k < n < 2m + 2 \quad (1)$$

In Eq. (1), the symbol k represents the number of data symbols being encoded and n represents the total number of code symbols in the encoded block.

For conventional R-S (n, k) code,

$$(n, k) = (2m - 1, 2m - 1 - 2t) \quad (2)$$

where t is the symbol-error correcting capability of the code and $n - k = 2t$ is the number of parity symbols.

The distance between two code words in non-binary codes is defined as the number of different bits in the sequences. For Reed-Solomon codes, the code minimum distance is given by

$$d_{\min} = n - k + 1 \quad (3)$$

The code can correct t bits or fewer errors than t bits and any combination of these errors, where t can be stated as

$$t = \left\lfloor \frac{d_{\min} - 1}{2} \right\rfloor = \left\lfloor \frac{n - k}{2} \right\rfloor \quad (4)$$

and $\lfloor x \rfloor$ represents the largest integer less than x . Eq. (4) for R-S codes shows that up to $2t$ bit parity symbols are needed to correct the t bit symbol error. The decoder has $n - k$ redundant symbols for error correction. A redundant symbol is used to locate each error. Another redundant symbol is used to find the correct value of the faulty value.

In implementation of (255, 251) code, it is desired to correct up to 3 symbol errors i.e. $t = 2$ and $m = 8$ which is the number of data bits per symbol. Numerically, it can be expressed as from Eq. (5).

$$(n, k) = (2^m - 1, 2^m - 1 - 2t) \quad (5)$$

RS Codes focus on the evaluation of polynomials over the elements in a finite field called as Galois Field (GF) [9]. The primitive polynomial for $m = 8$ is given by

$$f(x) = x^8 + x^4 + x^3 + x^2 + 1 \quad (6)$$

The RS code (255,251) is used in this research study.

C. Pseudo Noise (PN) Sequences and CDMA Implementation

A Pseudo-random Noise (PN) sequence which only includes binary numbers is used in this paper. The receiver should be able to reject other interfering the Spread Spectrum (SS) signals and/or prevent false correlation with CDMA systems [9]. In CDMA implementation, there are only two users i.e. $N = 2$ for this study. The BPSK modulated code functions are used for (255,251) code as

$$\text{Pseudo noise 1} = [0\ 0\ 0\ 1\ 0\ 0\ 1\ 1\ 0\ 1\ 0\ 1\ 1\ 1\ 1];$$

$$\text{Pseudo noise 2} = [1\ 0\ 0\ 0\ 1\ 1\ 0\ 0\ 1\ 0\ 1\ 1\ 1\ 1\ 0];$$

Two audio signals in the form of .wav file are recorded since there are two different data requirements for CDMA application.

III. WAVELET TRANSFORM

Wavelets are a method that can be applied to many different fields including applied mathematics, signal processing techniques, audio and image compression techniques. The

wavelets were first used by Jean Morlet and A. Grossman for geographic information systems. In fact, the basic beginning of the wavelets extends to Joseph Fourier and to his Fourier transformation. With the emergence of Fourier equations after 1807, mathematicians tented to frequency analyzes for signal recognition. In 1977, Esteban and Galand introduced a new filter concept, but in this way the error was high in regaining the main signal [13]. The wavelet term was first used in 1984 by Morlet and Grossman in quantum physics studies [14]. In 1987 Mallat emerged the relation between wavelet and filter groups. Meyer revealed the first wave named his name [15]. This was a function that could be used in continuous applications, as opposed to Haar wavelets. Over the years, Ingrid Daubhecies has become the basis for many of today's application by coming up with set of vertical base wavelet series [16]. Wavelet functions are derived from the main wavelet by varying various parameters.

IV. SIMULATION RESULTS

The five second length audio signals were recorded in MATLAB environment with $f_s = 8$ kHz sampling frequency and 8 bits resolution. The first and second audio signals are shown in Fig. 1 and Fig. 2 respectively. In the second step, amplitude values between -1 and 1 are mapped to the range of 0 to 255 and these values are expressed by the 8 bit binary number system. The signals obtained in the second step are transformed into Galois space and the G generator matrix is formed appropriately. RS channel coding is performed with these components. AWGN is added and the noisy signals are modulated with BPSK in the fourth step. After modulation process through, both audio signals are spreaded by using CDMA. Then, both signals are dispreaded and demodulated

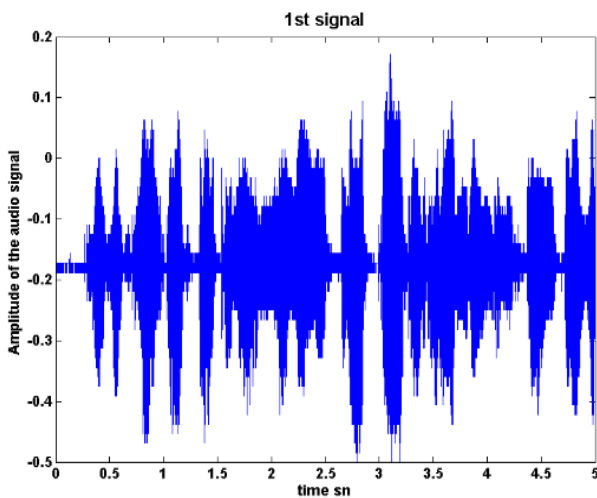


Fig. 1. 1st original signal

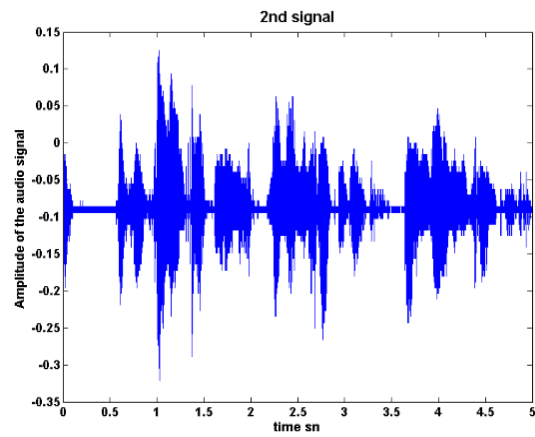


Fig. 2. 2nd original signal

In the second part of the study, four wavelet transform families at different levels were applied to the audio signals and the performances of these classes were compared. Using wavelet transform, instead of the original data, compressed data at different levels is inserted into the designed communication system and obtained signals at the output are observed. For example, the number of samples after compression with first order wavelet transform became 20000 (40000 samples before compression) samples. According to Table I and Table II, the Mean Square Error (MSE) performances of Daubechies wavelet family db1 are the best at level 4 for both signals.

TABLE I.
MSE PERFORMANCES OF WAVELET TRANSFORM FAMILIES FOR SIGNAL 1

Wavelet classes		MSE values			
		1. order	2. order	3. order	4. order
<i>Daubec.</i>	db1	1.03E-05	2.83E-06	1.56E-06	4.40E-07
	db2	4.77E-05	1.46E-04	6.49E-05	7.35E-06
	db3	1.17E-04	1.04E-04	-	-
<i>Symlet</i>	sym1	9.31E-06	4.82E-06	2.26E-06	8.39E-07
	sym2	4.89E-05	1.33E-04	6.10E-05	7.62E-06
	sym3	1.22E-04	1.03E-04	-	-
<i>Coiflet</i>	coif1	1.18E-04	9.95E-05	-	-
	coif2	2.02E-04	9.68E-05	3.24E-05	-
	coif3	1.51E-04	1.01E-04	-	-
<i>Biorth.</i>	bior1.1	1.29E-05	4.59E-06	8.27E-07	4.86E-07
	bior1.3	1.23E-04	1.17E-04	5.26E-05	-
	bior1.5	2.45E-04	1.34E-04	-	-

TABLE II.
MSE PERFORMANCES OF WAVELET TRANSFORM FAMILIES FOR SIGNAL 2

Wavelet classes		MSE values			
		1. order	2. order	3. order	4. order
<i>Daub.</i>	db1	7.39E-06	1.66E-06	2.91E-07	9.64E-08
	db2	1.15E-05	8.78E-06	3.21E-06	6.04E-07
	db3	1.57E-05	7.50E-06	-	-
<i>Symlet</i>	sym1	7.02E-06	2.21E-06	6.03E-07	2.92E-07
	sym2	1.15E-05	7.79E-06	2.68E-06	6.83E-07
	sym3	1.48E-05	6.90E-06	-	-
<i>Coiflet</i>	coif1	1.47E-05	7.65E-06	-	-
	coif2	1.81E-05	5.35E-06	1.66E-06	-
	coif3	1.68E-05	7.42E-06	-	-
<i>Bior.</i>	bior1.1	7.67E-06	2.09E-06	8.54E-07	1.68E-07
	bior1.3	1.60E-05	6.65E-06	2.67E-06	-
	bior1.5	1.92E-05	8.11E-06	-	-

The differences between the received signals and original signals are examined by using BER vs EbNo plot as shown in Fig. 3. The bit error rate varies inversely with the signal noise value.

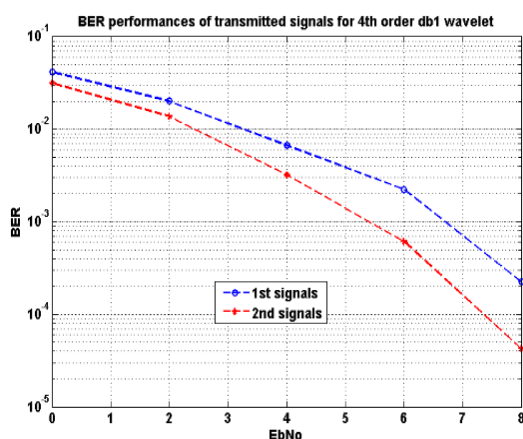


Fig. 3. BER performances of transmitted signals for 4th order db1 wavelet

V. CONCLUSION

According to the obtained results, RS coding method is a suitable method which can be used for channel coding. The BER performance curve is obtained inversely proportional to the signal-to-noise ratio. The coding of the channel by the RS

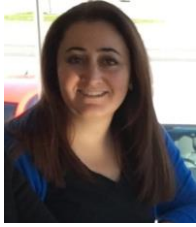
coding method has reduced the error effect of the AWGN in the transmitted operation. In the second part of this study, four wavelet transform families at different levels were applied to the audio signals and the performances of these families were compared. MSE performances were obtained at db1 of the Daubechies wavelet family at the 4th best level for both signals. After the first audio signal is transmitted from the AWGN channel, there is no difference between the transmitted and received audio signal except for some acoustic differences. With RS coding, the sampling frequency can be increased and each sample can be expressed with more bits in order to achieve better performance. However, these increases will lead to a longer transmission of the audio signal from the channel.

REFERENCES

- [1] John G. Proakis and Masoud Salehi, *Digital Communications*, McGraw-Hill Inc., Fifth Edition, p.751, 2008.
- [2] Lin and Daniel J Costello, *Error Control Coding: Fundamentals and Applications*, Englewood Cliffs, Prentice Hall, NJ, p.2, 1983.
- [3] Moreira JC and Farrell PG, *Essentials of Error-Control Coding*, John Wiley & Sons, England, 2006.
- [4] Md. Sipon Miah, M. Mahbubur Rahman, T. K Godder, Bikash Chandra Singh and M. Tania Parvin, "Performance comparison of AWGN, flat fading and frequency selective fading channel for wireless communication system using 4QPSK", *International journal of computer and information technology (IJCIT)*, Vol. 01, Issue 02, pp. 82-90, 2011.
- [5] Béchir Taleb Ali, Geneviève Baudoin, Olivier Venard, "Data Transmission Over Mobile Voice Channel Based on M-FSK Modulation", *Wireless Communications and Networking Conference (WCNC) Proc.*, 2013.
- [6] Md. Golam Rashed, M. Hasnat Kabir, Md. Selim Reza, Md. Matiquel Islam, Rifat Ara Shams, Saleh Masum, Sheikh Enayet Ullah, "Transmission of voice signal: BER performance analysis of different FEC schemes based OFDM system over various channel", *International journal of advanced science and technology*, vol. 34, pp.89-100, 2011.
- [7] Tantioukas Nikolaos, "Effects of the Wireless Channel, Signal Compression and Network Architecture on Speech Quality in VOIP Networks", *Master of Science in Electrical Engineering Thesis*, Naval Postgraduate School Monterey, June 2007.
- [8] Ali Tariq Bhatti, "Cyclic channel coding algorithm for original and received voice signal at 8 khz using ber performance through additive white gaussian noise channel", *International journal of innovative science, engineering & technology (IJSET)*, Vol. 2 Issue 4, pp. 843-852, 2015.
- [9] Ali Tariq Bhatti, Dr. Jung H. Kim, "implementation of reed-solomon (rs) and cdma for signaling a voice through AWGN at 8 KHz sampling frequency using BPSK", *International journal of advent research in computer and electronics (IJARCE)*, vol.2, no.8, pp.13-27, August 2015.
- [10] Thuraya Mahmood Qaradaghi, Fatima Kamil Faek, Diana Hayder Hussein, "Investigating the Effect of Error Correcting Codes on the Compressed Speech Signals", *1st International Conference on Engineering and Innovative Technology, SU-ICEIT 2016*, Salahaddin University-Erbil, Iraq, April 12-14, 2016.
- [11] G. Tzanetakis, G. Essl, P. Cook, "Audio Analysis Using the Discrete Wavelet Transform", *Proc. Conf. Acoustics and Music Theory Applications*, September 2001.
- [12] Bernard Sklar, *Digital Communications Fundamentals and Applications Second Edition*, Prentice Hall P T R Upper Saddle River, New Jersey 07458.
- [13] Croisier, A., Esteban, D., and Galand, C., "Perfect Channel Splitting by Use of Interpolation/Decimation/TreeDecomposition Techniques", *In Proc. Int. Conf. On Info. Sciences and Systems*, Greece, p. 443-446, 1976.
- [14] P. M. A. K. Louis and A. Rieder, *Wavelets Theory and Applications*. John Wiley & Sons, 1997.
- [15] S. G. Mallat, "A theory for multiresolution signal decomposition: the wavelet representation," vol. 11, pp. 674-693, July 1989.

- [16] I. Daubechies, Ten lectures on wavelets, vol. 61 of CBMS-NSF Regional conference series in applied mathematics, Philadelphia, PA: Society for industrial and applied mathematics (SIAM), 1992.

BIOGRAPHIES



SERAP KARAGOL received the B.E. degree in Computer Engineering from the Karadeniz Technical University, Trabzon, Turkey, in 2002, and the M.S. and Ph.D. degrees in electrical engineering from North Carolina A&T State University, Greensboro, NC USA, in 2006 and 2011, respectively. She is currently an Assistant Professor in the Department of Electrical and Electronics Engineering, Ondokuz Mayıs University, Samsun Turkey. She is engaged in teaching and conducting research in circuits and systems, signal processing, modeling, system identification and wireless sensors networks. She is the advisor for more than 10 M.S. and 3 Ph. D. students.



DOGAN YILDIZ born in Istanbul in 1989. He received the B.S. degree in Electrical-Electronics engineering and Mathematics from Fatih University, Istanbul, in 2013 and the M.S. degree in electrical-electronics engineering from Ondokuz Mayıs University, Samsun, in 2016.

Since 2013, he has been working as research assistant with the Electrical-Electronics Engineering Department in Ondokuz Mayıs University. His research interests include wireless sensor networks, localization, signal processing, telecommunication and applications, electromagnetic waves and electromagnetic radiation measurements.

Data Mining Through Data Visualization: A Case Study on Predicting Churners on Telecommunications Data Set


M.S. Başarslan, F. Kayaalp


Abstract— Data mining is the process of extracting meaningful information from a large, raw data. These processes are carried out by various, detailed methods. And, the obtained results are used to make various interpretations and to draw conclusions. Deductions can either be made by interpreting the data after various operations or by plotting the data in various forms of graphs. This type of interpretation over graphics is called data mining through data visualization. Generating graphs that can be used to draw various conclusions on a telecommunications data set with the help of some packages included in the R program is presented in the paper. It does not require upper-level math skills to interpret these graphics; and everyone having knowledge about the industry and data set of the graphs has the ability to plot similar graphs and make analysis and interpretations regarding the results obtained on the data set at hand. In this study, R language was preferred as the software infrastructure for data mining applications, and graphs were plotted for interpretation through data visualization with data mining.

Index Terms— Data visualization with data mining, R, Telecommunications.

I. INTRODUCTION

NOWAYDS various data mining methods are being used to turn large and complex data into usable form of data. Applying these methods requires a certain amount of time. However, the numerical results obtained as a result of these analyses cannot be interpreted easily by everyone. In order to make sense of these results, analysis graphs are plotted to draw conclusions. In this way, interpretations on telecommunications data set is performed using graphs, without any analysis made through the data mining methods. With these graphs, it is aimed to make some deductions that need to be considered in terms of advertising campaigns and campaigns in the telecommunications industry, without even needing an in-depth analysis of the data.

M. S. BASARSLAN, is with Department of Computer Programming, School of Advanced Vocational High School Istanbul Doğuş University, Istanbul, Turkey, (e-mail: mbasarslan@dogus.edu.tr). 

F. KAYAALP, is with Department of Computer Engineering, Düzce University, Duzce, Turkey, (e-mail: fatihkayaalp@duzce.edu.tr). 

Manuscript received September 13, 2017; accepted January 08, 2018.
DOI: [10.17694/bajece.410243](https://doi.org/10.17694/bajece.410243)

In important situations such as presentation and in-house auditing, it can be difficult to access information on complex tables instantly, and it can be difficult to explain the data in the table to the audience. In such cases, visualization of the data to be acquired from the tables provides both convenience and effectiveness in business. This is possible thanks to the graphs plotted through visualization and data mining. In this study, the plotting of the graphs that can be used to draw various conclusions on a telecommunications data set was explained with the help of the packages included in the R program. It does not require upper-level math skills to interpret these graphics; and everyone having knowledge about the industry and data set of the graph has the ability to plot similar graphs and make analysis and interpretations regarding the results obtained on the data set at hand [1].

II. DATA MINING

There are various definitions of data mining. One of the mostly used definitions is obtaining usable information from complex data [2]. Data mining, or the knowledge discovery as called in the literature, is the process of extracting potentially useful and beneficial information in the complex and vast amounts of data. During this procedure, multiple scientific study fields are used. These fields of study are the data management systems, statistics, artificial intelligence and machine learning. The knowledge discovery on the data by combining all these fields together is called data mining [3]-[5]. In short, data mining is the search for relationships and rules in vast amounts of data using computers that will allow us to make estimations about the future [6].

III. VISUALIZATION OF DATA WITH DATA MINING

Data visualization is the gathering of complex and scattered data in the classical format and presenting them in an understandable and interpretable forms through easily identifiable visuals or graphics.

Schematic structures can be abstracted while visualizing the data. Visual elements such as tables and graphs can be used to provide a clear information flow. Thus, cognitive processes such as comparison, interpretation and analysis can be performed more effectively and efficiently [7].

In parallel with technological developments, a continuous increase in the data size is observed. As a result of this

increase, it becomes very difficult to extract meaningful and usable information from the data. Especially the subscriber-based companies like telecommunications, banking, insurance and etc. aim to obtain profitable and efficient information by using the data at hand. For this reason, subscriber-based companies have data analysis departments or outsource this service to data analysis companies. The work done by these departments is to perform visualization by plotting graphs that employees in each unit of the company can understand. By means of data visualization, the data become meaningful without requiring knowledge of mathematics and statistics to interpret the data in an efficient and easy manner.

IV. CUSTOMER CHURN ANALYSIS

In subscriber-based industries, the analysis carried out to prevent loss of existing customers is called churn analysis. It is a method of analysis that is typically used in telecommunications, banking or insurance industries for predicting the churn of current customers so as not to lose the customers. Thanks to these estimates, solutions can be generated within the scope of customer relationship management (CRM) to prevent customer churn. In the literature, the terms customer attrition, customer churn, customer turnover, customer defection are also used for the same concept. Customer churn is of great importance in the subscriber-based industries such as telecommunications, banking, and insurance, because retaining existing customers requires lower cost than gaining new customers in general [8].

V. THE TELECOMMUNICATIONS DATA SET STUDIED

The telecommunications data set includes 8000 customer records and 20 variables which has been taken from one of the major telecommunications company of Turkey for a period of 10 months. The names, explanations and data types of these 20 variables are shown in Table 1.

```
> summary(telekomkat)
 age          age_of_line      tariff_type      device_type      last_reload_year      mmo_count_07
Min.   :16.00  Min.    : 49  Konturlu:5461  Mobil Tel   :3701  Min.    :1900  Min.    : 0.00
1st Qu.:28.00 1st Qu.: 266  Faturelli:2539  Akilli Telefon:3254 1st Qu.:1900 1st Qu.: 0.00
Median :36.00  Median : 705                                     : 786  Median :2013  Median : 15.00
Mean   :38.13  Mean  :1117  Uzb Modem    : 229  Mean   :1981  Mean   :40.63
3rd Qu.:46.00 3rd Qu.:1476  Tablet FC    : 17  3rd Qu.:2014 3rd Qu.: 54.00
Max.   :73.00  Max.  :2935  Modül       : 11  Max.   :2014  Max.  :1049.00
        (Other) : 2

 mmo_duration_07  mmo_non_count_07      mmo_non_duration_07      mmt_count_07      mmt_duration_07
0-2 saat :7245  Min.    : 0.00  0-500 saat :7213  Min.    : 0.00  0-500 saat :7346
2-4 saat : 591  1st Qu.: 2.00  500-1000 saat : 589  1st Qu.: 4.00  500-1000 saat : 415
4-6 saat : 107  Median : 24.00  1000-1500 saat :128  Median : 23.00  1000-1500 saat : 108
6-8 saat :  96  Mean   : 63.87  1500-2000 saat :  94  Mean   : 42.62  1500-2000 saat :  64
8-10 saat :  6  3rd Qu.: 82.00  2000-2500 saat : 16  3rd Qu.: 59.00  2000-2500 saat : 28
10-12 saat : 2  Max.   :1155.00  2500-3000 saat :  7  Max.   :629.00  2500-3000 saat : 16
        (Other) :  3  (Other) : 13  (Other) : 23

 mmt_non_count_07      mmt_non_duration_07      mmo_total_count_07      mmo_total_duration_07
Min.    : 0.00  0-500 saat :7506  Min.    : 0.00  0-500 saat :6104
1st Qu.: 2.00  500-1000 saat : 412  1st Qu.:  6.00  500-1000 saat :1176
Median : 24.00  1000-1500 saat :  88  Median : 23.00  1000-1500 saat :  98
Mean   : 63.87  1500-2000 saat : 16  Mean   :107.6  1500-2000 saat : 163
3rd Qu.: 82.00  2000-2500 saat :  5  3rd Qu.:153.0  2000-2500 saat :  64
Max.   :1155.00  2500-3000 saat :  1  Max.   :1533.0  2500-3000 saat :  51
        (Other) :  2  (Other) :  64

 mmt_total_count_07      mmt_total_duration_07      mmo_count_07      callcenter_count_07      churn_2013_07
Min.    :  0  Min.    :  0  Min.    :  0  Min.    :  0  Min.    :  0
1st Qu.: 19  1st Qu.:1981  1st Qu.:  1  1st Qu.:  1  1st Qu.:  0
Median : 69  Median :10447  Median : 15  Median :  0  Median :  0
Mean   : 97  Mean   :19009  Mean   : 403  Mean   :  0  Mean   :  0.9441
3rd Qu.:138  3rd Qu.:24524  3rd Qu.:172  3rd Qu.:  1  3rd Qu.:  1
Max.   :883  Max.   :808596  Max.   :1644  Max.   :26.0000  Max.   :193
```

Fig.1. Overview of the Data Set

Figure 1 shows a summary of the telecommunication data set.

TABLE I ALL THE VARIABLES, VARIABLES, FORMATS AND TYPES RELATED TO TELECOMMUNICATION DATA SET

Attribute	Description	Data type
age	Age	Numerical
age_of_line	Customer lifetime duration	Numerical
tariff_type	Tariff type (Postpaid, Prepaid)	Nominal
device_type	Device type, Smartphone, Laptop, etc.	Nominal
last_reload_year	Last reload date (for Prepaid subscribers)	Nominal
mmo_count_07	Monthly number of conversations with its own subscribers (Call)	Numerical
mmo_duration_07	Monthly talk time with its own subscribers (Call)	Numerical
mmt_count_07	Monthly number of conversations with its own subscribers (In call)	Numerical
mmt_duration_07	Monthly talk time with its own subscribers (In call)	Numerical
mmo_non_count	Number of Monthly Calls Made with Other Operators (Call)	Numerical
mmo_non_duration	Monthly Talk Time with Subscribers in Other Operators (Call - min.)	Numerical
mmt_non_count	Number of Monthly Calls Made with Subscribes in Other Operators (In call)	Numerical
mmt_non_duration	Monthly Talk Time with Subscribers in Other Operators (In call)	Numerical
mmo_total_count	Number of Total Monthly Calls (Call)	Numerical
mmo_total_duration	Monthly Total Talk Time (Call)	Numerical
mmt_total_count	Number of Total Monthly Calls (Call)	Numerical
mmt_total_duration	Monthly Total Talk Time (In call)	Numerical
msmo_count_07	Number of SMSs per month	Numerical
callcenter_count_07	Monthly Call Center Complaints Call Count	Numerical
Churn_2013_07	Subscriber churned?	Binary

VI. CUSTOMER CHURN ANALYSIS APPLICATION THROUGH VISUALIZATION

In this study, the plotting of the graphs that can be used to draw various conclusions on a telecommunications data set was explained with the help of the packages included in the R program. It does not require advanced-level analytical skills to interpret these graphics; and everyone with professional knowledge on the issue and industry can plot similar graphs and make analysis and interpretations regarding the results obtained on the data set at hand.

In this section, a study on density and violin graphics with the help of the R graphic packages will be discussed [9]. In plotting these graphs, customer lifetime and churn status in a telecommunications operator were grouped and interpreted according to categorical attributes.

A. Graphics Obtained By Density Graphics

In this section, interpretations on the density graph obtained with the ggplot2 package of the R is discussed.

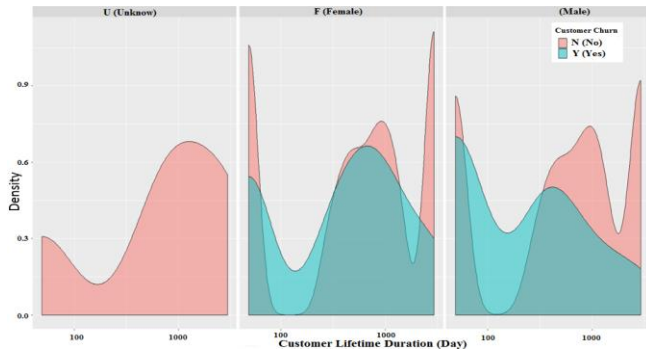


Fig.2. Grouping of Customer Lifetime and Churn Attributes by Gender

Figure 2 shows the churn status of the customers of female, male and unknown gender. According to the graph in Figure 2, churn status yes (Y) of males (M) is more instable than females (F). It is seen that none of the subscribers with unknown gender information churned (N).

Head and shoulders shots of authors which appear at the end of our papers.

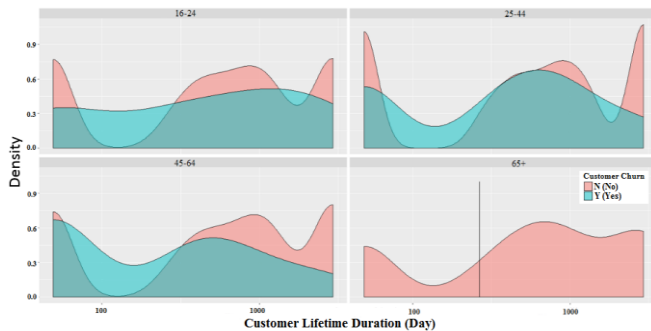


Fig.3. Grouping of Customer lifetime and churn attributes by age

The interpretation that can be made on the graph in Figure 3 is that users over 65 years of age do not churn (N) and use their phones only for making calls. There is a continuous fluctuation in the 16-24 and 25-44 age groups, and it can be said that they probably use smartphones and are looking for various campaigns.

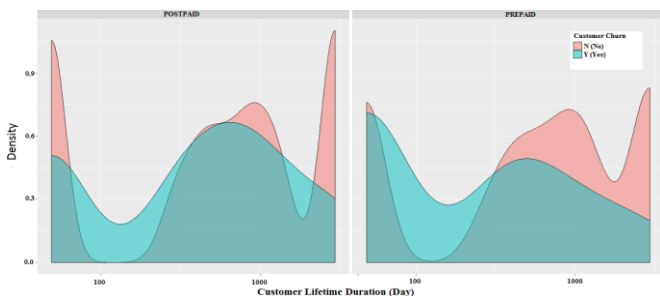


Fig.4. Grouping of Customer lifetime and churn attributes by the subscriber tariff type

Figure 4 shows that the rate of churn is higher in prepaid subscribers than the postpaid subscribers. This may be due to long-term contracts of postpaid subscribers.

B. Graphics Obtained By Violin Graphics

In this section, interpretations on the violin graph obtained with the ggplot2 package of the R is discussed.

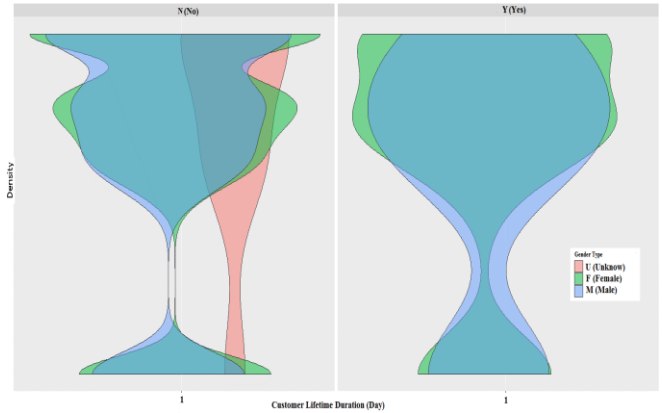


Fig.5. Grouping of Customer Lifetime and Churn Attributes by Gender

It is seen in the not-churned (N) section of the graph in Figure 5 that the churn of subscribers with unknown gender and male subscribers was more unstable than the churn of females. A similar interpretation is also made in the density graph.

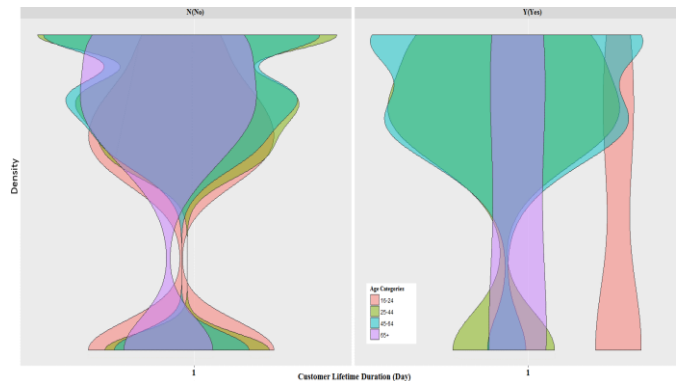


Fig.6. Grouping of Customer Lifetime and Churn Attributes by Age

The graph in Figure 6 shows that users who are over 65 years old are less likely to churn and that they only use their phones for making calls, similar to the interpretation of the density graph. There are various fluctuations in other age groups. Customer churn (Y) is observed to be low in young people in the 16-24 age group compared to the ones in the 25-44 age group.

In the graph in Figure 7, it can be seen that the tendency to churn is higher in prepaid subscribers compared to postpaid subscribers. This interpretation is observed to be the same in the density graph.

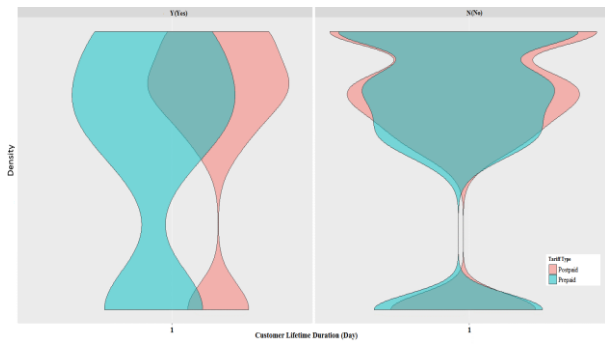


Fig.7. Grouping of Customer Lifetime and Churn Attributes by the Subscriber Tariff Type

VII. CONCLUSION

The main objective of this study is to develop a data visualization application that allows to obtain interpretable graphs without being overwhelmed by data mining methods. In the study, the complementary and verifying results obtained by density and violin packages of the R software were presented by using a telecommunications data set.

In this regard, it is observed that everyone having knowledge about the industry and data set of the graph has the ability to plot similar graphs and make interpretations on the results obtained. Therefore, it is now quite easy to plot and interpret graphs suitable for any data set.

REFERENCES

- [1] M. Kutlu, C. Küçüközmen, F. Çınar, *Büyük Veri Analizi, Görselleştirme ve Risk Yönetimi*, 12 Şubat 2015. [Online]. Available: <https://tr.linkedin.com/pulse/d%C3%BCnya-dillerine-en-son-ve-bir-yenisi-olarak-r-dili-analitik-%C3%A7ınar>.
- [2] Y. Özkan. *Veri Madenciliği Yöntemleri*, Türkiye: Papatya yayıncılık, 2013
- [3] J. Han, M. Kamber, *Data Mining: Concepts and Techniques*, USA: Morgan Kaufmann Publisher, 2000.
- [4] G.S. Gordon M. Berry. *Mastering data mining*, USA: John Willey and Sons, 2000.
- [5] L.B. Ayre, *Data Mining For Information Professionals*, San Diego, California: USA, 2006.
- [6] E. Alpaydın, "Ham veriden altın bilgiye ulaşma yöntemleri," Bilişim 2000 Eğitim Semineri, İstanbul, Türkiye, 2000.
- [7] Anonymous, *Veri Görselleştirme Nedir.*, 15 Mart 2016. [Online]. Available: <http://www.verigorsellestirme.com/veri-gorsellestirme-nedir/>
- [8] S. E. Seker, "Customer churn analysis", YBS Ansiklopedi, Vol. 3, No. 1, 2016.
- [9] W. Hadley, C. Winston, *KMggplot2*, 30 Aralık 2016. [Online]. Access: <https://cran.r-project.org/packages/RcmdrPlugin.KMggplot2>.

BIOGRAPHIES



Muhammet Sinan BAŞARSLAN Received the BS Degree in Computer Science from Düzce University in 2015, the MS Degree in Computer Science from Düzce University in 2017. Currently he is working as an Instructor in Doğuş University. His primary research interests include datamining, machine learning, Internet of Things, Artificial Intelligence and web technologies.



Fatih KAYAALP Received the BS Degree in Computer Science from Marmara University in 2000, the MS Degree in Computer Science from Sakarya University in 2005, and the PhD Degree in Computer Science from Sakarya University in 2014. Currently he is working as an Assistant Professor in Duzce University. His primary research interests include databases, web technologies, computer networks, wireless sensor networks and mobile computing.

Evaluation of Reconfigurable Multiple and Compact Micro-Strip Antennas for MIMO Systems

B. Aslan, O. Dikmen, S. Kulaç and A. M. Elbir

Abstract—In wireless communication systems, the improvement of data rate and quality is a priority as a result of users' requests. During the improvement of these priority situations, there will also be a number of losses in the signals. It is known that the techniques used in large systems to solve such problems are not efficient in small systems like modem. Therefore, when using a smaller system such as a modem, the recommended techniques will have to be different. Multimode antenna designs will be an important alternative for next generation wireless communication systems especially for MIMO systems due to the physical advantages of small antenna structures. In this study, MIMO channel structure is shown and performance analysis and theories of compact micro-strip and reconfigurable multiple antenna designs used for the development of MIMO communication systems are mentioned.


Index Terms—Compact Multimode Micro-strip Antennas, MIMO, Reconfigurable Multiple Antenna Systems.

I. INTRODUCTION

NOWADAYS, great advances are observed with the developing technology in wireless communication field. At the same time, wireless communication is widely used in many industrial environments. The wireless communication system is simply an event that the signal is transmitted from the transmitter to the receiver. The signal between the transmitter and the receiver is transmitted to the user through source coding, channel coding, modulator, demodulator, channel decoding and source decoding [1]. In wireless communication systems, improving data rate and quality performances is a priority as a result of users' requests.

B. ASLAN, was Undergraduate with Department of Electrical Electronics Engineering University of Duzce University, Duzce, Turkey, (e-mail: aslan54batuhan@gmail.com)

O. DİKMEN, is with Department of Electrical Electronics Engineering University of Duzce University, Duzce, Turkey, (e-mail: osmandikmen@duzce.edu.tr)

S. KULAÇ, is with Department of Electrical Electronics Engineering University of Duzce University, Duzce, Turkey, (e-mail: selmankulac@duzce.edu.tr) 

A. M. ELBİR, is with Department of Electrical Electronics Engineering University of Duzce University, Duzce, Turkey, (e-mail: ahmetelbir@duzce.edu.tr)

The reason why data rate and quality cannot be sent at the desired level is the loss of some of the electromagnetic wave that travels in space. This loss situation is described as fading in the literature [2]. Basically, if we consider the transmission between a high-power base station and a mobile station, the elimination of the fading effect of such a system can be achieved by improving the low quality as a result of increasing the power of the base station [3]. However, if we consider this scenario for a modem, it is not possible to make such an analysis in terms of design, cost and electronic materials used for the modem [3]. Several suggestions have been put forward to remove this problem. In one of these proposals in the literature, MIMO systems were introduced. MIMO is basically a phenomenon in which information symbols to be sent are separated from symbols with more than one information without the need for high bandwidth. In this way, by transmitting these separated information symbols to multiple antennas, each symbol will be subjected to different fading, thus achieving gains in terms of efficiency and data rate. At the same time, the complexity of MIMO systems will be proportional to the number of used antennas [4]. Achieving gain such as an efficiency, data rate and low bandwidth is maintained with using variations dimensional process. These variations are achieved by modulation, signal processing and coding techniques [5]. In the literature, diversity is classified into 3 categories. These are divided into time diversity, frequency diversity and spatial diversity. In time diversity, there are divided information symbols. These divided information symbols provide benefits by experiencing fading at different time intervals. In frequency diversity, the available bandwidth is divided into segments and a gain is provided using a sign for each segment. In the spatial diversity, the gain is obtained by dividing the channel into multiple parallel channels by means of multiple antennas [5].

The rest of the paper is as follows: In the second part, MIMO channel structure is mentioned. In the third part, a brief introduction to the micro-strip antennas used in the Compact Multimode Micro-strip Antenna design has been given. In the fourth part, the MIMO antenna solution which can be restructured is mentioned. In the fifth section, the performance evaluation for used design of the Reconfigurable MIMO Antenna is given. In the sixth chapter, scenario of the Compact Multimode Micro-strip Antenna is mentioned theoretically. In the seventh section, a performance analysis of the solution

Manuscript received September 13, 2017; accepted January 08, 2018.
DOI: [10.17694/bajece.410247](https://doi.org/10.17694/bajece.410247)

design Compact Multimode Micro-strip Antenna is explained.

II. MIMO CHANNEL STRUCTURE

MIMO is a channel structure implemented to avoid the need for high gain and high bandwidth. What is important here is that the channel information must be known by the receiver in order for the transmitted information to reach the receiver [6].

Significant differences are observed when the channel capacity for MIMO systems, i.e., data rate, is compared to single-input single-output systems. With the assumption that different MIMO systems with single-input and single-output systems have the same channel losses and that the coding matrix is completely known to the receiver, it is apparent that the performance of MIMO systems is clearly increased in Fig. 1 [6].

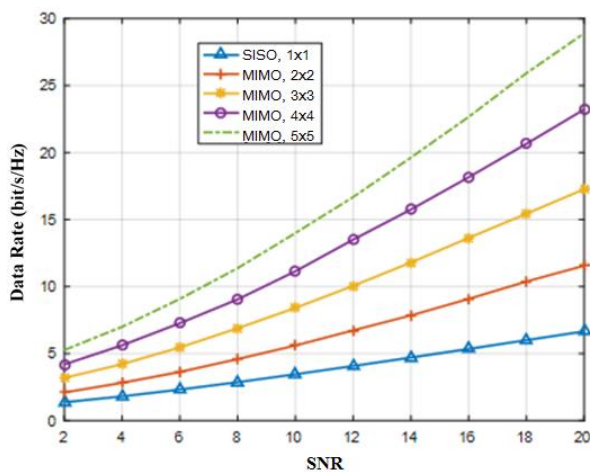


Fig.1. Data rate in MIMO Systems [6]

III. MICRO – STRIP ANTENNAS

In general, micro-strip antennas are the types of antennas that are important to gain the physical dimension. Having a low weight and flexible structure is a great physical advantage [3]. At the same time, having a shielded structure ensures that the deterioration of the assemblies is at a low level. In addition, the narrow frequency band, low output power, difficulty in formulating, and the delicate structure of power fluctuations are known as disadvantages. Fig. 2 is an example of a micro-strip antenna.

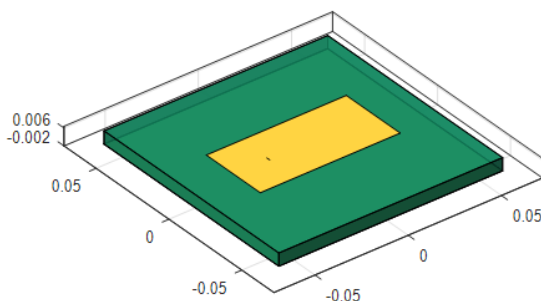


Fig.2. Rectangular micro-strip antenna

IV. SOLUTION OF RECONFIGURABLE MULTIPLE ANTENNA

The radiation pattern obtained in antenna structures used in a standard MIMO system is always stable. The element factor of this pattern is shown as the constant $F(\alpha, \beta)$. Depending on the position of the receiver, the changing factor depending on various parameters such as the radiation angle is denoted as $A(\alpha, \beta)$. The product of these two constants pattern is the main pattern. For the $A(\alpha, \beta)$ pattern, it is possible to improve with various coding techniques. For the $F(\alpha, \beta)$ element pattern, the reconfigurable antenna design is effective. For reconfigurable antenna design, antenna properties such as frequency, pattern, and polarization can be changed dynamically. It is possible to further increase this pattern gain with more than one reconfigurable MIMO antenna array. For a more detailed look at the system, there is a fixed transmitter with M antennas and a mobile receiver with N antennas. Equation (1) is used for the MIMO channel model. Here, the H channel matrix is used in determining the incoming signal. In this matrix, the channel gain coefficients change with the receiver's positional movements. In the MIMO channel structure, the matrix X comprises signal information and the information matrix is obtained from the P pre-coding matrix and the S vector set from the OFDM technique. We can express this with the following equation [7];

$$X = P * S \quad (1)$$

The above-mentioned $A(\alpha, \beta)$ pattern and the P pre-coding matrix can be obtained when properly selected according to the position of the receiver. This method is an application for classical MIMO systems. However, the reconfigurable antenna design has been introduced to change the elemental element $F(\alpha, \beta)$ factor. To this end, switching systems were created by adding diodes to the antenna design. Depending on the case where the pin diodes are conductive or insulator [5], appropriate modes are selected and gain is expected to be changed by changing the $F(\alpha, \beta)$ element factor. That is, the gain according to the position of the receiver will be obtained from both the factors of $F(\alpha, \beta)$ and $A(\alpha, \beta)$. The new gains will also affect the H -matrix due to the change in the pattern in the appropriate mode determined by the receiver's position. Previously, it has been mentioned that the matrix X must be known in the receiver. Due to this reason, the matrix H must also be known in the receiver. However, in order to select the appropriate mode and properly radiation pattern according to the H and P matrices in the transmitter, these matrix gains must also be known by the receiver. Therefore, this information is transferred to the receiver. In this design, which determines and matrices according to the mode of the appropriate k value for each position, three different mode suggestions have been made for the appropriate mode selection. The first one is the predictive mode. In this mode, the H and P matrices are reported to the receiver for all possible states, and the optimal mode is selected accordingly. According to this selection made new pattern is

obtained. In this way, the gain is increased by changing the previously unchanged $F(\alpha, \beta)$ pattern. Second, smart mode. In this mode selection, instead of transmitting each of the H and P matrices that can be generated to the receiver, only the necessary matrices are transmitted. The third mode is fast mode. In this application, it is predicted that a quick selection should be made by creating a data for previously matched matrices [5].

V. PERFORMANCE EVALUATION OF SOLUTION OF RECONFIGURABLE MULTIPLE ANTENNA

Experimental results for the reconfigurable antenna structure are compared with the conventional omni antenna performance in Fig. 3 [5].

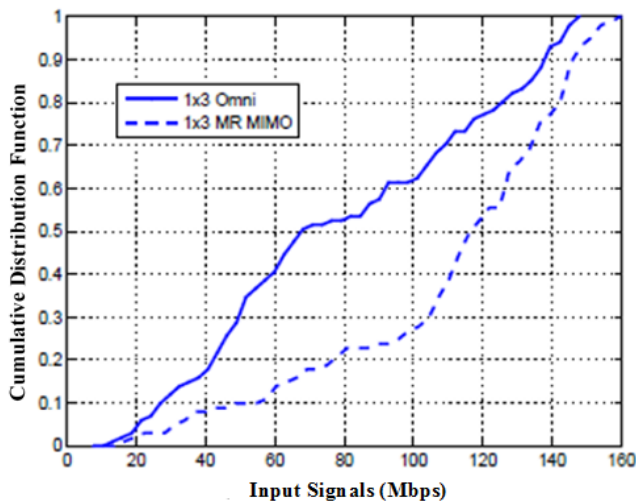


Fig.3. Corridor scenario- 1x3 SIMO [5]

Figure 1 shows the performance enhancement for the used reconfigurable antenna solution structure. However, studies done in the literature have some shortcomings as experimental and performance. In this system, it is seen that a performance improvement has been made in a reconfigurable MIMO antenna solution for systems that do not change the pattern factor of $F(\alpha, \beta)$ compared to a standard non-directional MIMO antenna, when examined on the basis of long distances. If we look at the system more objectively; this system is considered for short distances and the gain values are close to each other when the mode selection gain of the reconfigurable antenna design is compared with the fixed mode MIMO made with the standard directional antenna. Therefore, the situation where the performance gain of this system must be realized at suitable distances is a disadvantage. Besides, there is a mode selection with the assumption that only one user is in the experiments. In a multi-user case, the algorithms needed to select the appropriate mode are complex in the system. This is seen as one of the problems that arise in the development of the system. In cases where smart and fast modes are preferred, the most appropriate mode selection that should be selected introduces the use of intensive artificial intelligence. Here, the loss of the

system load due to the increase of the system load at a certain distance based on the Path-Loss method is apparent from the study in Fig. 4 [6].

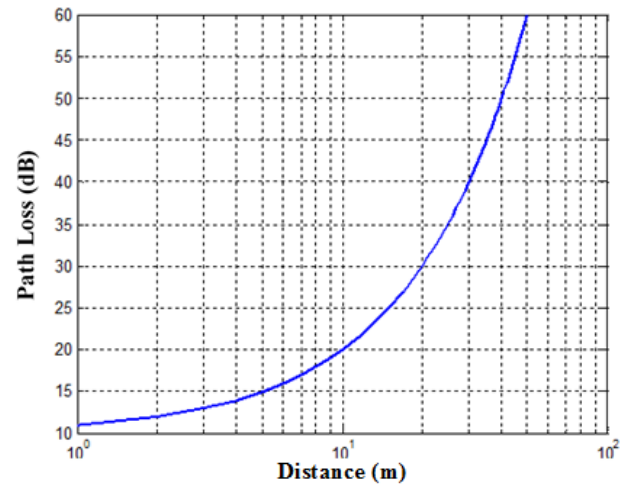


Fig.4. Power loss due to system software and hardware load [6]

In addition, there are some drawbacks to the mode selection operation determined by the position of the user. In the case of any artificial intelligence uncertainty, the pattern will not occur. Accordingly, breaks in the flow of data in correspondence will come into play. And at the same time, it is clear that there is no control of these situations during the system test. These are the disadvantages we have to consider.

VI. COMPACT MULTIMODE MICRO – STRIP ANTENNA

In the literature, a different design is revealed by considering the advantages of micro-strip antennas. A design was created by placing two circular micro-strip antennas with two different modes on top of each other in a suitable position. This solution is a simple system that can be understood as a system because it provides pattern formation over two fixed modes unlike the reconfigurable antenna design. Previously, it was mentioned that micro-strip antennas have good screening and will not affect each other's patterns. However, according to the process performed in this design, since it is desired to obtain a new pattern through two different modes, when the angle of the antenna at the bottom is lower than the antenna at the top, the two antennas disturb each other's patterns. To prevent this, the antenna mode at the bottom is always higher than the antenna mode at the top. According to the design of this antenna, it is seen that performance improvement is achieved in experimental studies [5].

VII. PERFORMANCE ANALYSIS COMPACT MULTIMODE MICRO – STRIP ANTENNA

The performance of the compact multi-mode micro-strip antenna is compared to the center feed (DP-ULA), dipole circular (CP-ULA) antennas using micro-strip antennas but with different sequences [7]. The compact multi-mode micro-strip antenna is also called SCP-ULA. The power correlation between the used channel model and the antennas and the

mode-dependent angle analysis are shown in Fig. 5 [7].

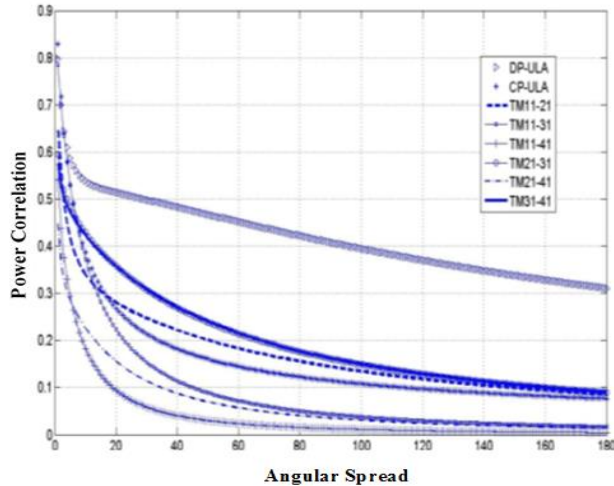


Fig.5. Antenna power correlation in different modes [7]

As can be seen from the graph in Figure 5, the compact micro-strip antenna solution (SCP-ULA) has a lower power correlation value than other antennas. A system with low power correlation has a higher spectral efficiency gain [8]. As we have already mentioned, and as can be seen from the analysis in Fig. 4, the pattern at the top, where the angle of the antenna in the top of the antenna has risen, has higher power correlation and reduced spectral efficiency. The compact multimode micro-strip antenna design, as it can be seen in the analysis, is a high performance alternative. In addition, it seems to be a great advantage for MIMO systems that need to be developed because of its low cost and design-enabling design. The high performance of the SCP-ULA design compared to other micro-strip antenna designs makes it reasonable to develop over the SCP-ULA system. However, when considering a design to be done by adding one more layer to the SCP-ULA antennas with multi-layer design, the pattern angles brought by the modes lead to major distortions in the triple structure. As a result, SCP-ULA antennas are a constraint for such a development. We can explain this degradation from the incident radiation performance of the micro-strip antennas shown in Fig. 6.

As already mentioned, since micro-strip antennas have mixed mathematical pattern subtraction equations, it presents a challenge in determining the appropriate modes to be selected. But it is easier to solve these mixed problems with developing computer technology. Unlike the reconfigurable antenna design, this is one of the advantages of using fixed modes in this application, so that it does not need unnecessary algorithms and artificial intelligence applications. Since the feedback of the micro-strip antennas is very sensitive to the pattern distortion, it is necessary that a micro-strip antenna application with a multi-layer structure has a much more sensitive feedback system.

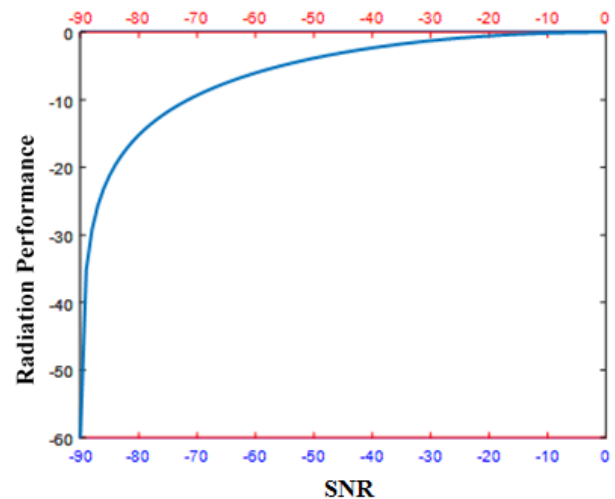


Fig.6. Performance of circular micro-strip antenna radiation-angle

VIII. CONCLUSION

In this study, antenna designs made for performance gain are investigated for two MIMO systems in the literature. These systems have been tried to be explained with the help of literature. At the same time, since the solution was recommended for the MIMO system, it is also mentioned about the MIMO channel structure and the necessity of MIMO systems. For better understanding of the systems, brief information is given about the types of antennas used in the designs. As a result, if the aim of this study is to be considered once more for the two systems, it has been tried to express the performance gains which are determined according to the position of the user as the basic logic and the optimum mode selection in the reconfigurable MIMO antenna design. It is understood that there are some disadvantages in these system tests, such as not testing the system in the case of multiple users and failing to obtain performance gains. Another solution proposal by the literature, the compact multimode micro-strip antenna, has been tried to specify the performance gains that can be achieved with a pattern that can be generated by a logical design in the case of fixed modes and fixed antenna types. In this paper, overall, the advantages that the antenna has brought are most efficiently utilized and the disadvantages are tried to be mentioned in the most objective manner.

REFERENCES

- [1] M. Viswanathan, Simulation of Digital Communication Systems using Matlab, 2013, p.422.
- [2] M. Viswanathan, On the Achievable Rate of Stationary Fading Channels, Springer, 2011, p.310.
- [3] İ. Görgeç, Design of Dual-Mode Stacked Circular Microstrip Patch Antennas and Correlation / Spectral Efficiency Analysis for Mimo Configurations, Master Thesis, 2009, p.121.
- [4] H. Zarrinkoub, Understanding LTE with Matlab, Wiley, 2014, p.508.
- [5] E. Kurtulmaz, Çoklu Yeniden Ayarlanabilir Çok Girişli Çok Çıkışlı Sistemlerde Dizayn ve Performans Analizi, Master Thesis, 2015, p.45.
- [6] Y. S. Cho, J. Kim, W. Y. Yang, C.G. Kang, MIMO-OFDM Wireless Communications with MATLAB, Wiley, 2010, p.544
- [7] A. Savaşçihabeş, Ö. Ertuğ, "IEEE 802.11n MIMO-OFDM WLAN haberleşme sistemlerinde kompakt multimod mikroşerit antenlerin korelasyon ve kapasite analizi", 3. Ulusal Haberleşme Teknolojileri ve Uygulamaları Sempozyumu, 2009, pp.127-132.

- [8] Ö. Çetin, B. Karakaya, H. A. Çırpan “3GPP LTE MIMO-OFDMA sistemlerde kanal kestirimi”, Signal Processing and Communications Applications Conference (SIU), April 2010, pp.129-132.

BIOGRAPHIES



BATUHAN ASLAN was born in Sakarya, Turkey in 1994. He received his bachelor's degrees in electrical electronics engineering department at Duzce University, in 2017. His research interests are: Wireless Communication, Signal Processing.



OSMAN DIKMEN was born in Yozgat, Turkey in 1989. He received his bachelors' degree in the Electronics Engineering Department at Gebze Technical University in 2013, master degree in the Electrical Electronics Engineering Department at Duzce University in 2017. And, he has been started PhD studying in the Electrical Electronics Engineering Department at Duzce University since 2017. He has been a research assistant in the

Duzce University since 2014. His major areas of interests are: Wireless Communication, Signal Processing.



SELMAN KULAÇ was born in Düzce, Turkey. He received the B.S. degree from Ankara University in 2002 and M.S. degrees in electronics engineering from Ankara University, Turkey, in 2004 and the Ph.D. degree electronics engineering from Ankara University, Turkey, in 2012.

From 2002 to 2007, he was a Research Assistant with the Electronics Engineering Department, Ankara University. Since 2012, he has been an Assistant Professor with the Electrical Electronics

Engineering Department, Duzce University. His research interests include telecommunication, wireless and mobile communication, cognitive radio, spectrum sensing, FPGA design, digital hardware design, video transmission, wireless implantable communication.



AHMET M. ELBİR was born in Malatya, Turkey in 1987. He received the B.S. degree from Fırat University in 2009 and the Ph.D. from Middle East Technical University (METU) in 2016, both in electrical engineering. He is the recipient of 2016 METU best Ph.D thesis award for his doctoral studies. Currently, he continues his studies at the Dept. of Electrical and Electronics Engineering, Duzce University, Turkey. His research

interests include statistical signal processing, array signal processing, sparsity-driven convex optimization, and deep learning for radar applications.

Noise Adaptive and Similarity Based Switching Median Filter for Salt & Pepper Noise

F. Katircioglu

Abstract—Works have been conducted recently to remove high intensity salt & pepper noise by virtue of adaptive and switching median filters. One of the cited works is the Noisy Adaptive Fuzzy Switching Median Filter (NAFSM) by which the noisy pixels are detected through utilization of image histogram. Noiseless pixels are left unprocessed while noisy pixels are passed through the noise adaptive median filter which expands for them. A filter mechanism which performs decision making in line with local similarity and similarity has been proposed for NAFSM. Local similarity information in 3x3 mask has been used for filtering mechanism in the study titled Noise Adaptive and Similar Based Switching Median Filter (NASBSM). Two thresholds with three regions were made by virtue of local similarity information. The logic of the approach was based on more intensive filtering for noisy pixels with high similarity value with neighboring pixels and less for those with less similarity value with neighboring pixels. According to the numerical and visual simulation results of the NASBSM mechanism, it was detected that it eliminates noises with high density.

Index Terms—Image processing, Local similarity, Median filter.

I. INTRODUCTION

DIGITAL IMAGES become deteriorated in the process of transfer or obtaining image. Transfer operations especially in noisy channels, faulty memory placement arising from the hardware and defective pixels created in the camera sensor lead to impulse noise [1]. Impulse noises are divided into two groups as salt & pepper noise and random noise. When the image is covered with salt & pepper noise, the noisy pixel takes a maximum or minimum value [2].

Standard Media Filter Filter (SMF) is utilized very often due to its noise reduction power and ease in computing. However, in as much as it makes regulation process for all noisy or noiseless pixels when the noise level increases some details emerge on the image or noise contamination occurs to the edges [3]. Adaptive Media Filter (AMF) has good performance in low density noise and in small window sizes however when the window size increases or when the density increases blurring also increases [4].

F. KATIRCIOGLU, is with Control and Automation Technology Department of Duzce Vocational High School of Duzce University, Duzce, Turkey, (e-mail: ferzankatircioglu@duzce.edu.tr) 

Manuscript received September 13, 2017; accepted January 08, 2018.
DOI: 10.17694/bajece.410249

Switching Media Filter (SMF) has been introduced with an eye to avoid damaging the pixels [5]. It is decided if the pixel should be corrected or not before filtering in AMF. Satisfactory improvements for details and edges have not been achieved in this filter in addition to its difficulty in selecting a threshold value.

SMF is applied to noisy pixel, as long as the Decision-Based Algorithm (DBA) noise pixel remains unchanged [6]. It is possible that the median value in the window can be noisy itself in a high noise intensive environment, in this case it is replaced by the neighboring pixel [7]. Noise Adaptive Fuzzy Switching Median (NAFSM) determines the noise pixels through utilization of histogram. It has performed the fuzzy switching process by creating local information in the filtering mechanism [8]. The sum of the valid pixel values in the recently recommended New Part Based Fuzzy Median Filter (NPBFMF) is obtained by weighting and this value becomes the output of the median filter. Fuzzy logic rules are used in the weighting process and the status of the input signal sequence is determined [9]. In another study, an adaptive fuzzy inference system was utilized in order to determine and eliminate random impulse noises. Intensity based on directional statistics is utilized in order to build adaptive fuzzy membership function [10]. However, satisfying noise reduction has not been achieved yet.

In the second part of this study, introduction of NAFSM filter has been made and the proposed NASBSM local similarity based filter mechanism has been briefly discussed. In the third part, NASBSM filter has been applied to images commonly used in image processing applications. The visual and numerical results obtained have been presented. In the last part, evaluations as regards this method have been made and proposals have been presented for future studies.

II. METHOD

A. Noise adaptive fuzzy switching median filter

NAFSM filter is a iterative double gradual filter, where it will perform the salt & pepper noise intensities detection before identifying the locations of possible noise pixels. L_{salt} and L_{pepper} , which are the two local maximum points, will be searched in the regions at the beginning and end of the noisy image histogram curve firstly in the NAFSM filter. When the L_{salt} and L_{pepper} , which are the two local maximum points are found, the search will be stopped. In Eq. (1), binary noise

mask $N(i,j)$ will be generated and the noisy pixels will be marked as mentioned the equality [8].

$$N(i,j) = \begin{cases} 0, & X(i,j) = L_{salt} \text{ or } L_{pepper} \\ 1, & \text{otherwise} \end{cases} \quad (1)$$

$X(i,j)$ in Eq. (1) is a pixel in (i,j) coordinates with a density of X . $N(i,j)=1$ represents the noiseless pixel while $N(i,j)=0$, represents the noisy pixel in the next step for filtering. Commonly preferred $W_{2s+1}(i,j)$ square filtering approach has been used in NAFSM filter.

$$W_{2s+1}(i,j) = \{X(i+m, j+n)\} \text{ where } m,n \in (-s, \dots, 0, \dots, s) \quad (2)$$

The term of $G_{2s+1}(i,j)$ which gives the number of noiseless pixels in the window is given as in Eq. (3).

$$G_{2s+1}(i,j) = \sum_{m,n \in (-s, \dots, 0, \dots, s)} N(i+m, j+n) \quad (3)$$

If the filtering does not have the minimum number of noisy pixels ($G_{2s+1}(i,j) < 1$), the filtering window is extended from of each of the four edges. This procedure ($G_{2s+1}(i,j) \geq 1$) is continued until the criterion met. According to Eq. (4), each of the noise-free pixels is a candidate for the selection of the median pixel.

$$M(i,j) = \text{median}\{X(i+m, j+n)\} \text{ with } N(i+m, j+n) = 1 \quad (4)$$

The filtering window size is limited to 7×7 because of the calculation time and the possibility of giving the wrong median term. If $e G_7(i,j) = 0$ is in 7×7 window size the first four pixels of the first 3×3 windows is taken into median operation [8].

$$W_3(i,j) = \{X(i+k, j+l)\} \text{ where } k,l \in (-1, 0, 1) \quad (5)$$

$$M(i,j) = \text{median}\{X(i-1, j-1), X(i, j-1), X(i+1, j-1), X(i-1, j)\}, \text{ when } s=3 \text{ and } G_7(i,j) = 0. \quad (6)$$

Four pixels in the upper left diagonal of the 3×3 filter window have been taken to ensure the repetition feature of NAFSM filter and behavior of making early process. $d(i,j)$ term which is the absolute luminance difference in the local 3×3 information window is present like in Eq. (7).

$$d(i+k, j+l) = |X(i+k, j+l) - X(i,j)| \text{ with } (i+k, j+l) \neq (i,j) \quad (7)$$

Eq. (7) provides local information with the maximum value of the absolute brightness differences in the window obtained.

$$D(i,j) = \max\{d(i+k, j+l)\} \quad (8)$$

Fuzzy logic is applied to the obtained local information as a part of filtering mechanism in NAFSM. The membership function of the accepted fuzzy set has been specified in Eq. (9).

$$F(i,j) = \begin{cases} 0, & : D(i,j) < T1 \\ \frac{D(i,j) - T1}{T2 - T1} & : T1 \leq D(i,j) < T2 \\ 1, & : D(i,j) \geq T2 \end{cases} \quad (9)$$

Local information $D(i,j)$ in Eq. (9), has been used as fuzzy input value. $T1$ and $T2$ are predetermined values of the threshold values 10 and 30 respectively. Finally, linear integration is made between the process pixel $X(i,j)$ and the median pixel $M(i,j)$ for making the restoration process of the designated noisy pixel. Restoration term $Y(i,j)$ is provided in Eq. (10) below [8].

$$Y(i,j) = [1 - F(i,j)].X(i,j) + F(i,j).M(i,j) \quad (10)$$

B. Noise adaptive and similarity based switching median filter

Similarity image forming the basis of NASBSM is a gray image in the form of white and black which emerges as result of examining the color difference values between pixels and makes the process of converting the image information to have a two-dimensional feature [11]. It will be used in the decision making process during the work to determine the relation between the pixels in the mask with the central pixel.

Distances between them must be found in order to find the similarity values in the mask with an eye to obtain local information. The distance between the pixels, due to working on gray level image, is in the form of one dimensional usage of Euclidean distance.

$$d_{(i+k, j+l)} = X_{(i,j)} - X_{(i+k, j+l)} \quad (10)$$

In Eq. (10) $d_{(i+k, j+l)}$, as the distance between the pixels, is present in all distances of all the pixels within a 3×3 mask to $X_{(i,j)}$ pixel respectively.

The linear function in Eq. (11) has been used for calculating similarity values of two pixels [12]. The dispersion range of similarity value varies in the (0,1) range. If the value obtained from this function is close to zero two pixels do not resemble each other, and if these values are close to 0, the result that resemble each other is obtained [13].

$$S_{(i+k, j+l)} = 1 - \frac{d_{(i+k, j+l)}}{D} \quad (11)$$

The D value normalizing coefficient and its value given in Eq. (11) has been determined as 255 which is the maximum value of gray level value. Equations (12), (13) and (14) are obtained by using the similarity values in the obtained mask.

$$\max_S = \max(S_i) \quad (12)$$

$$\min_S = \min(S_i) \tag{13}$$

$$\text{ort}_S = \frac{1}{9} \sum_{i=1}^9 S_i \tag{14}$$

Giving decision by using the Eq. (12) and (13), and adaptive threshold selection for switching operation is performed in Equation (15).

$$T = (\max_S - \min_S)/6 \tag{15}$$

$$F(i, j) = \begin{cases} 0, & : \text{ort}_S < T \\ \text{ort}_S, & : T \leq \text{ort}_S < 2 * T \\ 1, & : \text{ort}_S \geq 2 * T \end{cases} \tag{16}$$

Linear integration is made between the process pixel $X_{(i,j)}$ and the median pixel $M_{(i,j)}$ for making the restoration process of noisy pixel. Restoration term $Y_{(i, j)}$ is applied in the same way in Eq. (10).

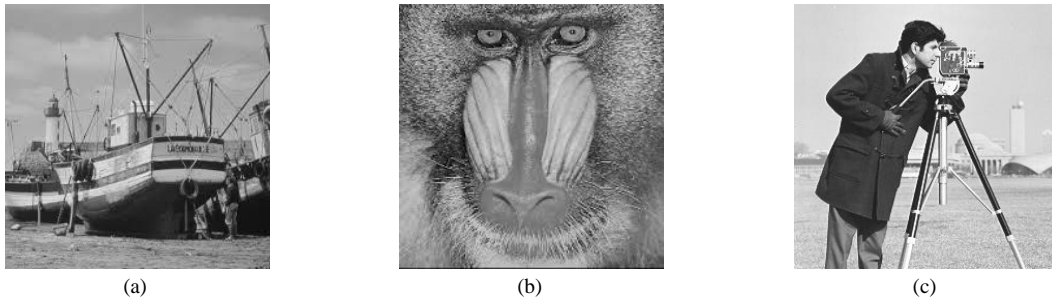


Fig. 1. Test images used in the application (a) Ship (b) Monkey (c) Camera man

NOISE DEN. (%)	Noisy Image	Filtered Image.	Noisy Image	Filtered Image	Noisy Image	Filtered Image.
	SHIP		MONKEY		CAMERA MAN	
20						
40						
60						
80						

Fig. 2. Results of application of NASBSM at various noise densities

III. RESULTS

The filtering algorithm performed with NASBSM has been tested in grayscale comparison images consisting of ship, monkey and camera man in Fig. 1. These images are in the

size of 225x225, 204x204 and 256x256 pixels respectively and is in JPEG format.

Some criteria are utilized with evaluation of achievements and compare the success of the noise reduction algorithms used. Some of these are listed as signal - to -

noise ratio (SNR), peak signal - to - noise ratio (PSNR) and mean square error (MSE).

$$MSE = \frac{1}{MN} \sum_{m=0}^{M-1} \sum_{n=0}^{N-1} [I_0(m, n) - K(m, n)]^2 \quad (17)$$

I_0 denotes noiseless image while K denotes the image which contains noise. M and N denote the number of rows and columns of the image pixels. MSE, from the signal noise ratio, represents the mean square error. The PSNR criterion, used as the first criterion in the application, is defined as follows [1].

$$PSNR = 10 \log_{10} \frac{M_I^2}{MSE} \quad (18)$$

M_I denotes the maximum number of gray levels in the image. This value has been determined as 255 in the application. A higher PSNR value denotes the fact that the restoration process has been done well. As a second criterion, MSSIM which calculates a similarity value between two images has been provided in Eq. (19) [14].

$$MSSIM(x, y) = \frac{1}{M} \sum_{j=1}^M \frac{(2\mu_{xj}\mu_{yj} + c_1)(2\sigma_{xyj} + c_2)}{(\mu_{xj}^2 + \mu_{yj}^2 + c_1)(\sigma_{xj}^2 + \sigma_{yj}^2 + c_2)} \quad (19)$$

μ_x and μ_y are the average of x and y respectively while c_1 and c_2 are constant values. σ_x and σ_y are the variance of x and y respectively while σ_{xy} is the covariance value of x and y . M denotes the number of pixels in the window within the image. The MSSIM value is present between 0 and 1, and if it is close to 1, it indicates that the performance of the application is good.

Fig. 2. includes visual results applied to ship, monkey and camera man images –which are commonly used in the literature- in NASBSM's %20, %40, %60 and %80 noise intensities. High-intensity salt & pepper covered images seem to have captured the original image. The risks of image's blurring and losing their edge properties have only been achieved in very small quantities in %80 application.

MSSIM value's being very high for all images used, emphasizes the proximity of the proposed work to real images according to the results in Table 1. PSNR value decrease as the noise intensity percentage value increases is normal and the decrease rate has been very low. NASBSM filter mechanism and performance are powerful and has been close to the original image to a large extent by eliminating the salt-and-pepper noise.

TABLE I
EVALUATION OF NASBSM PERFORMANCE

Noise Den. (%)	IMAGE.	MSE	PSNR	MSSIM
10	SHIP	38.611	32.263	0.971
30		114.622	27.538	0.910
50		200.768	25.103	0.837
70		309.572	23.223	0.740
90		639.024	20.075	0.544
10	MONKEY	50.774	31.074	0.957
30		165.478	25.943	0.858
50		284.329	23.592	0.740
70		413.919	21.961	0.598
90		791.809	19.144	0.362
10	CAMERA MAN	43.147	31.781	0.978
30		125.002	27.161	0.929
50		223.913	24.629	0.868
70		376.687	22.370	0.771
90		767.494	19.280	0.595

IV. CONCLUSION

Local similarity information in 3x3 mask for filtering mechanism has been used in this study. Two thresholds with three regions have been realized with local similarity information. The logic of the approach was based on more intensive filtering for noisy pixels with high similarity value with neighboring pixels and less for those with less similarity value with neighboring pixels. It has been detected by visual and numerical results that it makes the filtering process in

images covered with high-intensity salt & pepper noise and achieves the original image. MSE, PSNR and MSSIM have been preferred for performance evaluation. The risks of blurring of images and their losing edge properties were realized in a very small amount only in the %80 application NASBSM filter proposed in the next process will be compared with the median filters which are well-known in the literature and their performance evaluations will be detailed. Also its contribution to engineering applications by using the image processing application will be underlined.

REFERENCES

- [1] Bovik A., Handbook of image and video processing. New York: Academic, 2010.
- [2] Chan R. H., Ho C. W., Nikolova M., "Salt-and-pepper noise removal by median type noise detectors and detail-preserving regularization", Vol.14, No.10, pp. 1479-1485, 2005.
- [3] Nades T., Gallagher N., "The output distribution of median type filters", IEEE Transactions on Communications, Vol.22, No.5, pp. 532-541, 1984.
- [4] Hwang H., Haddad R. A., "Adaptive median filters: new algorithms and results", IEEE Transactions on image processing, Vol.4, No.4, pp. 499-502, 1995.
- [5] Wang Z., Zhang D., "Progressive switching median filter for the removal of impulse noise from highly corrupted images", IEEE Transactions on Circuits and Systems II: Analog and Digital Signal Processing, Vol.46, No.1, pp. 78-80, 1999.
- [6] Srinivasan K., Ebenezer D., "A new fast and efficient decision-based algorithm for removal of high-density impulse noises", IEEE signal processing letters, Vol.14, No.3, pp. 189-192, 2007.
- [7] Jayaraj V., Ebenezer D., "A new switching-based median filtering scheme and algorithm for removal of high-density salt and pepper noise in images", EURASIP journal on advances in signal processing, Vol.1, pp. 690218, 2010.
- [8] Toh K. K. V., Isa N. A. M., "Noise adaptive fuzzy switching median filter for salt-and-pepper noise reduction", IEEE signal processing letters, Vol.17, No.3, pp. 281-284, 2010.
- [9] Lin T. C., Lin C. M., Liu M. K., Yeh C. T., "Partition-based fuzzy median filter based on adaptive resonance theory", Computer Standards & Interfaces, Vol.36, No.3, pp. 631-640, 2014.
- [10] Habib M., Hussain A., Rasheed S., Ali M., "Adaptive fuzzy inference system based directional median filter for impulse noise removal", AEU-International Journal of Electronics and Communications, Vol.70, No.5, pp. 689-697, 2016.
- [11] Katircioglu F., "Segmentation of color images based on relation matrix and edge detection", Master of Science, Dept. Electrical Education, Duzce Universtiy, Duzce, Turkey, 2007.
- [12] M. Jourlin, J. C. Pinoli, "A model for logarithmic image processing", Journal of microscopy, Vol.149, No.1, pp. 21-35, 1988.
- [13] Demirci R., "Rule-based automatic segmentation of color images", Int. J. Electronics and Communication(AEU), Vol.60, pp. 435-442, 2006.
- [14] Wang Z., Bovik A. C., Sheikh H. R., Simoncelli E. P., "Image quality assessment: from error visibility to structural similarity", IEEE transactions on image processing, Vol.13, No.4, pp. 600-612, 2004.

BIOGRAPHIES



FERZAN KATIRCIOGLU he was born in Duzce City, in 1974. He received B.Sc. in 1996 at Marmara University, Faculty for Technical Education, M.Sc. in 2007 at A.I.B.U., Institute for Natural Sciences, Department of Electricity Education and Ph.D. at Duzce University, Faculty for Natural Sciences, Department of Electricity Electronic and Computer Engineering in 2016. From 1996 to 2000, he was a Electrical Teacher with Cerkes 19 May CPL School. He

has worked as academic staff in the Control and Automation Technology at Duzce University, Duzce Vocational High School since 2000. His current research interests are Image Processing and Heuristic Optimization.

Classification of Different Cancer Types by Deep Convolutional Neural Networks

H.S. Nogay

Abstract—In this study, ten different types of cancer were classified with deep convolutional neural networks (DCNN). A total of 10,000 MRI (Magnetic Resonance Imaging) data were used for ten cancer patients, including 1000 MRI data for each cancer type. Although the images were reduced to 28x28 pixels, the DCNN model performed classification with an accuracy rate of 0.98 after 27 seconds and 15 epochs of training. The error rate in the last epoch in the study is also very close to zero. A highly successful classification has been achieved with the proposed DCNN model.

Index Terms—Deep Convolutional Neural Network, Cancer Types, Classification, Accuracy

I. INTRODUCTION

CONVOLUTIONAL neural networks, which are recently enhanced and improved artificial neural networks, are one of the deep learning approaches used in many applications such as image recognition, classification and pattern recognition [1]. Nowadays, deep convolutional neural networks (DCNN) are used especially in the diagnosis and classification of fatal diseases such as cancer [1 – 4]. Cancer patients often learn by chance that they are cancerous. Because when they go to the doctor, the results of the examinations done to them are usually for the evaluation of other possibilities. People generally do not do any analysis unless they are sick or doctors need it. Early diagnosis of cancer is therefore very difficult. Which cancer type the cancer patients have is revealed by the doctor examining the patient's MR images or clinical data. However, since the metastases are so insidious, they are noticed very late. Knowing what is cancerous in a very practical and fast manner with MR images on hand is then very useful for early diagnosis before metastasis. Classification of information on different types of cancer in MR images may contribute to the understanding of metastatic conditions in the future together with their reasons for the examination and prophylaxis. In this study, it was aimed to classify cancer types with deep learning approach using ten thousand data of ten types of cancer patients. One thousand data of each cancer type was used. In the study, image patches recorded in jpg format are used. As a result, a fairly satisfactory classification rate has been achieved.

H. S NOGAY, is with Mustafa Cikrikcioglu Vocational College, Erciyes University, Kayseri, Turkey, (e-mail: nogay@erciyes.edu.tr) 

Manuscript received September 13, 2017; accepted January 08, 2018.
DOI: [10.17694/bajece.410250](https://doi.org/10.17694/bajece.410250)

II. MATERIALS

The data used in this study were obtained from The Cancer Imaging Archive (TCIA) website [5, 6]. In the study, 10,000 pieces of jpg format image data were used for 10 cancer types. In order to create the data set, 1000 image data of each cancer patient were collected and recorded separately. Figure 1 shows the data set and labels used in the study. In the data set shown in Figure 1, abbreviations such as the following are used as labels. In addition, each cancer type is numbered from zero to nine for classification.

BRN : Brain cancer (0)

BRST : Breast cancer (1)

COLN: Colon cancer (2)

HN: Head and neck cancer (3)

L : Lung cancer (4)

PROS: Prostate cancer (5)

PAC: Pancreas cancer (6)

RENL: Renal cancer (7)

SRKO: Sarkomas (8)

TROID: Thyroid cancer (9)

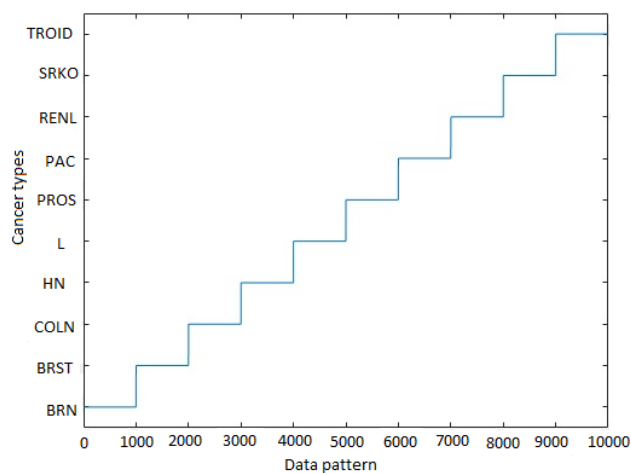


Fig. 1. Data set configuration

Each image patch in the data set is actually 216 x 256 pixels as shown in figure 2 in the sample brain MR image. All image patches have been reduced to a 28x28 size so that the operation can be faster and the data set is not overly saturated.

A sample dataset of 28 x 28 image patches consisting of 20 random data samples is shown in Fig. 3.

All images used in the study are only black and white, that is two-layer images. The aim is to determine which cancer type belongs to the MRI data, so no 3 or more layered images are needed. Rapid training of the model depends on whether the operating system to be used is GPU-supported, the number of data in the data set, the pixel of the data and whether it is layered. When all of these factors are considered, it can be seen that preferences made for the DCNN model are only considered to achieve rapid results.

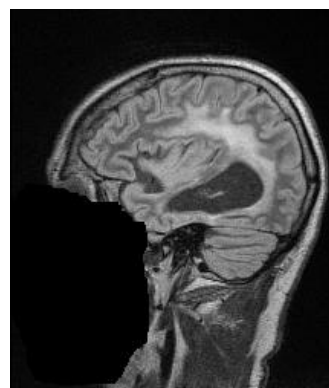


Fig. 2. A sample MR image of the brain in real size

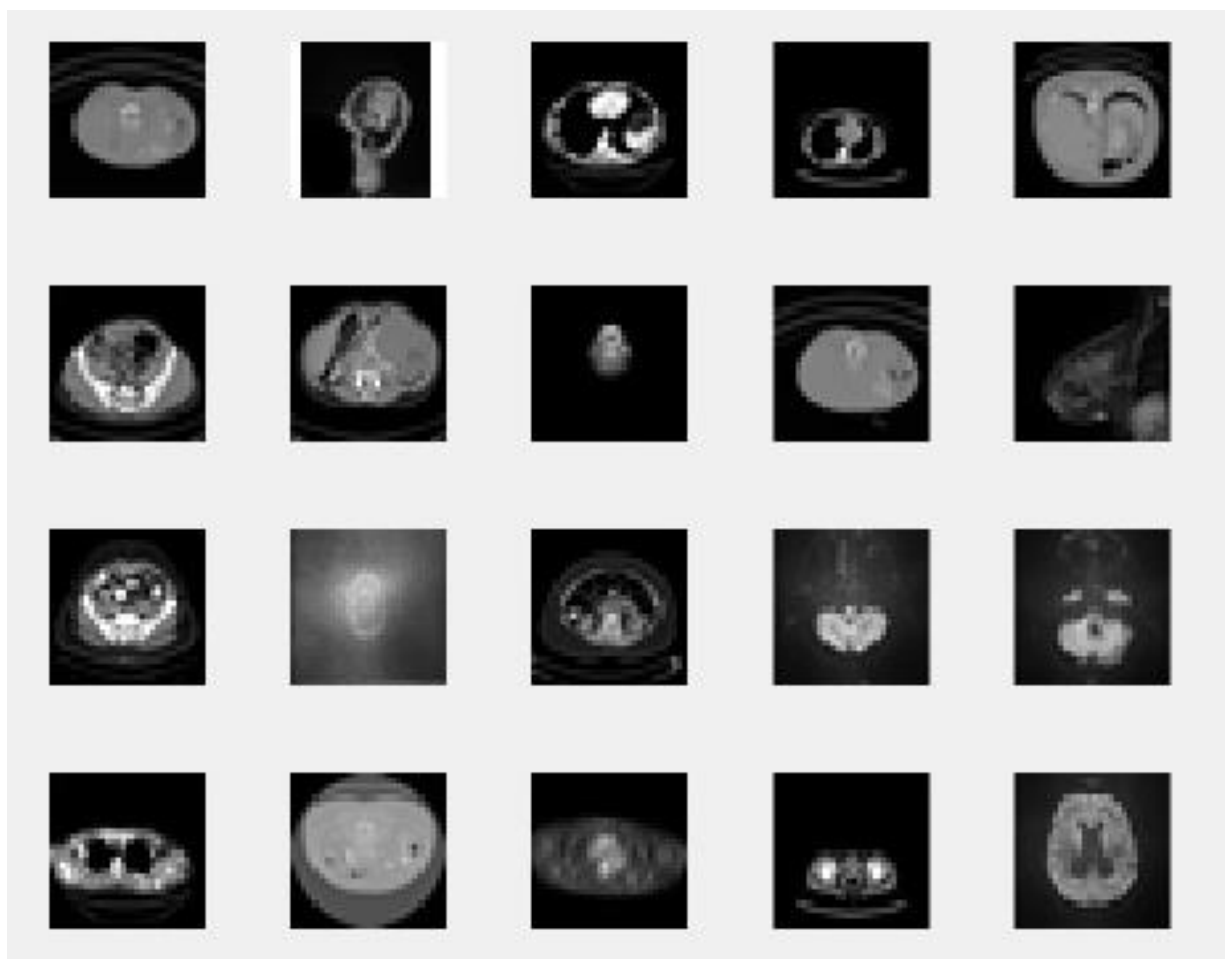


Fig. 3. Data set samples

III. METHODOLOGY

In the study, a deep convolutional neural network (DCNN) model, which is a kind of multi-layered perceptrons is used. Convolutional neural networks are an advanced deep learning approach based on artificial neural networks. In a convolutional neural network, there are generally the following layers: (i) the input layer is the layer at which the image data is recorded at the appropriate size and shape; (ii) the convolution layer is the layer from which a smaller pixel appearance is obtained using

the appropriate filter; (iii) the ReLU layer is co-worked with the convolutional layer, the normalization function of the activation function; (iv) The Max Pooling layer is known as the pooling layer, and some sort of filtering is possible; The layer by which the maximum number of image codes are filtered out; (v) full connected and soft max layer, the layer where the full connection is made. In this layer, connections are made to all the outputs. After this layer, there is an output layer with a classification output [7 - 11]. Often these layers are repeated in the construction of DCNN architects. That is,

two convolutional layers and two max pooling layers are used. In many studies, images can have multiple layers. If the images used are colored, they are images with 3 or more layers or sizes [11]. Two-dimensional black and white images were used in this study. The Deep Convolutional Neural Network model proposed in the study consists of 7 layers as shown in figure 4. The DCNN model is simply designed as a single level. These 7 layers are input layer, convolution 2d layer, relu layer, max pooling 2d layer, full connected layer, softmax layer and classification layer which is the last layer. 75% of the data set was used for testing and the remaining 25% was used for testing [12-14].

In a DCNN model, the most important method to minimize the total error is to use the gradient descent algorithm. For the model proposed in the study, the mini-batch gradient descent (MBGD) algorithm is used. In the MBGD algorithm, a much smaller number of samples are used for each iteration of the total dataset. In the study, the Rectified Linear Unit (ReLU) activation function, shown in equation (1), is used. If the input value is less than zero, the value is zero [15].

$$\text{ReLU}(x) = \text{Max}(0, x) \tag{1}$$

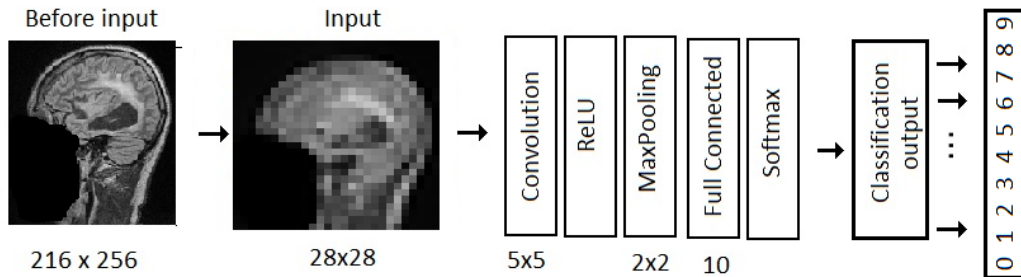


Fig. 4 Proposed DCNN architecture

In the convolution layer, a 5x5 filter was applied to the input image and the output was normalized by the ReLU activation function. After the ReLU layer, it was performed in 2 squares for the stride operation in the MaxPooling layer. The maximum epoch was selected as 15 for model training. The initial learning rate is 0.0001 as a starting point. In the next process, ten full connections are made for ten outputs.

testing process, and finally, the point at which the DCNN model was reached.

IV. RESULTS

As a result of the test made, the accuracy rate for the classification was obtained as 0.9948. Table 1 shows the training process of the model.

TABLE I. TRAINING PROCESS OF THE MODEL

Epoch	Iteration	Time Elapsed (Seconds)	Mini-batch Loss	Mini - Batch accuracy
1	1	0,14	4,8241	3,13
1	50	1,87	0,2849	94,53
2	100	3,41	0,1342	95,32
3	150	4,97	0,0679	97,66
4	200	6,52	0,0722	98,44
5	250	8,08	0,0472	99,22
6	300	9,64	0,0899	97,66
7	350	11,21	0,0252	99,22
7	400	12,74	0,0235	100
8	450	14,29	0,0555	98,44
9	500	15,83	0,0183	100
10	550	17,4	0,0256	99,22
11	600	18,94	0,0152	100
12	650	20,47	0,0043	100
13	700	22,02	0,0067	100
13	750	23,56	0,0062	100
14	800	25,09	0,0053	100
15	850	26,62	0,0113	100
15	870	27,24	0,0184	99,22

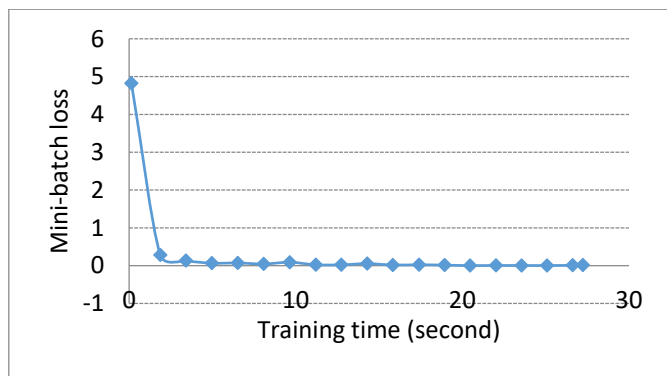


Fig.5 Training process

As Table 1 reveals, in the 15th epoch, a mini batch accuracy rate of 99.22% was achieved in 27.24 seconds, and a mini batch loss was obtained in the 15th epoch very close to zero at 0.00184. Figure 5 shows the training process and loss rates, and figure 6 shows the DCNN model in terms of training and

The reason for ending Epoch 15 is that the error does not fall further from the 12th epoch but increases slightly. The lowest error level is reached in the 12th epoch (0,0043). More importantly, the accuracy rate at the end of the first epoch begins with 94%.

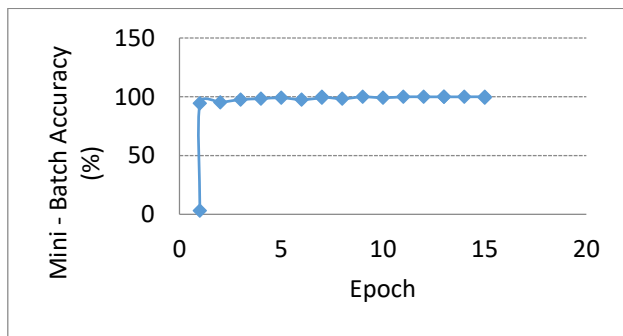


Fig. 6 Testing result of the DCNN model

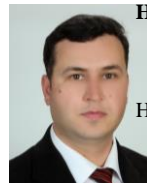
V. CONCLUSIONS

The training data used for the training of the proposed DCNN model in the study was reduced to a size of 28x28 pixels in the first stage. Although it is normally a very low pixel value, it is quite suitable for simple classification purposes only. On the other hand, it is very satisfactory that the accuracy rate obtained is 0.9948. The study was performed in a MATLAB environment on a PC with GPU support. Therefore, the training process continued until the 27th minute. Despite the accuracy achieved for the classification or prediction of different types of cancer, the error rate is also very close to zero. This study has produced very successful results in light of future studies.

REFERENCES

- [1]. U. Rajendra Acharya, Shu Lih Oh, Yuki Hagiwara, Jen Hong Tan, Hojjat Adeli, Deep convolutional neural network for the automated detection and diagnosis of seizure using EEG signals, *Computers in Biology and Medicine*, (2017) 1–9
- [2]. M.E. Paoletti, J.M. Haut, J. Plaza, A. Plaza, A new deep convolutional neural network for fast hyperspectral image classification, *ISPRS Journal of Photogrammetry and Remote Sensing*, 31, May, 2017, 1-28
- [3]. Pegah Khosravi, Ehsan Kazemi, Marcin Imielinski, Olivier Elemento, Iman Hajirasouliha, Deep Convolutional Neural Networks Enable Discrimination of Heterogeneous Digital Pathology Images, *EbioMedicine*, 2017, 1-12
- [4]. Y. Zheng, Zhiguo Jiang, F. Xie, H. Zhang, Y. Ma, H. Shi, Yu Zhao Feature extraction from histopathological images based on nucleus-guided convolutional neural network for breast lesion classification, *Pattern Recognition* 71 (2017) 14–25,
- [5]. Vallières, M. *et al.* Radiomics strategies for risk assessment of tumour failure in head-and-neck cancer, *Sci Rep*, 7, 10117 (2017). doi: 10.1038/s41598-017-10371-5
- [6]. <http://www.cancerimagingarchive.net/>, date of access: 10 Jan 2018,
- [7]. M. Dais Ferreira, Débora Cristina Corêa, Luis Gustavo Nonato, Rodrigo Fernandes de Mello, Designing architectures of convolutional neural networks to solve practical problems, *Expert Systems With Applications* 94 (2018) 205–217
- [8]. B. Krismono Triwijoyo, Widodo Budiharto, Edi Abdurachman, The Classification of Hypertensive Retinopathy using Convolutional Neural Network 2nd International Conference on Computer Science and Computational Intelligence 2017, ICCSCI 2017, 13-14 October 2017, Bali, Indonesia,
- [9]. U. Rajendra Acharya, Shu Lih Oh, Yuki Hagiwara, Jen Hong Tan, Muhammad Adam, Arkadiusz Gertych, Ru San Tan, A deep convolutional neural network model to classify heartbeats, *Computers in Biology and Medicine* 89 (2017) 389–396
- [10]. U.K. Lopes, J.F. Valiati, Pre-trained convolutional neural networks as feature extractors for tuberculosis detection, *Computers in Biology and Medicine* 89 (2017) 135–143.
- [11]. M. Dyrmann, H. Karstoft, H. Skov Midtby, Plant species classification using deep convolutional neural network, *biosystems engineering*, 151, (2016), 72 – 80
- [12]. S. Hussain, S. M. Anwar, M. Majid, Segmentation of glioma tumors in brain using deep convolutional neural network, *Neurocomputing*, (2017) 1–14
- [13]. H. Sharma, N. Zerbe, I. Klempert, O. Hellwich, P.Hufnagl, Deep convolutional neural networks for automatic classification of gastric carcinoma using whole slide
- [14]. S. Yu, SenJia, ChunyanXu, Convolutional neural networks for hyperspectral image classification, *Neurocomputing*, 219, (2017), 88–98
- [15]. I. Goodfellow, J., Warde-farley, D., ve Courville. AMaxout Networks. Proceedings of the 30th International Conference on Machine Learning, Atlanta, Georgia, USA. JMLR: W&CP.(2013). p. 28.

BIOGRAPHIES



H. H. SELÇUK NOGAY received B.S degrees in Electrical Education from Kocaeli University, and M.S. and Ph.D degrees in Electrical Education from Marmara University respectively 2002, 2003 and 2008. His research interests include Artificial Neural Network, Deep Learning and signal processing technique He has been working as a Professor in Vocational Scholl of Erciyes University in Kayseri, Turkey.

Publication Ethics

The journal publishes original papers in the extensive field of Electrical-electronics and Computer engineering. To that end, it is essential that all who participate in producing the journal conduct themselves as authors, reviewers, editors, and publishers in accord with the highest level of professional ethics and standards. Plagiarism or self-plagiarism constitutes unethical scientific behavior and is never acceptable.

By submitting a manuscript to this journal, each author explicitly confirms that the manuscript meets the highest ethical standards for authors and coauthors

The undersigned hereby assign(s) to *Balkan Journal of Electrical & Computer Engineering* (BAJECE) copyright ownership in the above Paper, effective if and when the Paper is accepted for publication by BAJECE and to the extent transferable under applicable national law. This assignment gives BAJECE the right to register copyright to the Paper in its name as claimant and to publish the Paper in any print or electronic medium.

Authors, or their employers in the case of works made for hire, retain the following rights:

1. All proprietary rights other than copyright, including patent rights.
2. The right to make and distribute copies of the Paper for internal purposes.
3. The right to use the material for lecture or classroom purposes.
4. The right to prepare derivative publications based on the Paper, including books or book chapters, journal papers, and magazine articles, provided that publication of a derivative work occurs subsequent to the official date of publication by BAJECE.
5. The right to post an author-prepared version or an official version (preferred version) of the published paper on an internal or external server controlled exclusively by the author/employer, provided that (a) such posting is noncommercial in nature and the paper is made available to users without charge; (b) a copyright notice and full citation appear with the paper, and (c) a link to BAJECE's official online version of the abstract is provided using the DOI (Document Object Identifier) link.



ISSN: 2147- 284X

Year: April 2018

Special Issue: The special issue consists of recent trends on electrical & computer engineering applications. And also, some studies have been selected from International Engineering Research Symposium, (UMAS 2017) for this special issue.

CONTENTS

- E. Huner, and C. Akuner;** The Design and Magnetic Analysis of MultiDisc and Layer Winding Toroidal Axial Flux Permanent Magnet Open Slotted (MLTAFPMOS) Synchronous Alternator,**1-5**
- H. Bakir, A. Ozturk, and S.Tosun;** Investigation of Power Flow Effect of Serial and Parallel FACTS Devices,**6-11**
- O. Akar, U.K.Terzi, and O. Ozgonenel;** A New Speed Control Technique for a Separately Excited Direct Current Motor by PID Controller,**12-17**
- M.K. Döşoğlu, and M. Dursun,** Response and Analysis of Permanent Magnet Synchronous Motor According to Different Reference Signals,**18-22**
- H.Uzun, O.Akar, A.Demirci, M.C.Akuner, U.K. Terzi;** Analyzing High Efficiency Asynchronous Motors Using Scalar Control Technique,**23-26**
- K. Erhan, M. Ayaz, and Y. Icer;** Conceptual Design of a Smart Parking Lot System for Electric and Hybrid Electric Vehicles,**27-32**
- Z.B. Garip and A.F. Boz;** The FIR Filter Design based on Genetic Algorithm,**33-36**
- S. Karagol, D. Yildiz;** Transmission of Audio Signal from Reed-Solomon AWGN Channel Using Wavelet Transform Families,**37-41**
- M.S. Başarslan and F. Kayaalp;** Data Mining Through Data Visualization: A Case Study on Predicting Churners on Telecommunications Data Set,**42-45**
- B. Aslan, O. Dikmen, S. Kulaç and A. M. Elbir;** Evaluation of Reconfigurable Multiple and Compact Micro-Strip Antennas for MIMO Systems,**46-50**
- F. Katircioglu;** Noise Adaptive and Similarity Based Switching Median Filter for Salt & Pepper Noise,**51-55**
- H.S. Nogay;** Classification of Different Cancer Types by Deep Convolutional Neural Networks,**56-59**

BALKAN JOURNAL OF ELECTRICAL & COMPUTER ENGINEERING

(An International Peer Reviewed, Indexed and Open Access Journal)

Contact

Istanbul Technical University
Department of Electrical Engineering,
Ayazaga Campus, Maslak, Istanbul-Turkey

Web: <https://www.bajece.com>
<http://dergipark.gov.tr/bajece>
e-mail: editor@bajece.com

